PROCEEDINGS QTS'26

CONTENTS

Krasnaya Polyana, Sochi, Russia March 1 – March 7, 2026
9th International School on Quantum Technologies

Coherent transport of atoms for scalable atomic quantum computer

Ivan Tsirulnikov[1*], **Gleb Struchalin**[1], **Ivan Bobrov**[1], **Stanislav Straupe**[1,2]

[1] *Quantum Technology Centre and Faculty of Physics, M.V. Lomonosov Moscow State University, 1 Leninskie Gory Street, Moscow 119991, Russian Federation*
[2] *Russian Quantum Center, Russia, Moscow, 121205, Bol'shoy bul'var 30 building 1*
*E-mail: tzirulnikov21@yandex.ru

Abstract

In this work, we investigate the coherent transport of single atoms between the sites of an optical lattice - a key operation for scaling neutral-atom quantum processors. We present combined numerical and experimental results, comparing various transport protocols. Our goal is to maximize the probability of transferring atoms between traps and the final fidelity of the quantum state, minimizing errors caused by non-adiabatic excitations and various sources of decoherence. The results determine optimal transport strategies and establish practical requirements for system stability to enable large-scale quantum computing.

Introduction

Arrays of neutral atoms trapped in optical tweezers are one of the most promising platforms for building a quantum computer[1]. This platform demonstrates both long coherence times and high fidelity for single-qubit as well as two-qubit gates. However, executing complex quantum algorithms requires not only high-quality operations on individual qubit pairs but also the ability to create arbitrary connectivity among multiple qubits in the array. To achieve this, an architecture with dynamic array reconfiguration, based on coherent transport of atoms between lattice sites or individual tweezers, has been proposed and is actively being developed[2], [3]. In such an architecture, groups of qubits can be physically brought together to perform multi-qubit gates and then separated again, minimizing parasitic interactions. Thus, the coherent shuttling operation becomes key for scaling.

Transport protocol

The coherent atom transport protocol consist of three stages. Initially, the atom is captured from a static optical trap by a tweezer whose potential is adiabatically deepened to a value exceeding the original trap depth by a factor of 5–6. This ensures reliable capture and minimises the probability of loss. Subsequently, the transport is carried out. The position of the deepened tweezer is displaced following a prescribed trajectory $x_0(t)$, thereby transferring the potential well and the atom to the target location. A key requirement is to choose a trajectory that minimises non-adiabatic heating while simultaneously completing the operation as rapidly as possible. Finally, upon reaching the target, the original tweezer is adiabatically switched off, concluding the atom transfer process.

Results

To simulate probability of transport of atoms (see Fig.1) we numeracaly solve classical equations of motion in time-dependent potential (see Equation (1)) for each of the N initial conditions sampled from the Maxwell-Boltzmann distribution. To investigate the coherence of the atomic ensemble, we numerically solved the coupled system of Bloch equations and classical equations of motion. This approach allowed us to perform a comparative analysis of the Ramsey interferometry scheme in a static trap versus a modified Ramsey protocol (see Fig.2) that incorporates preliminary coherent atom transport.

$$U(x,y,z,t) = U_A(x,y,z) + U_B(x,y,z) + U_M(x,y,z,t) \tag{1}$$

$$U_A(x,y,z) = -U_0\left(\frac{w_0}{w(z)}\right)^2 \exp\left(-\frac{2(x^2+y^2)}{w^2(z)}\right) \quad , \quad U_B(x,y,z) = -U_0\left(\frac{w_0}{w(z)}\right)^2 \exp\left(-\frac{2((x-S)^2+y^2)}{w^2(z)}\right)$$

$$U_M(x,y,x,t) = \begin{cases} -\frac{U_p}{\tau} t \left(\frac{w_p}{w_p(z)}\right)^2 \exp\left(-\frac{2((x-x_c)^2+(y-y_c)^2)}{w_p^2(z)}\right), & 0 \le t \le \tau \\ -U_p \left(\frac{w_p}{w_p(z)}\right)^2 \exp\left(-\frac{2((x-x_c-V(t)\cdot(t-\tau))^2+(y-y_c)^2)}{w_p^2(z)}\right), & \tau \le t \le T_m + \tau \\ -\frac{U_p}{\tau}\left(-t+(T_m+2\tau)\right) \left(\frac{w_p}{w_p(z)}\right)^2 \exp\left(-\frac{2((x-x_c-S)^2+(y-y_c)^2)}{w_p^2(z)}\right)), & T_m+\tau \le t \le T_m+2\tau \end{cases}$$

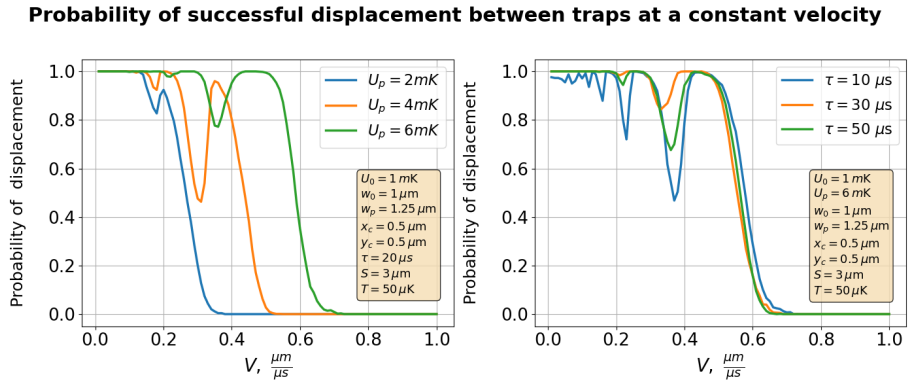

Figure 1: Graphs showing the dependence of the successful atom transfer probability on the tweezer velocity under various system and transport protocol parameters. The non-monotonicity of the curves is caused by vibrational resonances.

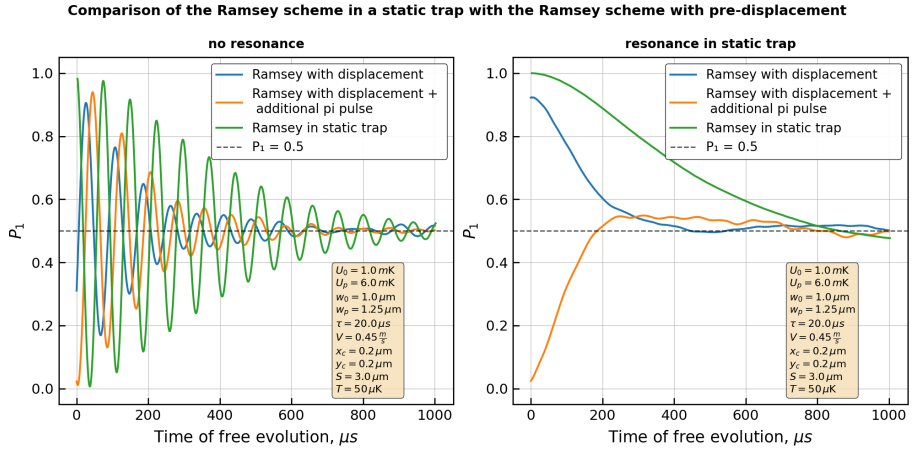

Figure 2: The graphs compare the results of three different protocols. The first protocol is the classic Ramsey scheme in a static trap. The second protocol is the Ramsey scheme with pre-transport. The third protocol differs from the second by the addition π-pulse at the center of the transport protocol

References

[1] *Radnaev A.G., Chung W.C., Cole D.C. et al.*, Universal Neutral-Atom Quantum Computer with Individual Optical Addressing and Nondestructive Readout. PRX Quantum. Vol. 6. P. 030334 (2025).

[2] *Bluvstein D., Levine H., Semeghini G. et al.*, A quantum processor based on coherent transport of entangled atom arrays. Nature. Vol. 604. P. 451–456 (2022).

[3] *Chiu N.C., Trapp E.C., Guo J. et al.*, Continuous operation of a coherent 3,000-qubit system. Nature. Vol. 646. P. 1075–1080 (2025).

Krasnaya Polyana, Sochi, Russia March 1 – March 7, 2026
9th International School on Quantum Technologies

Effective preparation of GHZ-like states from single photons

Suren Fldzhyan[1,2*], **Stanislav Straupe**[3,2,1], **Mikhail Saygin**[3,1]

[1] *Faculty of Physics, M. V. Lomonosov Moscow State University, Leninskie Gory 1, Moscow, 119991, Russia*
[2] *Russian Quantum Center, Bolshoy bul'var 30 building 1, Moscow, 121205, Russia*
[3] *Sber Quantum Technology Center, Kutuzovski prospect 32, Moscow, 121170, Russia*
*E-mail: fldzhyansa@my.msu.ru

Abstract

This work demonstrates a linear-optical technique for the resource-efficient generation of tunable Greenberger-Horne-Zeilinger (GHZ) like states from single photons. The method follows a staged scheme: single photons are converted into tunable intermediate states, which are then sequentially fused to increase the states' size, yielding the target GHZ-like state at the end. The proposed approach exhibits low resource cost, measured by the average number of photons per successful generation, and demonstrates scalable performance even for GHZ-like states with a large number of qubits.

Heralded multi-photon entanglement generation is a central bottleneck for photonic quantum computing, where resource costs typically grow exponentially with the target state size. The maximally entangled GHZ states are critical resources for universal quantum computation. The work [1] introduces the generation of N-qubit GHZ states using intermediate states, called "primates", and "bleeding" procedure. This work explores efficient methods for generating photon states with tunable entanglement. We focus on generating N-qubit GHZ-like states, and demonstrate that using variable-entanglement intermediate states and non-exhaustive bleeding can significantly reduce the photon resource cost compared to rigid approaches.

We define the family of target N-qubit GHZ-like states with variable entanglement parameter s as:

$$|\mathrm{GHZ}_N(s)\rangle = \sqrt{s}|10\rangle^{\otimes N} + \sqrt{1-s}|01\rangle^{\otimes N}, \tag{1}$$

where qubits are encoded in the dual-rail basis (one photon across two modes). The parameter $0 \leq s \leq 1$ controls the entanglement degree, with $s = 0.5$ corresponding to the maximally entangled GHZ state.

The building blocks of our construction are modified primate states — specialized photonic resource states that enable staged construction of larger entangled states. An n-photon primate state across $2n$ modes is defined as:

$$|\pi^{(n)}(\lambda, s)\rangle = \sqrt{\lambda}|s^{(n)}\rangle + \sqrt{1-\lambda}|0\rangle|\zeta\rangle|0\rangle, \tag{2}$$

where $|s^{(n)}\rangle = \sqrt{s}|2\rangle|01\rangle^{n-1}|0\rangle + \sqrt{1-s}|0\rangle|10\rangle^{n-1}|2\rangle$, $|\zeta\rangle$ is junk, and λ represents the weight of the useful component. The elementary primate $|\pi^{(1)}(1, s)\rangle$ can be generated from two single photons using an ancilla beamsplitter scheme with success probability $\frac{1}{2\max(s,1-s)}$. The resource cost of generating such state is however $\nu^{(1)}(s) = 4s - 2\sqrt{1-s}\left(\sqrt{s} - \sqrt{1-s}\right)$, provided we employ recycling of photons.

Larger primate states are constructed by fusing smaller ones using linear-optical networks and photon detection. The fusion operation $F^{(t)}$ (Fig. 1a) combines two primates $|\pi^{(n_1)}(\lambda_1, s_1)\rangle$ and $|\pi^{(n_2)}(\lambda_2, s_2)\rangle$ into $|\pi^{(n_1+n_2)}(\lambda', s')\rangle$ with success probability p. The updated parameters s' and λ' as well as probability p depend on which mode pairs are fused and the beamsplitter transmittance t. The resource cost of the $|\pi^{(n_1+n_2)}(\lambda', s')\rangle$ generation is then

$$\nu^{(n_1+n_2)}(s') = \frac{\nu^{(n_1)}(s_1) + \nu^{(n_2)}(s_2)}{p} \tag{3}$$

The final step transforms a primate state $|\pi^{(N)}(\lambda, s)\rangle$ into the target GHZ-like state $|\mathrm{GHZ}_N(s)\rangle$ using a balanced beamsplitter fusion ($t = 1/2$). The success probability is $\lambda/2$, maximized when λ is largest.

The bleeding technique (Fig. 1b,c) provides a more efficient fusion method. Instead of a single fusion attempt, the bleeding unit $B^{(c)}$ repeatedly passes photons through weakly transmitting beamsplitters until a single-photon detection heralds success. The parameter $c = \prod_x t_x^2$ quantifies how exhaustive

the bleeding process is, with $c = 0$ corresponding to fully exhaustive bleeding. By optimizing both the initial primate entanglement parameters s and the bleeding parameters c, we achieve significant reductions in the average photon number cost ν required to generate one target GHZ state. Fig. 1d shows that variable-entanglement primates combined with tunable bleeding parameters yield resource costs substantially below the fixed-parameter scaling of $N2^N$ [1].

Our work demonstrates that intermediate states with variable entanglement can reduce the resource costs for generating GHZ-like states in linear-optical quantum computing. The non-exhaustive bleeding technique provides particular advantages, showing that flexible state-generation strategies can outperform fixed protocols. These results suggest new pathways for efficient preparation of entangled resources in photonic quantum information processing.

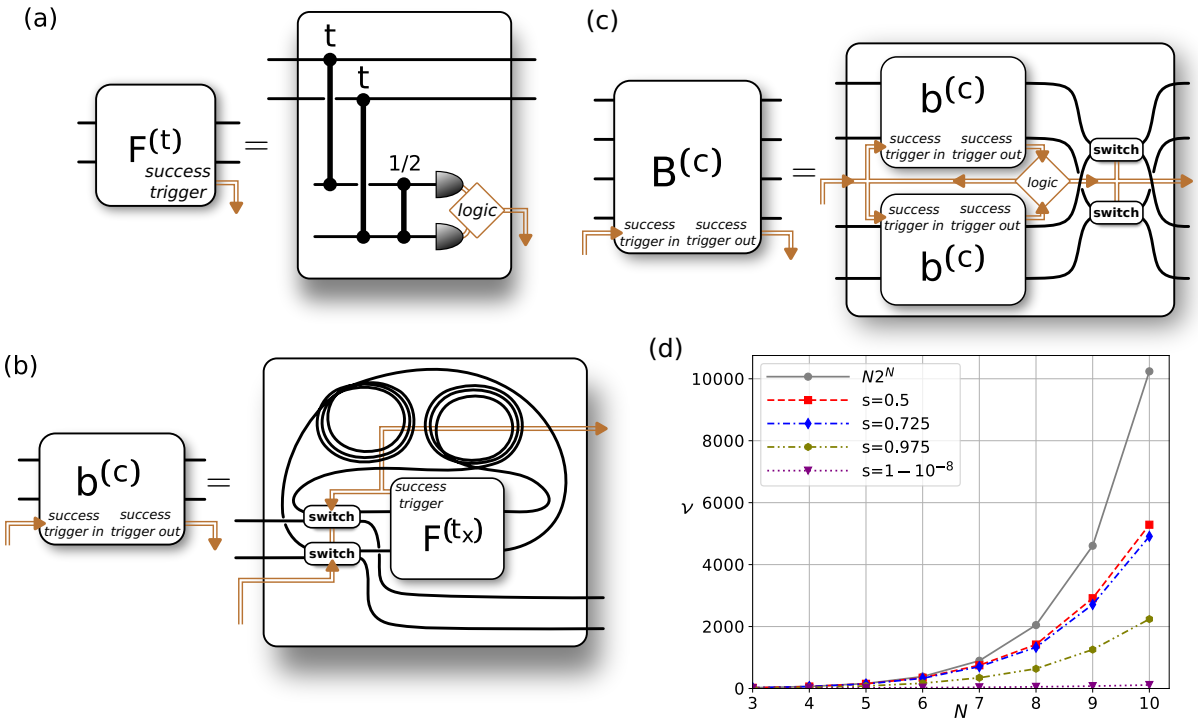

Figure 1: (a) Fusion unit $F^{(t)}$. A trigger signals success when exactly one photon is detected. Copper lines indicate classical signal flow. (b) Bleeding subunit $b^{(c)}$. An optical switch toggles from the bar to the cross state upon receiving a trigger. (c) Full bleeding unit $B^{(c)}$, using two parallel $b^{(c)}$ subunits. A logic unit discriminates photon counts, routes optical paths, and can halt the procedure. (d) Photon cost ν for generating $|\mathrm{GHZ}_N(s)\rangle$ via bleeding. The gray curve ($s = 0.5$, $c = 0$) scales as $N2^N$. Colored curves show improved costs with variable primates and tunable c.

Suren Fldzhyan acknowledges the support from the Foundation for the Advancement of Theoretical Physics and Mathematics (BASIS) (Project № 23-2-10-15-1) and the Scholarships of the President of the Russian Federation for postgraduate students.

References

[1] *S. Bartolucci, P.M. Birchall, M. Gimeno-Segovia, E. Johnston, K. Kieling, M. Pant, T. Rudolph, C. Sparrow, and M.D. Vidrighin* , Creation of Entangled Photonic States Using Linear Optics. arXiv:2106.13825, (2021).

Krasnaya Polyana, Sochi, Russia March 1 – March 7, 2026
9th International School on Quantum Technologies

Problems of Experimental Discrete-Continuum Optimization of Quantum Circuits in Josephson Integrated Circuits

Sergey Samarin[1,2], **Mikhail Sergeev**[1], **Aleksei Tolstobrov**[1,2], **Shtefan Sanduleanu**[2,3], **Gleb Fedorov**[2,3], **Oleg Astafiev**[1,2]

[1] *Skolkovo Institute of Science and Technology, Skolkovo, Russia*
[2] *Moscow Institute of Physics and Technology, Dolgoprudny, Russia*
[3] *Kotelnikov Institute of Radioengineering and Electronics of Russian Academy of Sciences, Moscow, Russia*
*E-mail: samarin.ss@phystech.edu

Abstract

Supervised quantum machine learning (QML) is an evolving interdisciplinary field that combines variational quantum algorithms and classical machine learning. Variational quantum circuits (VQCs) are among the most promising approaches in QML. However, selecting an appropriate VQC structure for a specific task remains largely empirical. When executed on noisy intermediate scale quantum (NISQ) devices, additional constraints arise: the circuit depth is limited by decoherence, and the hardware connectivity restricts the set of qubit pairs available for two-qubit gates [1]. Evolutionary optimization methods, such as genetic algorithms (GA), can mitigate these limitations by efficiently searching for near optimal circuits within the constrained solution space. In this work, a genetic algorithm is applied to state preparation task as well as to binary and multilabel classification tasks.

Algorithm description

Overview of the genetic algorithm approach in the state vector $|\psi_{\text{target}}\rangle$ preparation task [2]. (i) Create initial population $\{P_i\}$ of individuals, where each is a quantum circuit that generates the population states $|\psi(\vec{\theta})_{P_i}\rangle$, with the appropriate number of qubits and number of genes for the given state vector. (ii) Assess the fitness of the state vectors determined by each individual in the population:

$$f\left(|\psi(\vec{\theta})_{P_i}\rangle\right) = \left|\left\langle \psi_{\text{target}} \middle| \psi(\vec{\theta})_{P_i} \right\rangle\right|^2. \tag{1}$$

(iii) Apply crossover to the population, producing new circuits. (iv) Mutate the entire population with some probability p. (v) Run classical optimisation on each mutated individual to obtain the optimal $\vec{\theta}$ values between 0 and 2π, to achieve the highest fitness for their generated circuit. (vi) Apply roulette wheel selection to the population, to select the individuals for the next generation based on their assessed fitness. (vii) Repeat until the desired fitness is achieved or *maxiter* iterations since the last increase in fitness was achieved. (viii) If *maxiter* iterations since the last increase in fitness, increase the number of genes by 1 and return to (i). Such approach is applicable in other tasks with different measurement protocols and cost functions f. Gene space is constructed from hardware design constraints and sequences

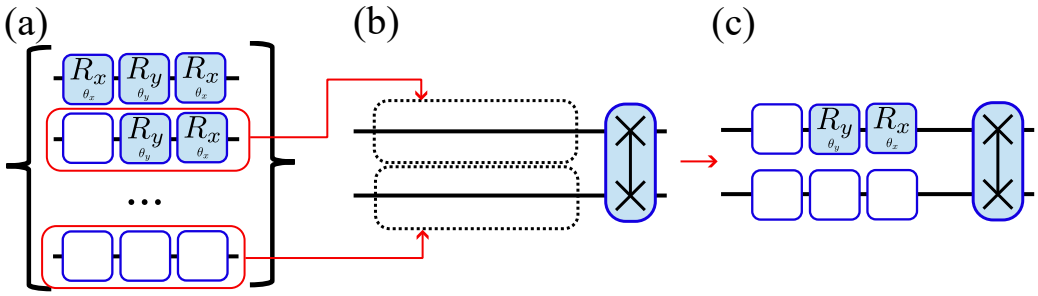

Figure 1: A single gene assembly procedure. (a) Gate sequences space. (b) A single gene template. (c) An example of a single gene.

of defined gates (see Fig. 1). We use maximum length 3 sequences of parametrized R_x and R_y rotations attached to two qubits, entangling through an iSWAP gate.

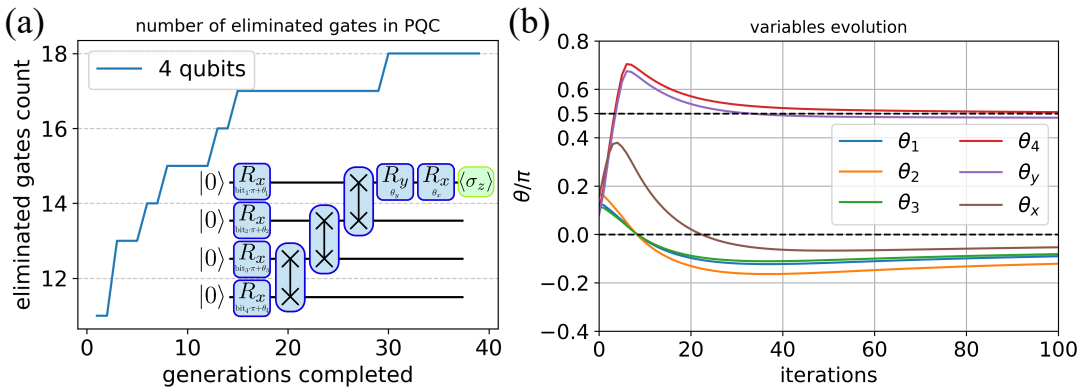

Figure 2: Binary string parity determination task solved using GA with iSWAPs . (a) Illustrates, how unnecessary gates were eliminated during GA. (b) Unnecessary parameters were eliminated as well.

Discussion

The analytical solution for **binary string parity determination** task using CNOT gates was already known. With GA the analytical solution was found using iSWAPs (see Fig. 2 (a) inset). It had been shown that it requires the same amount of two-qubit gates (even noisy ones). An added regularization coefficient allows us to get rid of unnecessary one-qubit rotations and to find a compact solution with only two additional $\pi/2$ rotations for an arbitrary length of a bitstring (Fig. 2 demonstrates the 4-qubits case). The solution remains viable in case of non-ideal gates.

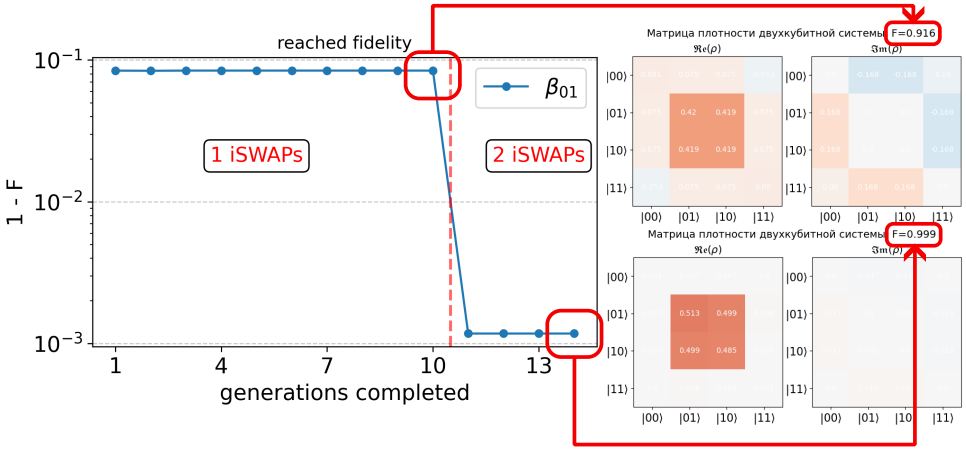

Figure 3: Bell's state preparation task in the presence of noise solved using GA.

GA also provides analytical solution for the **Bell's state preparation** task with only one iSWAP. However, in the presence of noise in the system one iSWAP is not sufficient to reach $F = 1$ due to entanglement power loss of non-ideal two-qubit gate. We demonstrated that two iSWAPs is sufficient to conquer this problem (see Fig. 3).

References

[1] *A. Tolstobrov, G. Fedorov, S. Sanduleanu, S. Kadyrmetov, A. Vasenin, A. Bolgar, D. Kalacheva, V. Lubsanov, A. Dorogov, J. Zotova, P. Shlykov, A. Dmitriev, K. Tikhonov, and O.V. Astafiev*, Hybrid quantum learning with data reuploading on a small-scale superconducting quantum simulator. Phys. Rev. A **109**, 012411 (2024).

[2] *F.M. Creevey, C.D. Hill, and L.C.L. Hollenberg*, GASP: a genetic algorithm for state preparation on quantum computers. Sci. Rep. **13**, 11956 (2023).

Expressivity study of quantum-inspired and classical analog neural network layers

Artem Popov[1*], **Stanislav Straupe**[2,1], **Mikhail Saygin**[2,1]

[1] *Faculty of Physics, M.V. Lomonosov Moscow State University, 1 Leninskie Gory, Moscow 119991, Russia*
[2] *Sber Quantum Technology Center, Kutuzovski prospect 32, Moscow, 121170, Russia*
*E-mail: popov.aa22@physics.msu.ru

Abstract

This work studies parameter-efficient replacements for dense neural network layers to reduce the computational burden of overparameterized models while maintaining expressivity. We evaluate quantum-inspired tensor layers and propose a new layer suited to classical analog photonic hardware, benchmarking both in MNIST classification and transformer fine-tuning. Results suggest analog photonic implementations may be more practical than digital simulation of quantum-inspired layers, while realization on quantum hardware appears even more challenging.

Over the past decade, advances in neural networks (NNs) have opened new avenues for addressing practical problems that were previously considered intractable. At the same time, deploying increasingly large NNs demands a commensurate increase in computational resources. This has motivated efforts to improve the efficiency of classical digital hardware and to explore alternative computing paradigms, including classical analog computing [1, 2] and quantum computing[3]. In typical NNs, the dominant computational cost is associated with linear algebra, most notably matrix–matrix multiplications. Importantly, many NNs are substantially overparameterized[4]: in many settings, multiplication by an N×M matrix with N*M trainable parameters can be replaced by multiplication by an N×M matrix whose entries are determined by a much smaller set of trainable parameters. Such parameterizations can reduce computational cost in both training and inference if implemented on the right hardware.
Therefore, lowering this cost is to simplify network layers by replacing traditional fully connected dense layers with parameter-efficient alternatives – linear layers in which the weight matrix depends on the trainable parameters through structured, typically nonlinear, mappings. The objective is to minimize the number of trainable (programmable) parameters without substantially sacrificing expressivity, i.e., the richness of the family of input–output transformations the layer can realize when embedded in an NN. Recently, quantum-inspired approaches have been proposed to construct parameter-efficient replacements of this kind [5, 6].
In this work, we investigate quantum-inspired tensor layers, which have been proposed as parameter-efficient substitutes for dense layers and as multiplicative adapters for neural network fine-tuning. In addition to these established constructions, we introduce a further parameter-efficient layer that can be implemented naturally in classical analog hardware, such as multimode programmable photonic interferometers. We assess the expressive capacity of these layers in both small models and larger transformer architectures. Concretely, we train a two-layer network for MNIST classification and fine-tune a pre-trained transformer. Our findings suggest that implementing certain parameter-efficient components directly on classical analog photonic platforms may be more practical than simulating quantum-inspired tensor layers on digital electronic hardware, while realizing the corresponding layers on quantum hardware is likely even more challenging.

References

[1] *Le Gallo, M., Khaddam-Aljameh, R., Stanisavljevic, M. et al*, A 64-core mixed-signal in-memory compute chip based on phase-change memory for deep neural network inference. Nat Electron 6, 680–693 (2023)

[2] *De Marinis, M. Cococcioni, P. Castoldi and N. Andriolli*, Photonic Neural Networks: A Survey. IEEE Access, vol. 7, pp. 175827-175841, 2019,

[3] *El Amine Cherrat, Iordanis Kerenidis, Natansh Mathur, Jonas Landman, Martin Strahm, and Yun Yvonna Li*, Quantum Vision Transformers. Quantum 8, 1265 (2024).

[4] *Florent Draye, Anson Lei, Ingmar Posner, Bernhard Schölkopf*, Sparse Attention Post-Training for Mechanistic Interpretability. arXiv:2512.05865

[5] Zhuo Chen, Rumen Dangovski, Owen Dugan, Charlotte Loh, Di Luo, Marin Soljačić, QuanTA: Efficient High-Rank Fine-Tuning of LLMs with Quantum-Informed Tensor Adaptation. Advances in Neural Information Processing Systems 37 (2024)

[6] Maolin Wang, Yu Pan, Zenglin Xu, Guangxi Li, Xiangli Yang, Danilo Mandic, Andrzej Cichocki, Tensor Networks Meet Neural Networks: A Survey and Future Perspectives. arXiv:2302.09019

Krasnaya Polyana, Sochi, Russia March 1 – March 7, 2026
9th International School on Quantum Technologies

Unitary t-design with an optimal number of parameters on a linear-optical platform

Robert Grinshtein[1*], **Ivan Dyakonov**[1,2], **Oksana Borzenkova**[1,2], **Stanislav Straupe**[1,2] **and Sergei Kulik**[1]

[1] *Quantum Technology Centre and Faculty of Physics, M.V. Lomonosov Moscow State University, Leninskie Gory Street 1, Moscow 119991, Russian Federation*
[2] *Russian Quantum Center, Bolshoy bul'var 30 building 1, Moscow 121205, Russian Federation*
*E-mail: grinshtein.ra21@physics.msu.ru

Abstract

Programmable interferometers are a key tool for realizing arbitrary unitary matrices on a linear-optical platform, a promising physical realization of quantum computing [1]. Constructing arbitrary Haar unitary matrices requires $\mathcal{O}(N^2)$ programmable phase shifters, which is a computationally and experimentally challenging task. However, many applications only require reproducing the first few moments of the Haar measure, leading to the use of unitary t-designs. In this work, we present a compact interferometer scheme that efficiently generates a 1-design using only $\mathcal{O}(N)$ parameters, and propose a general method for constructing t-designs of higher orders.

Problem description

Many quantum optical tasks, such as boson sampling, rely on implementing a unitary transformation U sampled from the Haar measure. While universal interferometers achieve this using $\mathcal{O}(N^2)$ parameters [2, 3], the computational necessity of strict Haar randomness is often questioned.

It is hypothesized that unitaries forming a t-design—which reproduce only the first t moments of the Haar measure—might suffice. Although t-designs can mimic the statistics, the critical challenge is proving that the resulting sampling problem remains computationally hard.

Motivated by the complexity of universal architectures, we propose a compact interferometer ansatz. Our goal is to generate random unitaries from a simpler, parameter-efficient class of matrices that effectively mimics the Haar measure by forming an efficient t-design. This approach is crucial for advancing both complex sampling problems and parameter-efficient variational algorithms.

Method

A unitary t-design [4] can be defined as a set of unitary matrices $S \subseteq U(d)$, such that for any polynomial $f_{t,t}(U)$ of matrix elements with homogeneous degree t in the entries of U and degree t in the entries of $U^\dagger$:

$$\frac{1}{|S|}\sum_{V\in S} f_{t,t}(V) = \int_{U(d)} f_{t,t}(U)\, d\mu_H(U) \tag{1}$$

where $\mu_H(U)$ is the Haar measure. Since finding an exact t-design is a complex problem, we use the frame potential metric for a uniform distribution ν over the set S:

$$F_\nu^{(t)} = \frac{1}{|S|^2}\sum_{U,V\in S} |\mathrm{Tr}\ (U^\dagger V)|^{2t} \tag{2}$$

where the Haar measure satisfies $F_{\mu_H}^{(t)} = t!$ for $t \leq d$. If equality holds between $F_\nu^{(t)}$ and $F_{\mu_H}^{(t)}$, the set S forms a t-design. The ε-approximate t-design can be characterized by the frame metric loss (FML) function

$$\left(F_\nu^{(t)} - F_{\mu_H}^{(t)}\right)^2 := \mathrm{FML}(t) \tag{3}$$

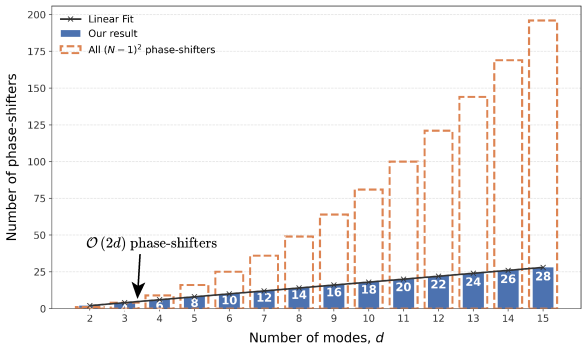

(a) Comparison of the number of parameters required for a 1-design (using our method) versus the $(d-1)^2$ phase shifters in a universal interferometer computed for up to $d = 15$ modes.

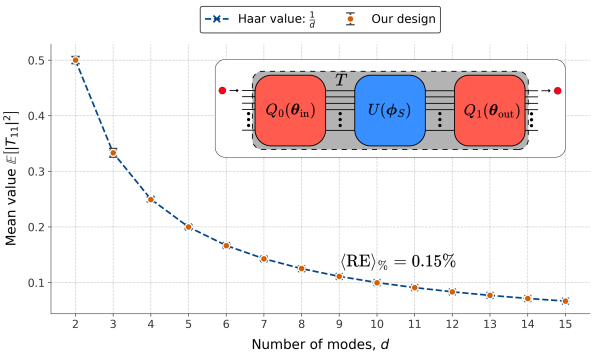

(b) Validation results of mean values averaged over 1000 different polynomials of matrix elements. The circuit T used for construction is shown in the inset.

which is bounded by ε.

We employ the Robust architecture [5] for building the set S, iteratively adding trainable layers of phase shifters until the FML(t) converges.

We implemented a verification procedure as shown in Fig. 1b, using the 1-design as an example. For input state $|\psi_{\text{in}}\rangle = |1\rangle \otimes |0\rangle^{\otimes(d-1)}$, we apply the unitary transformation

$$T(\boldsymbol{\theta}_{\text{in}}, \boldsymbol{\phi}_S, \boldsymbol{\theta}_{\text{out}}) = Q_0(\boldsymbol{\theta}_{\text{in}}) \cdot U(\boldsymbol{\phi}_S) \cdot Q_1(\boldsymbol{\theta}_{\text{out}}) \tag{4}$$

This comprises the preparation block $Q_0(\boldsymbol{\theta}_{\text{in}})$ and measurement block $Q_1(\boldsymbol{\theta}_{\text{out}})$ ansatzes, as well as our optimized Robust scheme $U(\boldsymbol{\phi}_S)$, which builds matrices from set S. The probability of measuring the input state at the output is given by $f_{1,1}(U) = |T_{1,1}|^2$, which is the polynomial of matrix elements of U that we averaged.

Results

Our results, presented in Fig. 1a, show that we need only $\mathcal{O}(2d)$ parameters to reproduce the first moment of the Haar measure with a mean relative error of 0.15% (see Fig. 1b). Additionally, we apply this optimization framework to constructing 2-designs. Preliminary investigations indicate that our robust architecture successfully converges for higher moments, offering a generalizable method for efficient t-design construction beyond the first order.

References

[1] *Jeremy L. O'Brien.* "Optical Quantum Computing", Science 318.5856 (2007)

[2] *M. Reck, A.Zeilinger et al.* Experimental realization of any discrete unitary operator. Phys. Rev. Lett. 73, 58 (1994)

[3] *William R. Clements et al.* "Optimal design for universal multiport interferometers," Optica 3, 1460-1465 (2016)

[4] *Mele A. A.* Introduction to Haar measure tools in quantum information: A beginner's tutorial, Quantum 8, c. 1340 (2024)

[5] *Saygin, M. Y., Kondratyev, I. V., Dyakonov, I. V., Mironov, S. A., Straupe, S. S., Kulik, S. P.* Robust architecture for programmable universal unitaries. Physical review letters, 124(1) (2020)

Erasure Error Detection and Correction in Neutral Atom Quantum Computer Architectures

Alexander Skokov[1*], **Stanislav Straupe**[3,2,1]

[1] *Faculty of Physics, M.V. Lomonosov Moscow State University, 1 Leninskie Gory, Moscow 119991, Russia*
[2] *Russian Quantum Center, Bolshoy bul'var 30 building 1, Moscow, 121205, Russia*
[3] *Sber Quantum Technology Center, Kutuzovski prospect 32, Moscow, 121170, Russia*
*E-mail: alexandre.skokov@gmail.com

Abstract

This work investigates approaches to handling erasure errors in neutral atom quantum architectures. Using numerical simulations, we study small quantum codes, erasure-detection protocols, and post-selection strategies under realistic noise models. The analysis highlights key limitations of minimal codes and outlines directions for developing more effective erasure-aware error mitigation schemes.

Neutral atom quantum computing platforms are a promising approach to scalable quantum information processing due to their long coherence times and flexible qubit connectivity.[1] At the same time, these systems exhibit characteristic error mechanisms that differ from those typically assumed in standard quantum error correction models. In particular, atom loss and leakage from the computational subspace give rise to erasure-type errors, where the affected qubit may be removed from the register or become inaccessible during computation.

Erasure errors play a central role in neutral atom architectures due to finite atom lifetimes, imperfect trapping, and loss processes during gate operations and measurements. While a variety of methods for mitigating such errors have been proposed, this work focuses on a specific class of erasure-aware strategies compatible with near-term neutral atom hardware. These strategies exploit partial information about loss events, when available, and are designed to operate under realistic experimental constraints.

In this work, we investigate an erasure-aware approach based on small quantum codes and low-overhead detection protocols tailored to neutral atom systems. In particular, we investigate an erasure-aware approach based on the [[4,2,2]] quantum error-detecting code and low-overhead detection protocols tailored to neutral atom systems.[2] We model the [[4,2,2]] code in conjunction with a Gottesman-type erasure detection scheme, with the goal of understanding how such a minimal code could be used for post-selection or error correction in realistic experimental settings.[3] Using numerical simulations with noise models relevant for neutral atom architectures, we analyze the behavior of this approach in the presence of both erasure events and additional operational errors. In parallel, research is ongoing on exploring dynamical quantum codes adapted to neutral atom architectures, which could provide additional flexibility in handling erasure events.[4]

Preliminary observations suggest a nontrivial trade-off between the potential benefits of erasure-aware encoding and the overhead introduced by additional operations and measurements. While partial erasure information can be leveraged in certain regimes, the associated overhead may limit the net performance gain for minimal-size codes. This ongoing study aims to clarify the conditions under which such erasure-aware schemes can provide a practical advantage and to guide the design of more effective protocols.

References

[1] M. Saffman, "Quantum computing with neutral atoms," *Quantum Information Processing* **10**, 221–260 (2011).

[2] A. Smith, B. Johnson, and C. Lee, "Logical Error Rates for a [[4,2,2]]-encoded Variational Quantum Eigensolver Ansatz," *Quantum* **5**, 123 (2021).

[3] D. Gottesman, *Stabilizer Codes and Quantum Error Correction*, PhD thesis, California Institute of Technology, 1997.

[4] E. X. Fu and D. Gottesman, "Error Correction in Dynamical Codes," QuICS, University of Maryland, College Park, MD 20742, USA; Computer Science Department, University of Maryland, College Park, MD 20742, USA, 2023.

Спектроскопия октупольного перехода в ионе Yb171+

Юрий Аносов[1*], **Александр Борисенко**[1], **Илья Заливако**[1], **Илья Семериков**[1], **Ксения Хабарова**[1], **Николай Колачевский**[1] [8pt]
[1] *ФИАН, Москва, Росссия*
*E-mail: uriy.anosov@yandex.ru

Аннотация

В данной работе представлена схема эксперимента по спектроскопии октупольного перехода в ионе Yb171+ для задач квантовой логики и метрологии.

Ионы иттербия в ловушке Пауля - одна из популярных платформ для квантовых вычислений. Манипуляция октупольным переходом (см Рис. 1) между уровнями $^2S_{1/2}(F=0) \longleftrightarrow ^2F_{7/2}(F=3)$ позволит использовать сверхтонкую систему уровня $^2F_{7/2}(F=3)$ как для кодирования информации, так и для считывания кубита, закодированного в сверхтонких подуровнях основного состояния $^2S_{1/2}$ при помощи техники шелвинга [1]. В данной работе представлена схема эксперимента по спектроскопии октупольного перехода, а также его предварительные результаты. Особенное внимание уделено схеме стабилизации частоты лазерного источника относительно фемтосекундной гребенки частот. Спектр и стабильность центральной частоты лазера на длине волны 467 нм имеют ключевое значение для данного эксперимента, так как естественная ширина перехода составляет всего 8 мГц [2].

Данная работа была поддержана госкорпорацией «Росатом» в рамках Дорожной карты по квантовым вычислениям (Договоры № 868-1.3-15/15-2021 от «5» октября 2021 года и № 868/1653-Д от «21» августа 2025 года.)

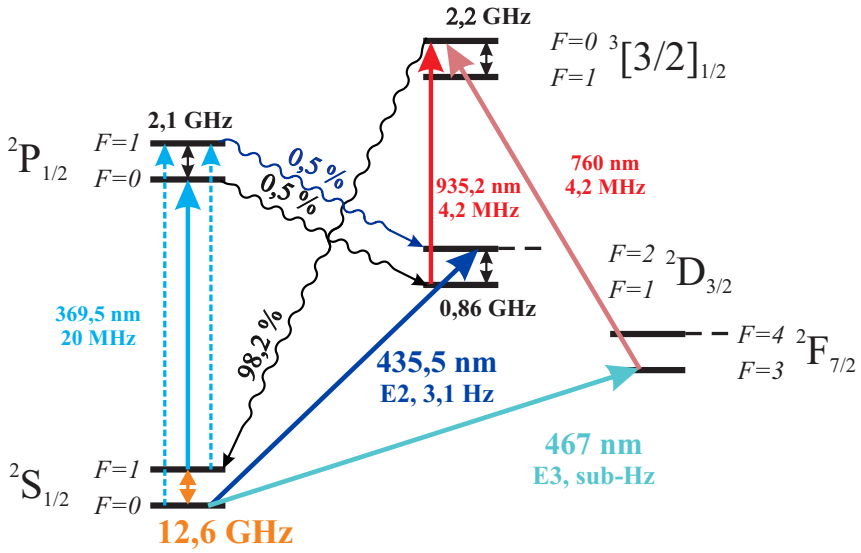

Рис. 1: Схема уровней Yb171+

Список литературы

[1] *Leibfried, Dietrich, et al.* Quantum dynamics of single trapped ions. Reviews of Modern Physics 75.1 (2003): 281.

[2] *Hosaka, K., et al.* Frequency measurement of the S 2 1/2-F 2 7/2 electric octupole transition in a single Y 171 b+ ion. Physical Review A—Atomic, Molecular, and Optical Physics 79.3 (2009): 033403.

Exploring the potential of D-Wave Advantage 2™ Quantum Annealer for Particle Tracking

Martin Bureš[1]

[1] *Joint Institute for Nuclear Research, 141980 Dubna, Moscow region, Russia*
*E-mail: bures@physics.muni.cz

Abstract

Reconstruction of charged-particle trajectories in modern high-energy physics experiments is a computationally demanding combinatorial optimization problem, exacerbated by the extremely high interaction rates expected in the high-luminosity era. In this work we investigate the suitability of quantum annealing for particle tracking by formulating the tracking task as a quadratic unconstrained binary optimization (QUBO) problem and studying its embedding and solution on the D-Wave Advantage2™ quantum annealer with the Zephyr qubit topology. We analyze how the increased qubit connectivity and reduced embedding overhead affect the scalability and performance of QUBO-based tracking models, in particular those based on triplets of detector hits. Our study indicates that the new topology enables more compact embeddings and opens a realistic path toward solving larger tracking instances on quantum hardware.

1 Introduction

One of the key stages in processing data obtained in particle physics experiments is the reconstruction of the trajectories (tracks) of charged particles based on discrete detector measurements (hits). As charged particles traverse tracking detectors, they leave signals whose association into tracks must be inferred from noisy and incomplete data. The extremely high frequency of interactions in modern and future accelerators poses a major challenge for classical data processing, motivating the exploration of new computational paradigms, including quantum algorithms.

Particle tracking can be naturally cast as a global optimization problem, where physically consistent track candidates are rewarded and unphysical combinations are penalized. Early approaches employed Hopfield neural networks to minimize carefully designed energy functions favoring smooth, non-bifurcating trajectories. More recently, this idea has been formalized in terms of quadratic unconstrained binary optimization (QUBO), enabling direct application of both classical and quantum annealing methods [1].

2 Particle Tracking as a QUBO Problem

In the QUBO formulation, binary variables represent elementary track constituents, such as doublets or triplets of detector hits. The objective function to be minimized takes the form

$$\min_{\mathbf{x}\in 0,1^n} ; \mathbf{x}^{\mathrm{T}} Q \mathbf{x} + \mathbf{h}^{\mathrm{T}} \mathbf{x}, \tag{1}$$

where the matrix Q encodes pairwise compatibilities or conflicts between candidates and $\mathbf{h}$ represents individual quality terms. Constraints, such as preventing hit reuse or track bifurcations, are incorporated as penalty terms.

A particularly effective model represents track candidates as triplets of hits. Compatible triplets that can form a valid quadruplet are assigned attractive couplings, while conflicting triplets are penalized. This formulation is computationally equivalent to an Ising Hamiltonian and is therefore directly amenable to quantum annealing.

3 Quantum Annealing and D-Wave Systems

Quantum annealing is a heuristic optimization technique in which quantum fluctuations are used to explore the low-energy landscape of an Ising model. D-Wave quantum processing units (QPUs) are

Figure 1: Schematic illustration three D-Wave topologies: Chimera, Pegasus, and Zephyr. In th Zephyr topology, each qubit is connected to up to 20 neighbors, enabling denser logical graph embeddings with shorter chains compared to earlier Chimera and Pegasus architectures [2].

designed to sample low-energy spin configurations by slowly transforming an initial Hamiltonian into one encoding the problem of interest. Unlike gate-based quantum computers, quantum annealers already provide thousands of physical qubits and can address certain real-world optimization tasks.

A practical limitation is the restricted qubit connectivity of the hardware, which necessitates *minor embedding* of the logical QUBO graph into the physical QPU topology. Embedding overhead, in the form of qubit chains, can significantly limit the effective problem size and solution quality.

4 Advantage2 and the Zephyr Topology

The recently introduced D-Wave Advantage2™ system represents a major step forward, featuring more than 4400 qubits and over 40,000 couplers arranged in the Zephyr topology. Each qubit is connected to up to 20 neighbors, compared to 15 in the previous Pegasus architecture. This increased connectivity allows for more compact embeddings with shorter chains, directly addressing one of the main bottlenecks in QUBO-based particle tracking.

From a practical perspective, the key question is how well the geometry of the tracking problem matches the Zephyr topology, and how much speedup or scalability improvement can be achieved for realistic detector layouts. More compact embeddings reduce chain-breaking errors and improve the probability of finding high-quality solutions, thereby increasing the effective size of solvable tracking instances.

5 Outlook and Conclusions

Our goal is to quantify how the new Zephyr topology accelerates the solution of the particle tracking problem on quantum annealing hardware. Preliminary studies on earlier D-Wave systems showed no clear advantage over optimized classical solvers, largely due to embedding overhead and problem decomposition [3]. Advantage2 mitigates several of these issues by enabling denser logical graphs to be embedded directly on the QPU.

Further progress will require algorithmic refinements, including improved pre-filtering of hit combinations, optimized triplet-based models, and better use of physical information such as the magnetic field. Together, these developments suggest that quantum annealing, combined with the enhanced connectivity of Zephyr, may become a viable component of real-time, low-power tracking solutions in future high-energy physics experiments.

References

[1] Bureš, M., Kadochnikov, I., Kovalenko, A. & Ososkov, G. Application of the Hopfield Network to SPD Track Reconstruction. *Communication Of The Joint Institute For Nuclear Research.* (2024), P11-2024-5

[2] Jaumà, G., García-Ripoll, J. & Pino, M. Exploring Quantum Annealing Architectures: A Spin Glass Perspective. *Advanced Quantum Technologies.* **7** (2024,3), http://dx.doi.org/10.1002/qute.202300245

[3] L. Linder, *Using a Quantum Annealer for Particle Tracking at LHC*, PhD thesis (2019).

Krasnaya Polyana, Sochi, Russia March 1 – March 7, 2026
9th International School on Quantum Technologies

Native entanglement of qubits embedded in multilevel carriers in a trapped ion quantum processor

Pavel Kamenskikh[1*], **Nikita Semenin**[1], **Ilia Zalivako**[1], **Ilia Semerikov**[1,2], **Nikolay Kolachevsky**[1,2]

[1] *Lebedev Physical Institute, Russian Academy of Sciences, Moscow, Russia*
[2] *Russian Quantum Center, Moscow, Russia*
*E-mail: kamenskikh.pa@lebedev.ru

Аннотация

Multi-level carriers (qudits) offer an efficient route to scaling quantum computers by encoding multiple qubits within a single ion. We identified the limitations of standard qubit-based Mølmer –Sørensen(MS) gates, which require multiple two-particle operations to realize embedded XX and ZZ interactions. To overcome this overhead, we introduced a generalized qudit MS gate that simultaneously couples multiple pairs of levels. We showed that this qudit MS gate enables the implementation of embedded two-qubit interactions using a single two-particle operation, reducing the required gate count by a factor of four compared to standard approach. Furthermore, we demonstrated that this gate can be efficiently applied to QAOA, where it allows for a compact realization of the Ising ansatz. These results establish the qudit MS gate as a powerful building block for scalable quantum computation with embedded qubits.

In this work, we focus on the implementation of two-qubit interactions of the type XX (or ZZ) between embedded qubits. We refer to this operation as *embedded* XX gate, which can be expressed as

$$\mathsf{XX}^{\mathsf{q}_{im}\mathsf{q}_{jn}}(\chi) = \exp(\imath\chi X^{\mathsf{q}_{im}} X^{\mathsf{q}_{jn}}), \tag{1}$$

where q_{im} denotes the m^{th} qubit embedded in the i^{th} ququart Q_i, and a Pauli operator $X^{\mathsf{q}_{im}}$ acts only on that qubit. For more details about embedding of qubits into qudits see Ref. [1]. The embedded ZZ operator has the same form, with the Z-pauli matrix replacing X.

Two types of two-qubit gates arise between embedded qubits. The first couples qubits q_{i1} and q_{i2} within a single ququart Q_i; the interaction is confined to a single ion and can be transpiled into single-qudit rotations [1]. The second type entangles qubits embedded in different ququarts Q_1 and Q_2, requiring two-particle interactions. In this work, we focus on the Mølmer–Sørensen (MS) gate [2], whose operator is defined as:

$$\mathsf{XX}^{ij|kl}(\chi) := \exp\big(\imath\chi X^{ij} \otimes X^{kl}\big), \tag{2}$$

where $X^{ij} = |i\rangle\langle j| + |j\rangle\langle i|$. It can be shown that implementing the embedded XX gate requires at least four two-particle gates:

$$\mathsf{XX}^{\mathsf{q}_{11}\mathsf{q}_{21}}(\chi) = \mathsf{XX}^{02|02}(\chi)\mathsf{XX}^{13|13}(\chi)\mathsf{XX}^{13|02}(\chi)\mathsf{XX}^{02|13}(\chi). \tag{3}$$

We propose a qudit version of the MS gate, shown in Fig. 1(a), in which the standard MS interaction is applied simultaneously to multiple level pairs within a qudit. Thus, we refer to this gate as a *qudit* MS gate. While a related concept was introduced in Ref. [3], its application to entangling embedded qubits has not been explored. The resulting evolution operator for a qudit MS gate is given by:

$$\mathsf{XX}_{\theta}^{ij\|kl}(\chi) = \exp\left(\imath\chi\left(X^{ij} + \theta X^{kl}\right)^{\otimes 2}\right), \tag{4}$$

where the MS interaction couples the transitions $|i\rangle \leftrightarrow |j\rangle$ and $|k\rangle \leftrightarrow |l\rangle$. The parameter θ is defined as the factor between Rabi frequencies in different pairs of transitions, i.e. $\Omega^{kl}(t) = \theta\Omega^{ij}(t)$. The qudit MS gate can be implemented using either two bichromatic laser beams or a single laser with four spectral tones. As shown in Fig. 1(b), this gate enables an efficient implementation of the embedded XX gate using a single two-particle operation, in contrast to the four required for the standard MS gate. The qudit MS gate therefore serves as a native operation for embedded qubits.

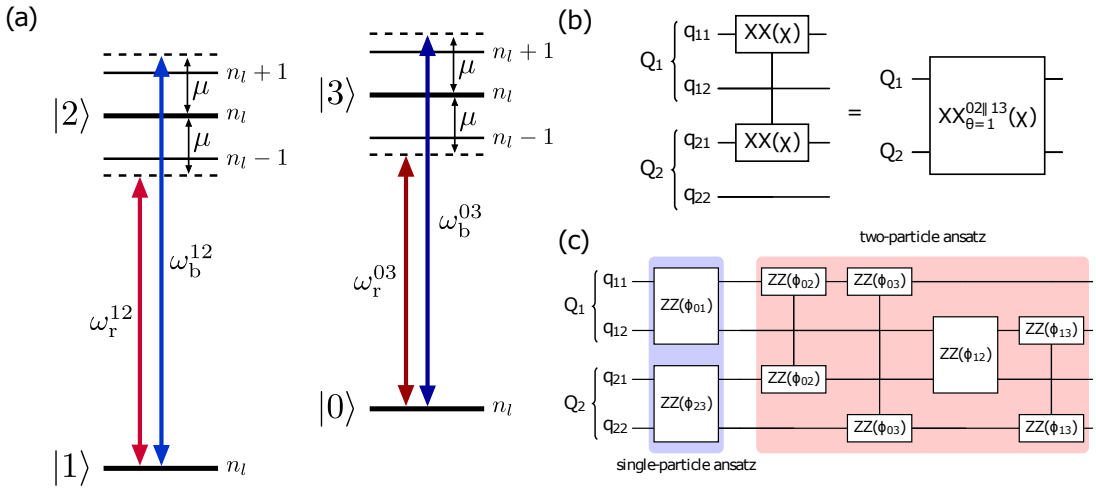

Рис. 1: (a) Schematic representation of the parallel Mølmer–Sørensen gate. Red and blue lines represent the spectral components of the two bichromatic laser beam. (b) Transpilation of the embedded XX gate between qubits q_{11} and q_{21} using qudit MS gate. Realization of the XX gate on other qubit pairs requires also one two-particle operation. (c) Quantum curcuits for an Ising anzatz for 4 qubits

Another important feature of the qudit MS gate is that it can be efficiently employed in the Quantum Approximate Optimization Algorithm (QAOA) [4], which is based on preparing a parametrized ansatz state. A central challenge in constructing this ansatz is implementing the Ising evolution operator:

$$e^{-\imath\gamma\mathcal{H}_C} = e^{\imath\sum_{i<j}\phi_{ij}Z^{q_i}Z^{q_j}} = \prod_{i<j} e^{\imath\phi_{ij}Z^{q_i}Z^{q_j}}. \tag{5}$$

Figure 1(c) illustrates the realization of the Ising ansatz on four qubits using 6 two-qubit gates. When using embedded qubits, the single-particle part of the ansatz requires no two-particle operations. In this work we show the way, how to implement the two-particle ansatz with a single qudit MS gate. By eliminating unnecessary two-particle operations in the single-particle part of the ansatz and compressing the two-particle ansatz into a single qudit MS gate, our approach significantly reduces the number of two-particle gates, thus give an opportunity to make more layers in QAOA.

This research was supported by the Russian Roadmap on Quantum Computing, Contract No. 868/1653-D dated 21 August 2025.

Список литературы

[1] *A.S. Nikolaeva, E.O. Kiktenko, and A.K. Fedorov,*, Universal quantum computing with qubits embedded in trapped-ion qudits. Physical Review A, 109(2), 022615 (2024).

[2] *A. Sørensen,, and K.Mølmer,* Quantum computation with ions in thermal motion. Physical review letters, 82(9), 1971 (1999).

[3] *P. J.Low, B. M. White , A. A. Cox, M. L. Day, and C.Senko,* Practical trapped-ion protocols for universal qudit-based quantum computing. Physical Review Research, 2(3), 033128 (2020).

[4] *E. Farhi, J. Goldstone, S. Gutmann.* A quantum approximate optimization algorithm. arXiv preprint arXiv:1411.4028 (2014).

Adaptive Variational Quantum Algorithm with Error Mitigation on the Example of the F2 Molecule

Artem Maslennikov[1*], **Gleb Struchalin**[2], **Artem Rozanov**[1,3]

[1] *Faculty of Space Research, M.V.Lomonosov Moscow State University, Moscow, Russia*
[2] *Quantum Technology Centre, M.V.Lomonosov Moscow State University, Moscow, Russia*
[3] *P.N. Lebedev Physical Institute, Moscow, Russia*
E-mail: artmasl04@gmail.com

Аннотация

We present Qubit-ADAPT variational quantum eigensolver enhanced with Zero Noise Extrapolation (ZNE) for error mitigation. The algorithm adaptively constructs the quantum circuit by selecting operators with maximal gradients [1], while ZNE suppresses hardware errors through controlled noise scaling and extrapolation [3]. Applied to the F_2 molecule (8 qubits), this approach achieves chemical accuracy (1.6 mHa error) under realistic noise conditions where standard methods fail. The noise model incorporates depolarizing and phase errors with probability $p = 0.06$, derived from experimental data matrices (single-qubit gates and two-qubit gates), and we demonstrate significant error reduction compared to unmitigated calculations, enabling reliable quantum chemistry simulations on near-term hardware.

Methodology

Qubit-ADAPT is an adaptive variational quantum algorithm that dynamically builds an efficient quantum circuit ansatz for molecular simulations. Unlike fixed-ansatz approaches, it selects Pauli operators based on gradient magnitudes, adding only those that significantly impact the energy. At each iteration, the algorithm:

1. Computes energy gradients for all operators in the pool
2. Selects the operator with the largest gradient magnitude
3. Adds the corresponding unitary rotation to the ansatz
4. Optimizes all parameters using SPSA optimizer [2]

This adaptive strategy minimizes circuit depth while maintaining accuracy. For noise modeling, we used realistic error matrices: single-qubit error matrix and two-qubit CNOT error matrix, which were derived from experimental calibration data with error probability $p = 0.06$. When combined with ZNE error mitigation, the algorithm scales noise levels and extrapolates to the zero-noise limit, effectively suppressing hardware errors.

Таблица 1: F_2 ground state energy calculations (Ha)

	Energy (Ha)	Absolute Error (Ha)
Exact (FCI)	-195.9701972	–
Noiseless	$-195.970197200 \pm 1.1 \cdot 10^{-9}$	$2.3 \cdot 10^{-9}$
Noisy (no mitigation)	-63.4 ± 3.6	132.6
Noisy + ZNE (linear)	-195.97 ± 19.35	0.0015

Figure 1 presents the ZNE extrapolation results for the F_2 molecule, averaged over 10 independent runs. The linear extrapolation of energy values at different noise levels (λ) demonstrates how ZNE effectively recovers the exact energy value from highly distorted noisy measurements. The green line represents the exact FCI energy (-195.970197 Ha), while the red square shows the ZNE-extrapolated energy (-195.96874 Ha), achieving chemical accuracy within 1.5 mHa. The method uncertainty (standard

deviation from 10 runs) is shown as error bars. The results in Table 1 show that without error mitigation, the energy error is catastrophic (132.6047 Ha), while with ZNE, we achieve an error of 1.5 mHa, which is below the chemical accuracy threshold of 1.6 mHa.

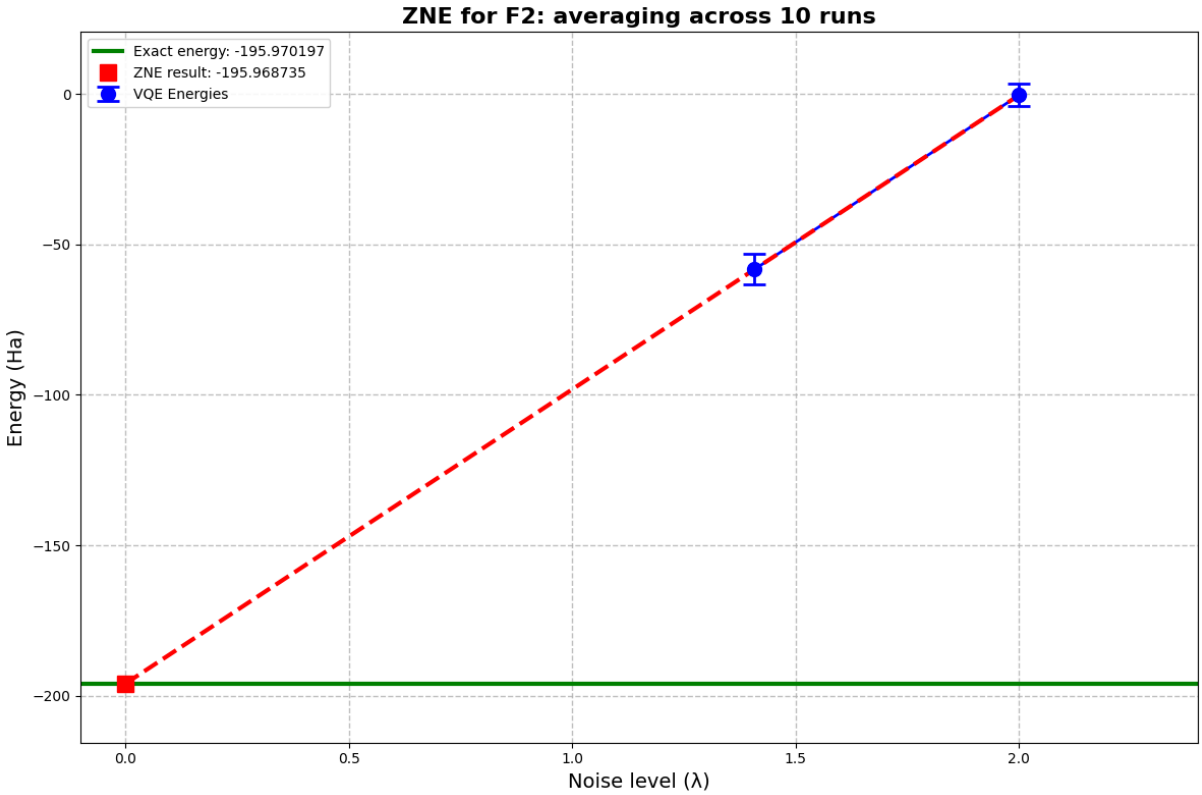

Рис. 1: ZNE results for F_2 molecule averaged over 10 runs. The green line shows the exact energy, the red square shows the ZNE-extrapolated energy, and the blue points show the VQE energies at different noise levels (λ). The dashed line represents the linear extrapolation to zero noise.

Conclusion

The integration of adaptive circuit construction with ZNE error mitigation enables quantum chemistry calculations at chemical accuracy levels on noisy hardware. For the F_2 molecule, the noiseless Qubit-ADAPT achieves near-exact results, while the noisy implementation without mitigation fails catastrophically with an error of 132.6047 Ha. With ZNE mitigation, we recover chemical accuracy (1.5 mHa error) despite realistic noise conditions (error probability $p = 0.06$). This demonstrates a practical pathway for applying quantum computing to complex molecular systems on current NISQ devices. Future work will extend this approach to larger molecules and explore optimization of the operator pool for efficient scaling.

Список литературы

[1] H.L. Tang, V.O. Shkolnikov, G.S. Barron, H.R. Grimsley, N.J. Mayhall, E. Barnes, and S.E. Economou, "qubit-ADAPT-VQE: An adaptive algorithm for constructing hardware-efficient ansätze on a quantum processor," Phys. Rev. Research **2**, 043287 (2020).

[2] J.C. Spall, "Multivariate Stochastic Approximation Using a Simultaneous Perturbation Gradient Approximation," IEEE Trans. Autom. Control **37**, 332 (1992).

[3] K. Temme, S. Bravyi, and J.M. Gambetta, "Error mitigation for short-depth quantum circuits," Phys. Rev. Lett. **119**, 180509 (2017).

Characterization of a Surface-Electrode Paul Trap for Ion-Based Quantum Computing

Alexey Russkikh[1,2] , **Ilya Gerasin**[1,2,3], **Nikita Zhadnov**[1,3], **Ilia Zalivako**[1,3], **Alexander Borisenko**[1,3], **Ilya Semerikov**[1,3], **Nikolay Kolachevsky**[1,3]

[1] *P.N. Lebedev Physical Institute of the Russian Academy of Sciences, Moscow, Russia*
[2] *Moscow Institute of Physics and Technology, Dolgoprudny, Russia*
[3] *Russian Quantum Center, Moscow, Russia*
*E-mail: russkikh.am@phystech.edu

Аннотация

This work focused on developing quantum logic using a chain of ultracold ions confined in a surface-electrode Paul trap. We successfully demonstrated single-ion confinement, performed spectroscopy on the clock transition, and observed coherent Rabi oscillations. Furthermore, we characterized the trap's secular frequencies and measured the magnetic field inside the vacuum chamber.

Trapping ultracold ions in radiofrequency (RF) Paul traps constitutes one of the most promising platforms for building a scalable quantum processor [1]. To scale these systems, the Quantum Charge-Coupled Device (QCCD) architecture is employed. This architecture relies on multiple interconnected traps that enable controlled ion transport. A particularly effective implementation of this approach uses surface-electrode Paul traps, which consist of a planar system of electrodes that generate a confining pseudopotential. This design facilitates the precise shuttling of individual ions and ion chains, their transport between functional zones, and guidance through junctions connecting different traps [2]. At

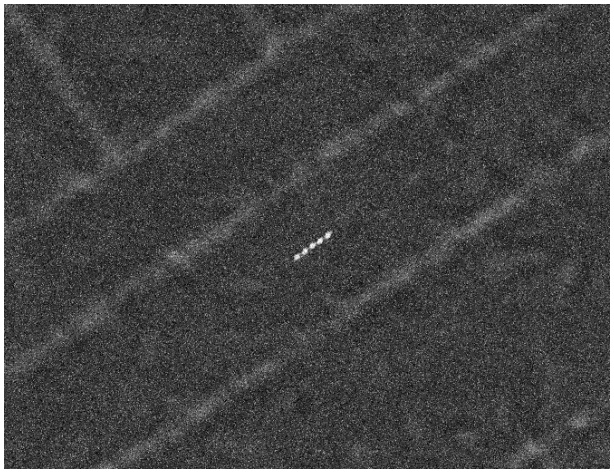

Рис. 1: Caption of ion chain

FIAN, a 70-qubit quantum computer based on $^{171}YB^{+}$ ions in a 3D Paul trap has been demonstrated. To advance scaling further, work is underway to implement quantum logic operations on a planar surface-trap system. This system is designed not only for ion confinement but also for comprehensive trap characterization via optical and microwave spectroscopy. In the present study, we performed spectroscopy on the quadrupole transition $^2S_{1/2}$ $(F = 0)$-$^2D_{3/2}$ $(F = 2)$, which serves as an optical qubit, and characterized its Rabi oscillations. Using the resolved sideband mode, we determined the trap's secular frequencies and extracted the magnetic field inside the vacuum chamber. Furthermore, we optimized the ion readout parameters, including micromotion compensation via minimization of the micromotion sideband.

Future work includes implementing ground state cooling, testing ion shuttling protocols, and performing two-qubit gate operations.

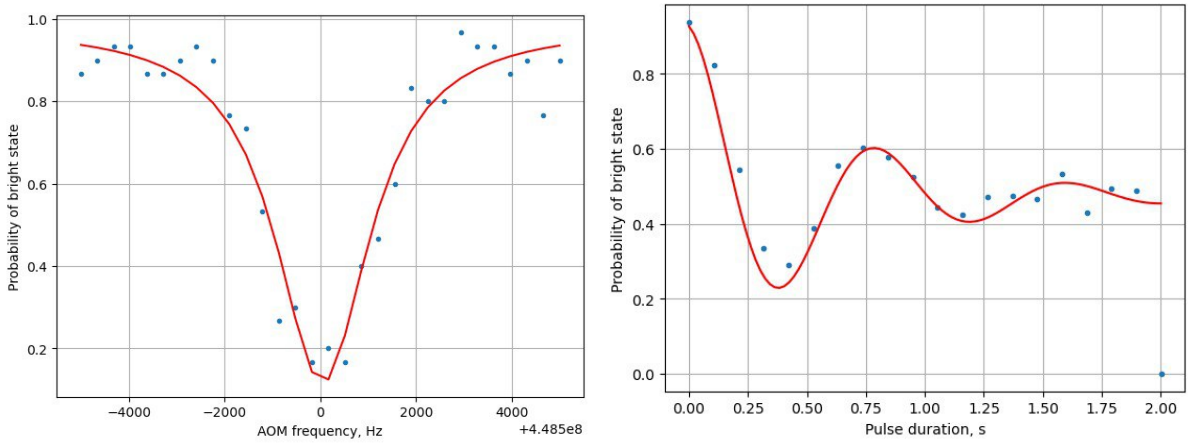

Рис. 2: Clockline and Rabi oscillations of optical qubit

This research was supported by the Russian Roadmap on Quantum Computing, Contract No. 868/1653-D dated 21 August 2025.

Список литературы

[1] *Ransford A. et al.*, Helios: A 98-qubit trapped-ion quantum computer //arXiv preprint arXiv:2511.05465. – 2025.

[2] *Burton W. et al.*, Scalable transport of trapped-ion qubits in a surface-electrode RF Paul trap //SMT 2025. – 2025.

Optomechanical Platform Based on Controllable Spatial Bifurcation for Ising Machine Applications

Elizaveta Soboleva[1*], **Semyon Rudiy**[1], **Andrei Ivanov**[1]

[1] *International Research and Educational Center for Physics of Nanostructures, ITMO University, St. Petersburg, Russia*

*E-mail: eliz.sobol239@gmail.com

Аннотация

The aim of this work is to demonstrate that a levitated optomechanical system based on a hybrid electrodynamic–optical trap for a charged microparticle can serve as a physical platform for an analog Ising machine, by exploiting a controllable pitchfork-type spatial bifurcation to encode binary spin states. We analytically and numerically investigate the dynamics of a silica nanoparticle in a planar hybrid trap with transparent ITO electrodes and a perpendicular Gaussian laser beam. We establish the functional dependence of the bifurcation parameter on laser power, RF voltage, and trap geometry, show that the effective potential matches the Duffing oscillator model, and propose a time-multiplexed hybrid feedback scheme to implement programmable spin–spin couplings for solving combinatorial optimization problems (e.g. MAXCUT). Our results confirm that the system exhibits a laser-controlled transition from a single-well to a double-well potential, enabling robust bistable dynamics suitable for spin encoding ($\sigma = sign(Y)$). Unlike phase-sensitive coherent Ising machines, our platform is stable, compact, and relies only on intensity-based control. This establishes a promising foundation for a scalable, room-temperature analog Ising solver based on levitated optomechanics.

Ising machines offer a promising alternative by mapping the combinatorial optimization problem onto the ground state search of an Ising Hamiltonian [1]. We proposed a novel optomechanical platform for analog computation based on a hybrid trap for charge microparticle[2]. The hybrid trap combines electrodynamic module (transparent planar electrodes [3]) and optical module (a perpendicular Gaussian laser beam), see Fig.1 a. The system demonstrates a controllable pitchfork-type spatial bifurcation: by tuning the laser power, the effective potential transitions from a single-well to a double-well configuration, enabling bistable dynamics (Fig.1 b, c).

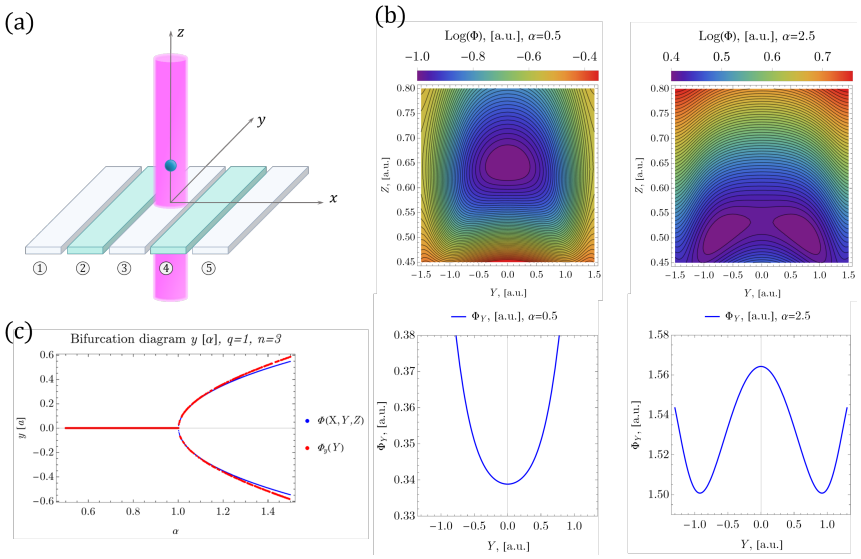

Рис. 1: (a) Scheme of the hybrid trap. (b) Section of the effective potential distribution $\log[\Phi](X, Y, Z)$ at $X = 0$ and the corresponded 1D fitted effective potential $\Phi_y(Y)$ for $n = 3$ and $q = 1$ depending on the α-value. (c) Bifurcation diagram for $Y(\alpha)$. Comparison of 3D and 1D potential.

The particle's dynamics can be described in terms of the effective Duffing-like potential [4]:

$$\Phi_y(Y) \approx Y^2 A(\alpha, q, n) + Y^4 B(\alpha, q, n) + O(Y^6) + const, \tag{1}$$

where α is the bifurcation parameter and proportional to laser power, q depends on AC-voltage amplitude, and n is the electrode geometry factor. At $A > 0$, $B > 0$ — single-well regime; at $A < 0$, $B > 0$ — double-well regime with two stable states $Y = \pm Y_0$.

We adopt a time-multiplexed hybrid architecture Ising machine (inspired by Böhm et al. [5]). A single particle sequentially emulates N spins, then particle's position Y is measured and digitized as $\sigma = \text{sign}(Y)$. Then we compute the feedback signal:

$$f = \beta \sum_j J_j \sigma_j. \tag{2}$$

where $\sigma_n = \pm 1$ denotes the Ising spin variable associated with the n-th node of the graph, J_{mn} is the coupling matrix that encodes the structure of the optimization problem (with $J_{mn} = -1$ for connected nodes in MAXCUT and $J_{mn} = 0$ otherwise), and β is the dimensionless coupling strength that controls the influence of neighboring spins on the dynamics of the n-th spin.

The laser power is modulated to set the next effective $\alpha \propto f$. This loop allows the system to evolve toward the ground state of the target Ising Hamiltonian. This approach offers a stable, phase-insensitive alternative to coherent Ising machines.

This work was supported by the Russian Science Foundation (project 24-79-00225).

Список литературы

[1] *N. Mohseni, P. L. McMahon, and T. Byrnes*, Ising machines as hardware solvers of combinatorial optimization problems. Nat. Rev. Phys. **4**, 363 (2022).

[2] *E.V. Soboleva, S.S. Rudiy, D.P. Shcherbinin, and A.V. Ivanov*, Controllable spatial bifurcation in optomechanical system: Analytical and numerical study. Physica D: Nonlinear Phenomena. **484**, 134982 (2025).

[3] *D. Shcherbinin, V. Rybin, S. Rudyi, A. Dubavik, S. Cherevkov, Y. Rozhdestvensky, and A. Ivanov*, Charged hybrid microstructures in transparent thin-film ITO traps: Localization and optical control. Surfaces. **6**, 133 (2023).

[4] *D. I. Albertsson, A. Rusu*, Ising machine based on bifurcations in a network of duffing oscillators. in: Proceedings of the 2023 IEEE International Symposium on Circuits and Systems (ISCAS). **659**, 1-5 (2023).

[5] *F. Böhm, G. Verschaffelt, and G. Van der Sande*, A poor man's coherent Ising machine based on opto-electronic feedback systems. Nat. Commun. **10**, 3538 (2019).

Numerical analysis for erasure and Pauli error thresholds in different FBQC schemes

Gareeva A. R.[1*], **Dyakonov I. V.**[1,2], **Avanesov A. S.**[3], **Straupe S.S.**[1,2,3]

[1] *Faculty of Physics, Lomonosov Moscow State University, Moscow, Russia*
[2] *Quantum technology centre, Faculty of Physics M.V. Lomonosov Moscow State University, Moscow, Russia*
[3] *Russian Quantum Center, Moscow, Russia*
*E-mail: gareeva.ar22@physics.msu.ru

Abstract

We investigate the fault-tolerant properties of different fusion-based quantum computation (FBQC) models [1], [2], [3] by determining their threshold probabilities for tolerable measurement outcome loss and Pauli errors.

Fusion-based quantum computation (FBQC) includes two main properties: resource states (small entangled states) and fusion measurements (entangling measurements). It also enables efficient quantum error correction protocols [1], [2], [3]: redundancy between the Pauli operators measured during fusion and the stabilizers of the resource states define a non-trivial check operator group for error detection. The fusion network's syndrome graph consists of measurements (represented by the edges) and parity checks (represented by the nodes). When studying its fault-tolerance, we usually consider two types of noise effects: a loss (or erasure of the measurement) and an error (fusion outcome flip).

The percolation theory [4] can be applied to the erasure model: each edge is erased with a probability p and a logical error is introduced when there is a path of erased edges connecting one face of a syndrome graph with another.

In the case of Pauli errors, we also consider a model where each edge suffers from the error with probability p. We compute the syndrome and run a decoder (in our case, it is implemented in PyMatching library). The outcome of the decoder is then compared with the actual error chain and if there is a non trivial logical cycle, the decoding procedure has failed.

The algorithm was used to find threshold values of measurement erasures for three different syndrome graph geometries. These geometries correspond to different schemes of FBQC presented in the literature [2], [3]: the ten-qubit, four-qubit and six-ring models (Fig. 1, a, b, c respectively). The program was written in Python. Percolation thresholds were found by plotting curves for different lattice sizes $L = 12, 16, 20$ (where L is the number of nodes per row) and finding their intersection point. We used at least 10^4 samples. Results of simulations are presented in Fig. 2, Fig. 3 and Table 1.

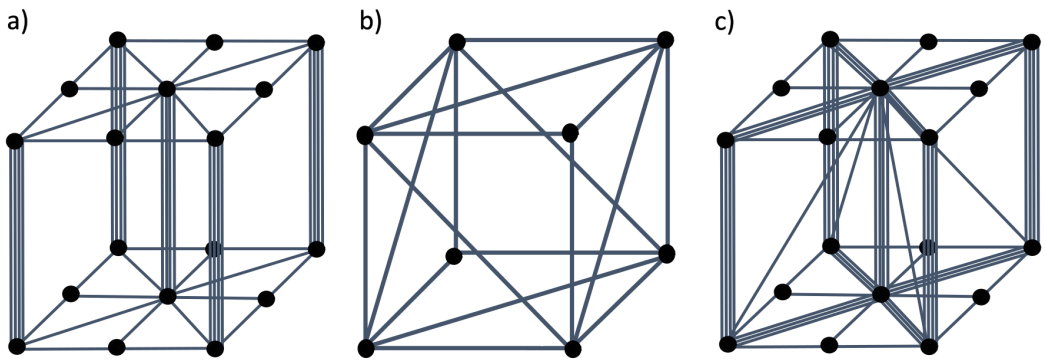

Figure 1: Different geometries of syndrome graphs: a) ten-qubit model, b) six-ring model, c) four-qubit model

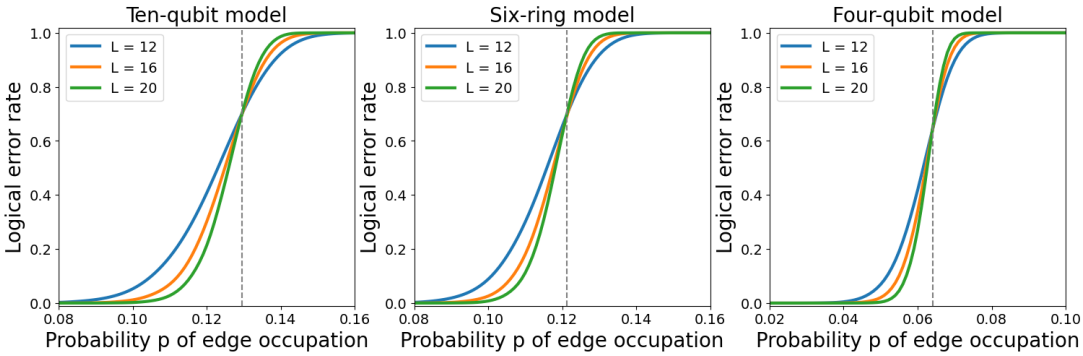

Figure 2: Simulation results for erasures

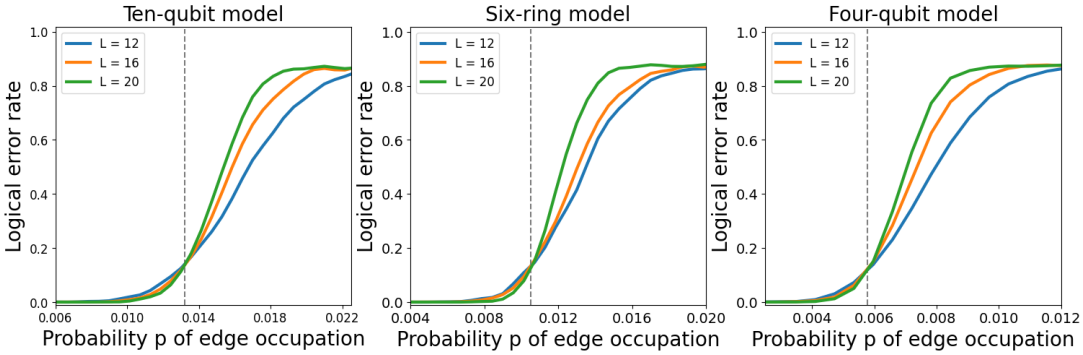

Figure 3: Simulation results for Pauli errors

Table 1: Computational results (standard deviations are presented in brackets).

model	erasure probability	error probability
ten-qubit	0.1295 (0.0001)	0.0133 (0.0002)
six-ring	0.1212 (0.0003)	0.0106 (0.0002)
four-qubit	0.06400 (0.00003)	0.0058 (0.0002)

References

[1] *S. Bartolucci, P. Birchall, H. Bombín et al.*, Fusion-based quantum computation. Nat. Commun. **14**, 912 (2023).

[2] *A. Avanesov, A. Shurinov, I. Dyakonov and S. Straupe*, Building a fusion-based quantum computer using teleported gates. Quantum **9**, 1762 (2025).

[3] *H. Bombin, I. H. Kim, D. Litinski, N. Nickerson et al.*, Interleaving: Modular architectures for fault-tolerant photonic quantum computing. Preprint. *https://arxiv.org/abs/2103.08612* (2021).

[4] *M. E. J. Newman and R. M. Ziff*, Fast Monte Carlo Algorithm for Site or Bond Percolation. Phys. Rev. E **64**, 016706 (2001).

A Comparative Study of the Quantum Autoencoder Model

Sofya Manko

InfoTeCS Scientific Research and Advanced Developments Centre, Moscow, Russia
Skolkovo Institute of Science and Technology, Moscow, Russia
E-mail: Sofia.Manko@infotecs.ru

Abstract

This work presents a comparative analysis of the Quantum Autoencoder (QAE), a hybrid quantum-classical model adapted from classical deep learning. As quantum machine learning gains prominence as a near-term application of quantum computing across a wide range of tasks, we investigate the potential of QAE to deliver practical advantages. The study aims to benchmark the performance of a quantum autoencoder against its classical counterpart, exploring hypothesized benefits such as parameter efficiency, superior data compression, and improved convergence. Our results contribute to understanding both the practical viability and the current limitations of quantum autoencoder models on near-term hardware.

In the current landscape where modern quantum processors are noisy and limited in scale (NISQ devices), Variational Quantum Algorithms (VQAs) are emerging as a primary practical tool. Their architecture, which combines shallow parameterized quantum circuits with classical optimization, affords them inherent noise resilience [1]. Precisely because of this, VQAs are viewed as a strategy capable of delivering practical utility long before the advent of fully fault-tolerant (error-corrected) quantum computers, whose reliability requirements are orders of magnitude beyond current technological capabilities [2].

One of the most significant and rapidly developing applications of VQAs is quantum machine learning. Currently, this field is primarily developing through the direct transfer of various ideas from the more established and somewhat mature field of classical machine learning, with the hope of discovering an advantage in the quantum versions of the corresponding models (such as better convergence, fewer trainable parameters, etc.). In this work, we have chosen to investigate the capabilities of one such model – the Quantum Autoencoder (QAE) [3, 4].

The autoencoder addresses two key interrelated problems, based on a single core mechanism: it learns to reconstruct "normal" data with minimal loss but cannot correctly reproduce data that falls outside this learned distribution. One of the most important applications of these models, particularly relevant for information security, is anomaly detection [5, 6]. Since the model is not adept at effectively encoding and reconstructing unusual patterns absent from the training data, it yields a high reconstruction error when processing them. This anomalously high error serves as the signal for identifying failures, intrusions, or defects. Another significant application is noise removal (denoising). In this task, the model learns to recover "clean" data from its noisy versions [6]. Crucially, an autoencoder is trained not to memorize specific instances but to capture their underlying structure and patterns. Therefore, when presented with a noisy image or signal, it seeks to "project" it onto the space of correct ("clean") data and, as an output, reproduces a cleaned version, filtering out random noise and distortions in the process.

Potential advantages of quantum autoencoders over classical ones may include reduced trainable parameter count, more efficient data compression, efficient handling of quantum data, faster training convergence, and effectiveness with limited datasets. The aim of this study is to empirically explore the potential of a quantum autoencoder model against its classical counterpart across several different tasks, assessing its performance and practical viability in the NISQ era.

References

[1] *K. Sharma, S. Khatri, M. Cerezo, and P. J. Coles*, Noise resilience of variational quantum compiling. New J. Phys. **22**, 043006 (2020).

[2] *M. Cerezo et al.*, Variational quantum algorithms. Nat. Rev. Phys. **3**, 625 (2021).

[3] *J. Sharma, J. Olson, and A. Aspuru-Guzik*, Quantum autoencoders for efficient compression of quantum data. Quantum Sci. Technol. **2**, 045001 (2017).

[4] *C. Bravo-Prieto*, Quantum autoencoders with enhanced data encoding. Mach. Learn.: Sci. Technol. **2**, 035028 (2021).

[5] *R. Frehner, and K. Stockinger*, Applying quantum autoencoders for time series anomaly detection. Quantum Mach. Intell. **7**, 1 (2025).

[6] *J. Wu et al.*, Quantum circuit autoencoder. Phys. Rev. A **109**, 032623 (2024).

Hybrid Tensor Network Error Mitigation via Adaptive Circuit Contraction

Daniil S. Bagaev[1,4*], **Nadezhda V. Khrapai**[2,4], **Aleksey K. Fedorov**[3,4], **Evgeniy O. Kiktenko**[3,4,5]

[1] *Faculty of Physics, Lomonosov Moscow State University, Moscow, Russia*
[2] *Moscow Institute of Physics and Technology, Moscow, Russia*
[3] *National University of Science and Technology MISIS, Moscow, Russia*
[4] *Russian Quantum Center, Skolkovo, Russia*
[5] *Steklov Mathematical Institute, Moscow, Russia*
*E-mail: d.bagaev@rqc.ru

Abstract

Reliable estimation of expectation values on noisy quantum processors is a key prerequisite for practically useful quantum computations. We propose a hybrid tensor-network workflow for mitigating errors in Pauli-string observables that adaptively combines classical contraction with hardware execution. Whenever the circuit is classically contractable under a prescribed tensor-network budget, the observable is evaluated exactly without running on a quantum device. Otherwise, only the non-contractable residual fragment is executed, and the resulting measurement data are post-processed with scalable tensor-network error mitigation to reduce noise-induced bias.

Near-term quantum devices operate in the noisy intermediate-scale regime, where imperfections in state preparation, control, and readout lead to biased estimates of expectation values. Quantum error mitigation (QEM) addresses this issue without the full overhead of fault-tolerant error correction and is therefore a practical ingredient for near-term experiments [1]. At the same time, many mitigation approaches face a scalability bottleneck as circuit size increases.

We propose a hybrid workflow that combines classical tensor-network processing with quantum-hardware execution in a resource-aware manner. The method aims to reduce the reliance on hardware whenever parts of the target computation can be handled classically within a prescribed budget, while still enabling the evaluation of circuits that exceed classical capabilities. A schematic overview of the overall pipeline is shown in Fig. 1.

At a high level, the approach uses a tensor-network representation of the ideal circuit to perform as much classical processing as possible under a user-defined resource constraint. When the circuit is amenable to classical treatment, the desired observable can be evaluated without hardware runs. In more demanding cases, the procedure delegates only the remaining portion to the quantum processor and combines the resulting measurement data with classical tensor-network objects in a post-processing stage.

Finally, to further suppress noise-induced bias, we apply a scalable tensor-network-based mitigation procedure [2]. This yields improved expectation-value estimates while keeping additional quantum resources modest, and naturally interpolates between fully classical evaluation and hardware-assisted execution depending on the available classical budget and circuit structure.

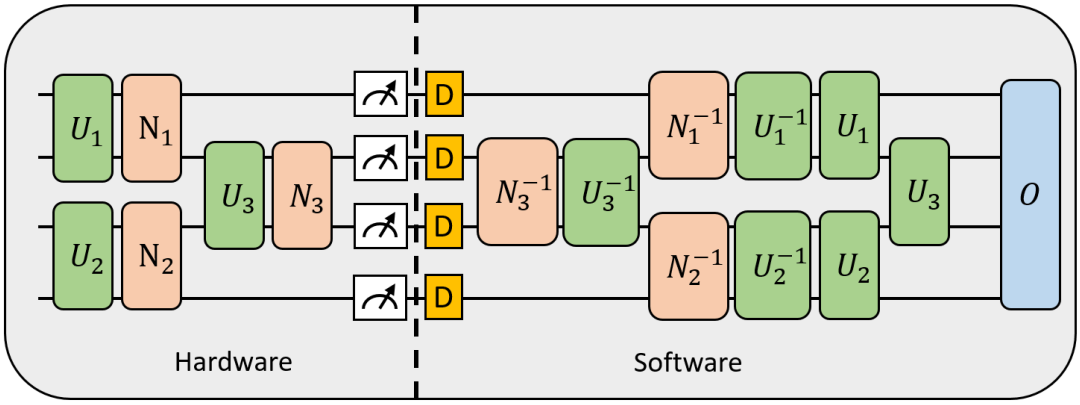

Figure 1: Pipeline for circuits with interleaved ideal layers U_k and noise maps $\mathcal{N}_k$ executed on hardware, followed by a software post-processing stage that applies an approximate inverse-noise model and ideal inverse layers to obtain a mitigated estimate of the target observable O.

Acknowledgements

The work was supported by Rosatom in the framework of the Roadmap for Quantum computing (Contract №868/2059-D dated 24.12.2025).

References

[1] *Z. Cai, R. Babbush, S. C. Benjamin, S. Endo, W. J. Huggins, Y. Li, J. R. McClean, and T. E. O'Brien*, Quantum error mitigation. Rev. Mod. Phys. **95**(4), 045005 (2023). doi:10.1103/RevModPhys.95.045005.

[2] *S. Filippov, M. Leahy, M. A. C. Rossi, and G. García-Pérez*, Scalable tensor-network error mitigation for near-term quantum computing. arXiv:2307.11740 (2023).

Krasnaya Polyana, Sochi, Russia March 1 – March 7, 2026
9th International School on Quantum Technologies

Boosting linear-optical type-I fusion gates with single photons

Aleksandr Melkozerov[1,2*], **Stanislav Straupe**[1,2], **Mikhail Saygin**[2]

[1] *Russian Quantum Center, Moscow, Russia*
[2] *Faculty of Physics, M. V. Lomonosov Moscow State University, Moscow, Russia*
*E-mail: melkozerov.alex@gmail.com

Abstract

Linear-optical approaches to fault-tolerant quantum computing rely on the creation of constant-sized entangled resource states and performing probabilistic entangling fusion measurements on subsets of their qubits. Fusion gates, which play a key role in such approaches, achieve a maximum success probability of 50% using only linear optical elements. Here we demonstrate how to achieve a success probability 75% for Type-I fusion gates using single-photon ancillary states. We study the performance of the scheme and show how it's incorporation significantly reduces resource requirements for photonic entanglement creation methods.

Introduction

Entangling operations are probabilistic at the qubit level in linear-optical platform. Modern linear-optical quantum algorithms, such as fusion based quantum computing [1], suppose implementing probabilistic entangling measurements, called fusions, on small, constant-sized entangled resource states.

Type-I fusion gates apply an entangling measurement on two photonic qubits, destroying one of the initial qubits. Without additional photonic resources, the success probability of fusing two maximally entangled qubit states is limited by 50%. It has been recently shown that the success probability of type-I fusion gates can be boosted to 75% using an entangled ancillary state similar to the photonic Bell state in a dual-rail encoding [2]. The creation of such states, however, is a highly nontrivial probabilistic task in linear optics, requiring a minimum of 4 single photons [3] in schemes with low success probabilities.

Here present a scheme that reaches a success probability of 75% for type-I fusion gates requiring only $50:50$ beam splitters, PNRDs, and four ancillary unentangled single photons.

Creation of entangled states

Large entangled photonic can be created by fusing smaller states together. Type-I fusion gate allows to efficiently create larger entangled states from smaller ones since it measures only one qubit during it's action. However, modern approaches for linear-optical quantum computing require fusion success probabilities above 50% threshold [1, 4], which was known to be achievable only using entangled ancillary states [2]. Here we show the way to boost the success probability of type-I fusion gates using only single photons.

The proposed gates can also be implemented in multiplexing schemes for near-deterministic creation of large entangled states. We show that this technique allows to significantly reduce the resource requirements for such schemes. Thus, for example, notable scheme for near-deterministic generation of 5-qubit GHZ state from 2-qubit resource states requires approximately 768 single qubits using standard type-I fusions, and only 517 single qubits using the proposed boosted gates.

References

[1] *Sara Bartolucci, Patrick Birchall, Hector Bombín, Hugo Cable, Chris Dawson, Mercedes Gimeno-Segovia, Eric Johnston, Konrad Kieling, Naomi Nickerson, Mihir Pant, Fernando Pastawski, Terry Rudolph, and Chris Sparrow*, Fusion-based quantum computation. Nature Communications, 14(1) (2023)

[2] *Sara Bartolucci, Patrick M. Birchall, Mercedes Gimeno-Segovia, Eric Johnston, Konrad Kieling, Mihir Pant, Terry Rudolph, Jake Smith, Chris Sparrow, and Mihai D. Vidrighin*, Creation of Entangled Photonic States Using Linear Optics. arXiv:2106.13825 (2021)

[3] *Stasja Stanisic, Noah Linden, Ashley Montanaro, and Peter S. Turner*, Generating entanglement with linear optics. Physical Review A, 96(4) (2017)

[4] *Mercedes Gimeno-Segovia, Pete Shadbolt, Dan E. Browne, and Terry Rudolph*, From Three-Photon Greenberger-Horne-Zeilinger States to Ballistic Universal Quantum Computation. Physical Review Letters, 115(2) (2015)

Reflectors on directional couplers for weakly guiding waveguides fabricated by femtosecond laser writing

Nikita Kostyuchenko[1*], Sergey Zhuravitskii[1], Nikolay Skryabin[2], Michael Saygin[1,3], Ivan Dyakonov[1,2], Alexander Kalinkin[1], Alexander Korneev[1], Stanislav Straupe[1,2], Sergey Kulik[1,3]

[1] *Quantum Technology Centre and Faculty of Physics, M. V. Lomonosov Moscow State University, Moscow 119991, Russia*
[2] *Russian Quantum Center, 30 Bolshoy bul'var building 1, Moscow 121205, Russia*
[3] *Laboratory of Quantum Engineering of Light, South Ural State University (SUSU), 76 Prospekt Lenina, Chelyabinsk 454080, Russia*
*E-mail: kostiuchenko.ns20@physics.msu.ru

Abstract

A compact 180° turn design for waveguides fabricated by femtosecond laser writing was proposed and experimentally characterized. The design employs a pair of coupled waveguides terminated by a mirrored facet to overcome the large bending radii imposed by the low refractive index contrast. The measured loss was around 1 dB. Potential applications of this design include forming 180° turns in multi-channel integrated optical circuits and constructing ring resonator devices.

The scalability of integrated quantum photonic circuits is limited by optical routing challenges. While low-refractive-index-contrast platforms enable multi-channel interferometers, their large waveguide bend radii (tens of millimeters) hinder miniaturization [1, 2]. Alternative approaches using total internal reflection (TIR) suffer from fabrication-sensitive mode-matching losses [3], incompatible with quantum applications where loss directly impacts state fidelity.

We propose a robust 180° turn architecture combining a directional coupler with a mirrored facet. Light couples adiabatically between waveguides via evanescent fields before reflection, inherently tolerant to fabrication variations. The design is fabricated in fused silica using femtosecond laser writing [4], with the mirror formed by angled cleavage and metal coating.

The fabrication process involves pre-calibration of the directional couplers and careful selection of the waveguide writing mode to achieve optimal performance. Detailed characterization of the mode allows for the expected values of the turn in the reflectors to be obtained before deposition of the end faces.

Initial experimental characterization demonstrates < 1 dB loss per turn ($\approx 79\%$ efficiency), already surpassing typical TIR-based designs while occupying significantly less space than conventional bends. Theoretical analysis suggests further optimization could reduce losses through coupler length tuning and improved mirror reflectivity.

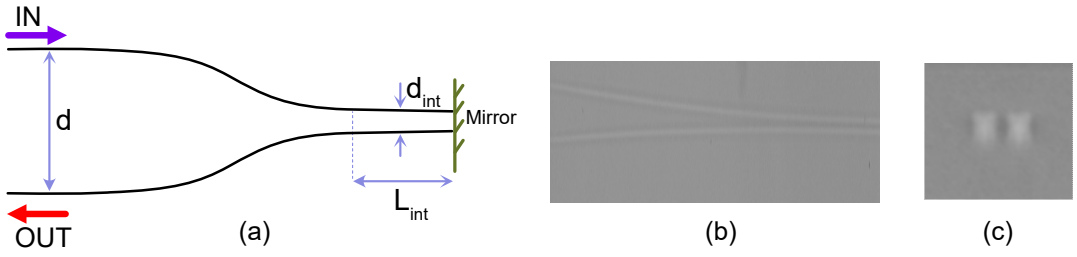

Figure 1: (a) Schematic diagram of the reflector; morphology of the modifications on the top (b) and the side end (c)

The proposed design is applicable not only to multichannel interferometers but also to the creation of ring resonators. To fabricate such structures, deposits can be created on both sides of the sample, thereby creating a closed loop for light transmission.

In this study, we investigated a fundamentally new solution for optical waveguide 180° turns based on a directional coupler and a mirrored facet. The key advantage of our design is minimal optical loss during the turn, which is crucial for building scalable quantum photonic devices.

The work was supported by Rosatom in the framework of the Roadmap for Quantum computing (Contract № 868/1759-D dated 3 October 2025 and Contract № 11-2025/1 dated 14 November 2025).

References

[1] *G. Corrielli, A. Crespi, and R. Osellame*, Femtosecond laser micromachining for integrated quantum photonics. Nanophotonics **10**, 3789 (2021)

[2] *T. Lee et al.*, Low bend loss femtosecond laser written waveguides exploiting integrated microcrack. Sci. Rep. **11**, 23770 (2021)

[3] *J. Lv et al.*, Transmission performance of 90°-bend optical waveguides fabricated in fused silica by femtosecond laser inscription. Opt. Lett. **42**, 3470 (2017)

[4] *N. N. Skryabin et al.*, Femtosecond-laser-written low-loss multiscan waveguides in fused silica. Phys. Rev. Appl. **22**, 064079 (2024)

Decoherence in Single-photon Emission of Resonantly Pumped Telecom C-Band InAs/InGaAs Quantum Dots

Alexey Veretennikov*, **Yuriy Serov, Aidar Galimov, Maxim Rakhlin, Tatiana Shubina, Alexey Toropov**

Ioffe Institute, St. Petersburg 194021, Russian Federation
*E-mail: veretennikov.a@mail.ioffe.ru

Abstract

This work is devoted to the study of dephasing mechanisms in a state-of-the-art single photon source designed for the telecom C-band. Quantum interferometric measurements of single-photon indistinguishability at various temperatures revealed the influence of phonons on dephasing processes. Analysis of experimentally observed Rabi oscillations allowed us to obtain microscopic coupling parameters and their variation with temperature and power for describing the processes.

Epitaxially grown quantum dots (QDs) are one of the most promising platforms for fabricating deterministic single-photon sources (SPSs), offering short radiative lifetimes and high internal quantum efficiency. SPSs for the telecom C-band (1.55 μm) are of particular interest due to the minimal optical losses in silica optical fibers, which can be used for both far-distance communications and within optical computers. Along with emission efficiency and single-photon purity, a key parameter of SPSs designed for linear optical quantum computing and certain quantum communication algorithms is the indistinguishability of emitted photon wave packets. The indistinguishability is necessary to ensure two-photon interference effects, but is often insufficiently high. Therefore, it is necessary to investigate the mechanisms responsible for reducing these parameters in state-of-the-art QD-microcavity systems for the C-band.

In this work, we present a systematic study of dephasing mechanisms in a telecom C-band SPS based on InAs/InGaAs QDs grown above an $In_xGa_{1-x}As$/GaAs metamorphic buffer layer (MBL) with graded composition profiles [1, 2] located inside a 3λ-cavity in a composite semiconductor-dielectric cylindrical microresonator. The source demonstrates high single-photon purity with a second-order correlation function $g^{(2)}(0)$=0.019, high single-photon counting rate of 4.2 MHz, and photons indistinguishability reaching 35% at 8.3 K. These parameters correspond to the highest world level for C-band photon sources.

Quantum interference measurements allowed us to determine the pure dephasing time T_2^*, which is known to play a significant role in controlling the coherence dynamics in QDs (a typical histogram is shown in Fig. 1a). Temperature-dependent coincidence measurements near zero delay show a decrease in T_2^* from 790 ps at 8.3 K to 245 ps at 18 K (Fig. 1b presents the corresponding dephasing rate), indicating an enhanced influence of phonons on decoherence with increasing temperature. In contrast, no significant dependence of T_2^* on the time delay between interfering photons was observed. This highlights a minor role of spectral diffusion in decoherence; otherwise, the phase difference of sequentially emitted single photons should rise with increasing delay.

Measurements of the power dependence of single-photon emission intensity upon resonant excitation of QDs allowed us to directly observe Rabi oscillations, a typical pattern of which is shown in Fig. 1c. A strong decay of the overall decoherence rate with increasing excitation power was observed, which may also be due to the influence of phonons. To model the Rabi oscillations, we numerically solved the optical Bloch equations, assuming a power dependence of the pure dephasing rate. Furthermore, we took into account possible multiphoton generation at even-π-area excitation pulses, which can also change the shape of the Rabi oscillations.

Simulations and comparative analysis of experimental data allowed us to extract quantitative coupling parameters characterizing dephasing mechanisms. We demonstrated that ensuring decoherence control can lead to a peak excited state population of approximately 75%. Furthermore, our study provides practical guidance for optimizing SPS performance for C-band telecommunications applications.

This work is supported by the State Corporation Rosatom within the Quantum Computing Roadmap (contract No. 868/1734-D dated September 22, 2025).

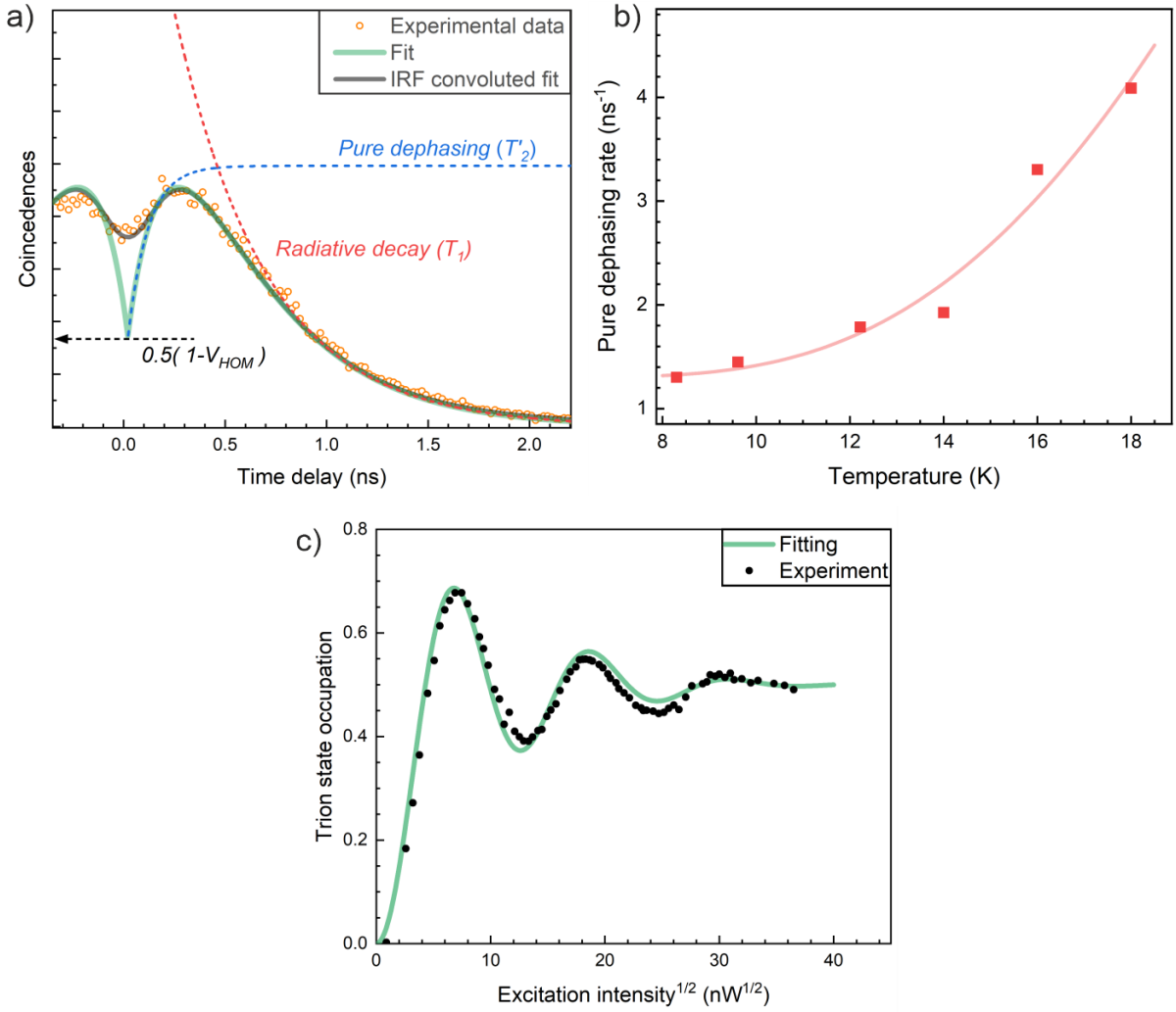

Figure 1: a) Typical coincidence histogram measured using the Hong-Ou-Mandel scheme near zero delay. The red and blue dashed lines show the impact of radiative decay and pure dephasing on histogram, respectively; the green and black lines are fitting. b) Temperature dependence of the pure dephasing rate $1/T_2^*$ (squares) and the Boltzmann fit (solid line). c) Experimentally observed Rabi oscillations (dots) and the numerically obtained fit (solid line).

References

[1] *S.V. Sorokin, G.V. Klimko, I.V. Sedova, A.I. Veretennikov, et al.* Metamorphic InAs/InGaAs Quantum Dot Heterostructures for Single-Photon Generation in the C-Band Spectral Range. JETP Lett. **120**, 694 (2024).

[2] *A.I. Veretennikov, M.V. Rakhlin, Y.M. Serov et al.* Single-Photon Emission in the Telecom C-Band in a Micropillar Cavity with an InAs/InGaAs Quantum Dot. JETP Lett. **121**, 170 (2025).

Programming of integrated optical interferometers with a high level of thermal cross-talk interference

Artem Argenchiev[1*], **Ilya Kondratyev**[1], **Kseniia Urusova**[1], **Nikolay Skryabin**[1,2], **Ivan Dyakonov**[1,2], **Stanislav Straupe**[1,2], **Sergey Kulik**[1,3]

[1] *Lomonosov Moscow State University, Quantum Technology Centre, Moscow, Russia*
[2] *Russian Quantum Center, Moscow, Russia*
[3] *South Ural State University, Chelyabinsk, Russia*
*E-mail: argenchiev.as20@physics.msu.ru

Abstract

In this study, a complete numerical model of a 16-mode interferometer was obtained by calibrating all thermo-optic phase shifters and reconstructing the parameters of all internal elements. Parameter reconstruction was performed via numerical optimization. The optimization was carried out using the PyTorch library with the Adam optimizer. As a result, the algorithm identified 1231 real-valued parameters that fully describe the physical 16-mode interferometer: 120 power reflectivity coefficients, phase shifts, output-loss parameters and crosstalk matrices. The coefficient of determination $R^2 = 0.9966$ indicates a high correlation between the experimentally measured calibration points and those predicted by the numerical model.

A multi-mode optical interferometer is the core operational unit of a boson sampler, where single photons interfere in a non-classical manner and form a complex high-dimensional state. The transformation implemented by an N-mode interferometer is described by an $N \times N$ unitary matrix U, and the probability of a given outcome is computed via the permanent of a submatrix of U. Computing the permanent is a highly demanding task that belongs to the complexity class of #P-complete problems.

In this work, we calibrated a 16-mode interferometer fabricated in fused silica using femtosecond laser writing [1]. The interferometer consisted of eight layers of MZI arranged in a Clements pattern [2] and contained 120 beam splitters and 64 phase shifters (Fig. 1a). The ultimate goal of the calibration is to obtain a complete computer model of the interferometer that enables reconstruction of the transfer matrix of the optical chip for specified values of the control electrical currents.

Continuous coherent laser radiation was used to calibrate the thermo-optic phase shifters. The laser light was sequentially coupled into each input port of the sample. For a selected input port, all thermo-optic phase shifters were calibrated one by one by applying an electrical current over a predefined range from 0 to 15 mA with a step of 0.1 mA. The output light was measured using an array of photodetectors—individually for each output port. In this way, the calibration dataset required to build a complete numerical model of the interferometer was acquired.

Calibration measurements were performed according to a specially developed algorithm consisting of three main stages:

1. Calibration of the primary thermo-optic responses of all 60 main phase shifters.
2. Calibration of the mutual thermo-optic crosstalk between groups of phase shifters that influence each other.
3. Calibration of additional thermo-optic crosstalk effects.

At the first stage, light was injected into every second input port of the interferometer; then all heaters located along the same horizontal line were calibrated. For example, for the 2nd input port, heaters 1, 9, 16, 24, 31, 39, 46, and 54 were calibrated, as shown in Fig. 1a. For each heater, immediately after recording the experimental output-intensity data, the calibration curves were automatically fitted with the dependence:

$$I_{ij}(x) = A + B\cos(a \cdot x^2 + \varphi_0). \tag{1}$$

From this fit, the current values corresponding to phases π and $\pi/2$ were determined. The current corresponding to phase π was then automatically applied to the heater, and the procedure moved on to the next heater in the given horizontal line.

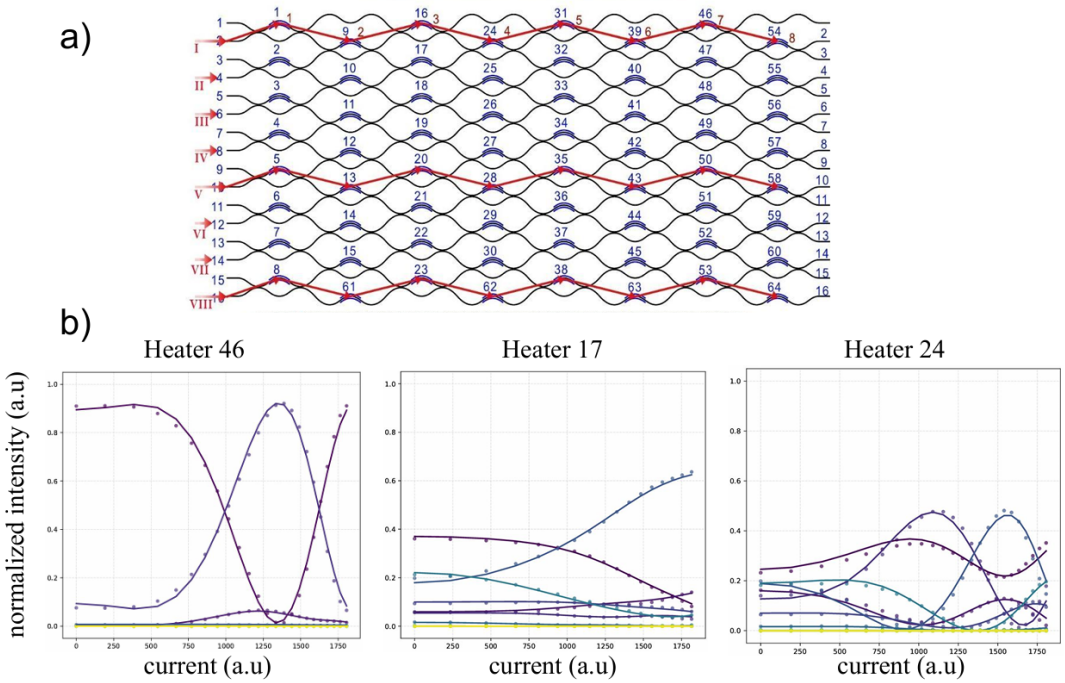

Figure 1: (A) Schematic of the 16-channel integrated optical interferometer and the first calibration stage of the experimental sample. (B) Simultaneous approximation of experimental data with light coupled into the second channel. These results encompass three calibration stages: primary thermo-optic response, mutual thermo-optic crosstalk, and additional crosstalk effects. Measured normalized optical powers at the output ports are depicted as dots, while approximation curves are shown as lines. The coefficient of determination is $R^2 = 0.9966$.

As a result, the optimization using the PyTorch library and the Adam optimizer converged with a coefficient of determination $R^2 = 0.9966$ calculated between the experimental calibration data and the model predictions (Fig. 1b), and 1231 real-valued interferometer physical parameters were reconstructed.

In future work, the fabricated and calibrated 16-mode interferometer will be used in boson-sampling experiments with single photons and superconducting detectors.

The work was supported by Rosatom in the framework of the Roadmap for Quantum computing (Contract № 868/1759-D dated 3 October 2025 and Contract № 11-2025/1 dated 14 November 2025).

References

[1] *N.N. Skryabin et al.*, Femtosecond-laser-written low-loss multiscan waveguides in fused silica. Phys. Rev. Applied. **22**, 064079 (2024).

[2] *William R. Clements et al.*, Optimal design for universal multiport interferometers. Optica **3**, 12 (2016).

Variational preparation of entangled states in a system of transmon qubits

Alexander Yeremeyev[1*], Aleksei Tolstobrov[2,1], Gleb Fedorov[1], Shamil Kadyrmetov[1], Aleksey Bolgar[1], Daria Kalacheva[1], Oleg V. Astafiev[2,1]

[1] *Laboratory of Artificial Quantum Systems, Moscow Institute of Physics and Technology, Dolgoprudny, Russia*
[2] *Center for Engineering Physics, Skolkovo Institute of Science and Technology, Moscow, Russia*
*E-mail: eremeev.am@phystech.edu

Abstract

The conventional method for generating entangled states in qubit systems relies on applying precise two-qubit entangling gates alongside single-qubit rotations. However, achieving high-fidelity entanglement demands high accuracy in two-qubit operations, requiring complex calibration protocols. In this work, a minimally calibrated two-qubit iSwap-like gate, tuned via straightforward parameter optimization (flux pulse amplitude and duration) is used, to prepare Bell states and GHZ state experimentally in systems of two and three transmon qubits. Integration of this gate into a variational quantum algorithm (VQA) bypasses the need for intricate calibration while maintaining high fidelity. The proposed methodology employs variational quantum algorithms (VQAs) to create the target quantum state through imperfect multiqubit operations. Furthermore, a violation of the Clauser–Horne–Shimony–Holt (CHSH) inequality for Bell states is experimentally demonstrated, confirming their high fidelity of preparation.

Introduction

In this work [1], we focus on the experimental variational preparation of two-qubit Bell states and the three-qubit Greenberger–Horne–Zeilinger (GHZ) state [2] using the superconducting quantum computing platform. Typically, Bell states are generated using high-precision two-qubit entangling gates, such as $\sqrt{\text{iSwap}}$ [3, 4] or cPhase [5]. Obviously, the fidelity of the resulting states is highly sensitive to the accuracy of the gates, which in turn demands intricate calibration procedures [6]. To show that this challenge may be addressed, in this work we develop a fully automatic calibration routine based on a gradient-descent VQA that incorporates a quantum circuit comprising minimally calibrated fixed iSwap-like gates [7] and single-qubit X and Y rotations with tunable angles. Our approach introduces an alternative methodology for learning accurate quantum evolution using non-ideal multi-qubit gates, and, simultaneously, exhibits a clear example of a practical application for variational quantum algorithms in realistic experimental settings.

Process of preparation of Bell's states and GHZ state

The experiment was conducted on three transmon qubits [8] (I, II, and III, left to right) as shown in Figure 1a. Figure 1b,c illustrates the quantum circuit designed for preparing the two-qubit Bell states. The circuit comprises 12 parameterized single-qubit rotations, 6 around the X-axis and 6 around the Y-axis of the Bloch sphere, along with two non-ideal iSwap-like entangling operations. Following the state preparation block, the circuit includes a module for quantum state tomography and qubit measurement. The parameters of the quantum circuit are optimized using Nesterov's accelerated gradient descent algorithm [9].

Figure 2 presents the optimization data for one of the Bell states $|\beta_{00}\rangle = (|00\rangle + |11\rangle)/\sqrt{2}$: density matrices of the two-qubit states obtained from quantum state tomography (showing both real and imaginary parts), the dependence of the loss function $\mathcal{L}$ on the algorithm iteration, the evolution of the parameters θ_{1-12} as a function of the algorithm iteration number.

Results

This work demonstrates the application of variational quantum algorithm (VQA) to prepare entangled Bell states and Greenberger–Horne–Zeilinger (GHZ) states. By utilizing a simple variational circuit

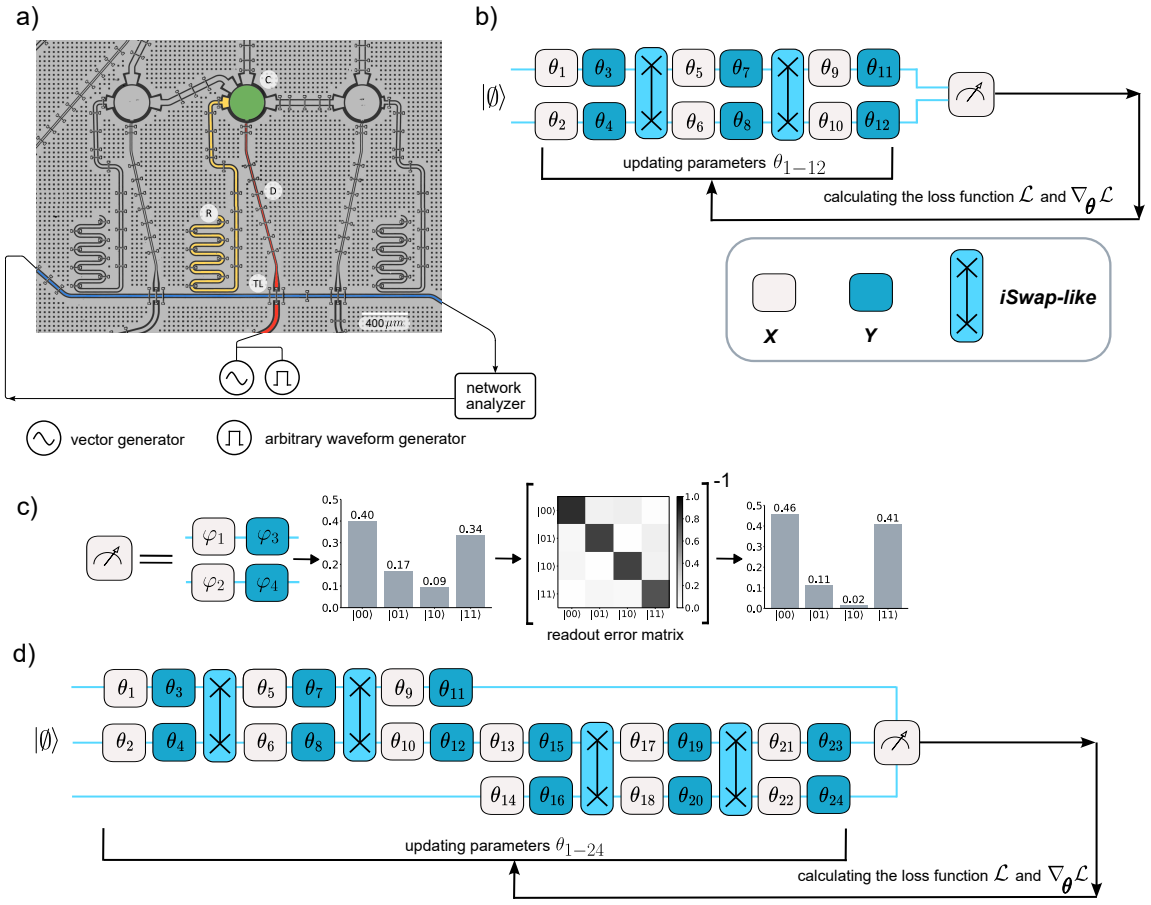

Figure 1: a) Micrograph of the three transmons used in this experiment (false-colored). Green (C) represents the transmon shunt capacitance, yellow (R) denotes the readout resonator, red (D) indicates the drive-bias control line, and blue (TL) corresponds to the transmission readout line. b) The state readout protocol involves three sequential steps: (1) tomography rotations to prepare various measurement bases, (2) statistical averaging through repeated measurements (2000 shots) to determine basis state populations, and (3) application of readout error correction using the inverse error matrix method. c) Quantum circuit for preparing Bell states with two qubits. d) Quantum circuit for preparing GHZ states with three qubits.

incorporating non-ideal iSwap-like gates and single-qubit X and Y rotations, we achieved high-fidelity preparation of these states. The average fidelity of the Bell's prepared states is 0.956 ± 0.007. For the GHZ state, the fidelity is 0.869 ± 0.003. The key advantages of our approach lie in the simplicity of the circuit design with the minimal calibration required for the iSwap-like gates so that an ideal quantum evolution can be reproduced using a variational circuit containing imperfect (non-digital, native) two-qubit gates. We would like to reiterate that this is a proof-of-concept experiment demonstrating the capability of VQAs with parametrization of single-qubit gates, and further work is certainly needed.

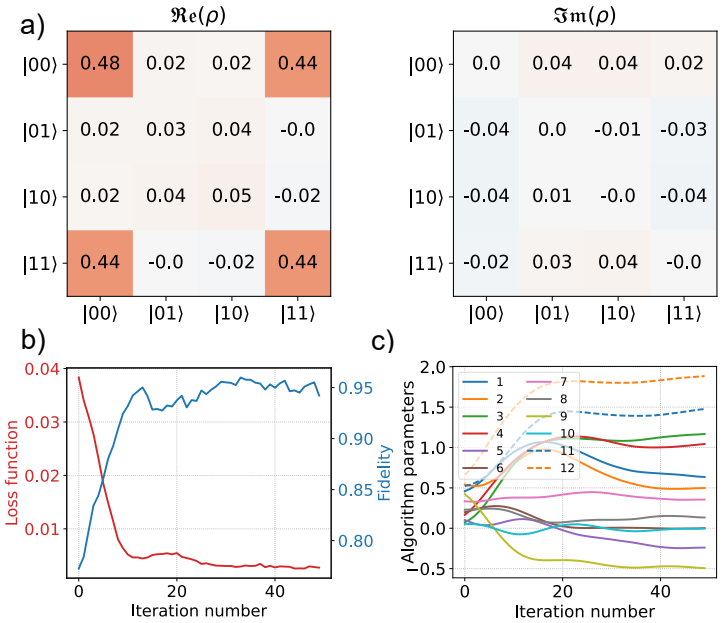

Figure 2: a) For the Bell state $(|00\rangle + |11\rangle)/\sqrt{2}$, the figure presents the experimentally measured density matrix at the last iteration of the algorithm, showing both real and imaginary components. b) The evolution of the loss function $\mathcal{L}$ as a function of algorithm iteration number, demonstrating the convergence behavior. c) The parameters optimization trajectory, showing the dependence of quantum circuit parameters on the algorithm iteration number.

References

[1] *Yeremeyev, A., Tolstobrov, A., Fedorov, G. et al.*, Variational preparation of entangled states in a system of transmon qubits. Advanced Quantum Technologies, e00316. (2025)

[2] *M. A. Nielsen and I. L. Chuang*, Quantum Computation and Quantum Information. 10th Anniversary Edition, Cambridge University Press, Cambridge. (2010)

[3] *Matthias Steffen et al.*, Measurement of the Entanglement of Two Superconducting Qubits via State Tomography.Science 313,1423-142. (2006)

[4] *Ansmann, M., Wang, H., Bialczak, R. et al.*, Violation of Bell's inequality in Josephson phase qubits. Nature 461, 504–506. (2009)

[5] *DiCarlo, L., Chow, J., Gambetta, J. et al.*, Demonstration of two-qubit algorithms with a superconducting quantum processor. Nature 460, 240–244. (2009)

[6] *Arute F. et al.*, Observation of separated dynamics of charge and spin in the Fermi-Hubbard model. arXiv:2010.07965. (2020)

[7] *Foxen B. et al.*, Demonstrating a continuous set of two-qubit gates for near-term quantum algorithms. Physical Review Letters, 125(12), 120504. (2020)

[8] *Koch J. et al.*, Charge-insensitive qubit design derived from the Cooper pair box. Physical Review A—Atomic, Molecular, and Optical Physics, 76(4), 042319. (2007)

[9] *Y. Nesterov*, A method for solving the convex programming problem with convergence rate $\mathcal{O}(1/k^2)$, Proceedings of the USSR Academy of Sciences 269, 543. (1983)

Spectroscopy of a transmon in straddling regimes

Julia Zotova[1*], **Ekaterina Lavrina**[2,1], **Gleb Fedorov**[1], **Oleg Astafiev**[2,1]

[1] *Moscow Institute of Physics and Technology, Institutskiy Pereulok 9, Dolgoprudny 141701, Russia*
[2] *Skolkovo Institute of Science and Technology, 121205 Moscow, Russia*
*E-mail: yuliya.zotova@phystech.edu

Abstract

We investigated the spectral features of a superconducting artificial atom-transmon in the straddling regime, when the frequency of the readout resonator lies between adjacent transition frequencies in the transmon. It was found that the resonator's dispersion shift discontinuously changes sign in the spectral features. These features are caused by the hybridization of the system's high-lying energy levels at given magnetic fluxes.

The system consists of a superconducting artificial atom – a transmon – capacitively coupled to a readout resonator. The transmon frequency can be tuned by an applied external magnetic flux, which changes the Josephson energy in the transmon's SQUID. For a particular value of the external magnetic flux, the readout resonator frequency ω_r lies between the first two transmon transition frequencies: $\omega_{fe} < \omega_r < \omega_{eg}$.

It has been found [1], that in the straddling regime, when $\omega_{fe} = \omega_r$, the system changes the sign of the dispersive shift of the readout resonator. However, there has been no study of the system behavior when the resonator frequency lies between other adjacent transmon levels.

At the same time, spectral features resembling quasi-avoided crossings have been observed [2]. These features could be related to the straddling regime but were observed for different frequency relations.

In this work, we close the gap in understanding the spectroscopic behavior of the system (see Fig. 1) in the straddling regime. We also identify different orders of the straddling regime, each with its own spectroscopic signature, and analyze them numerically.

The authors are grateful to the Russian Science Foundation Project No. 25-72-00088 for financial support. The authors acknowledge Alexei Bolgar, Victor Lubsanov, Daria Kalacheva, and Eugene Korostylev for the sample fabrication.

References

[1] *J. Koch, T. M. Yu, J. Gambetta, A. A. Houck, D. I. Schuster, J. Majer, A. Blais, M. H. Devoret, S. M. Girvin, and R. J. Schoelkopf*, Charge-insensitive qubit design derived from the Cooper pair box, Physical Review A 76, 042319 (2007).

[2] *J. Zotova, S. Sanduleanu, G. Fedorov, R. Wang, J. S. Tsai, and O. Astafiev*, Control and readout of a transmon using a compact superconducting resonator, Applied Physics Letters 124 (2024).

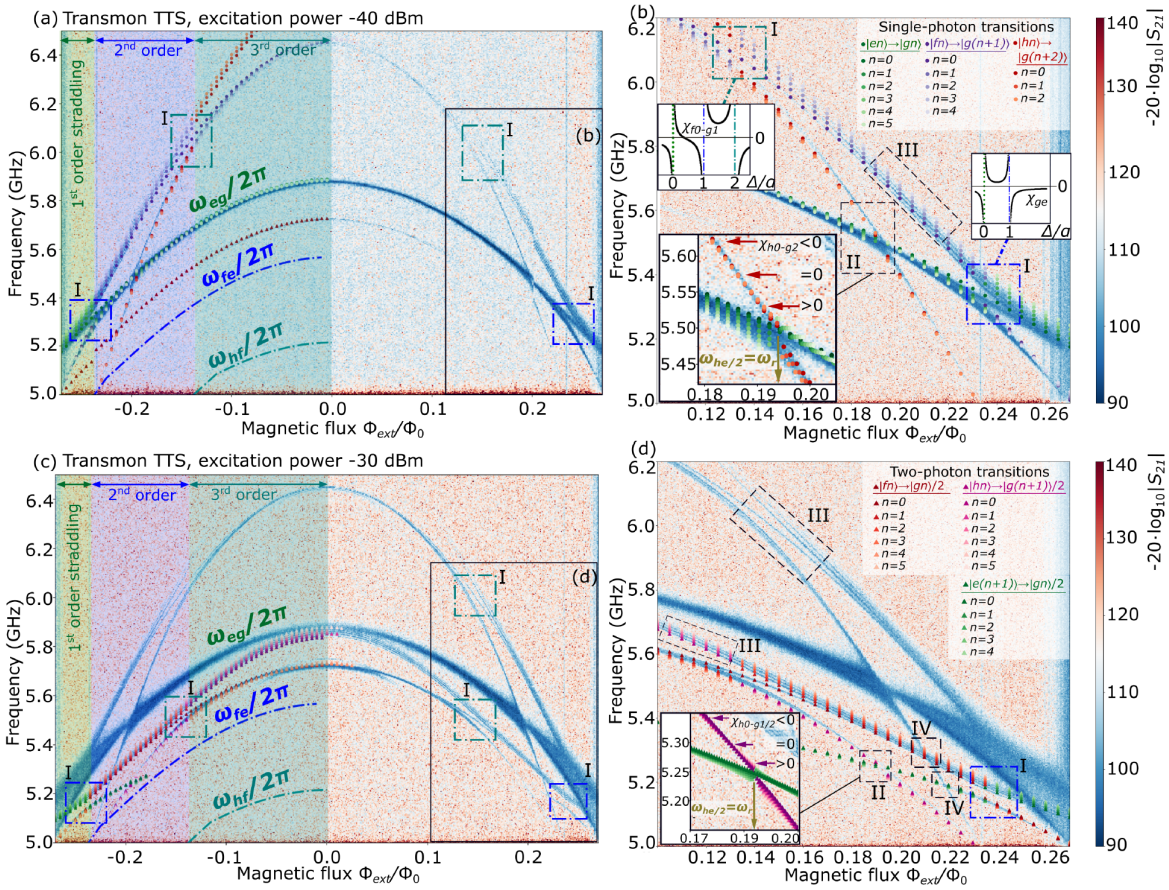

Figure 1: Two-tone spectroscopy of the transmon artificial atom. (a)(b) Analysis of the single-photon transitions for an excitation power of -40 dBm from the microwave signal source. (c),(d) Analysis of the two-photon transitions for an excitation power of -30 dBm. (b) and (d) are insets in subplots (a) and (c), respectively. Roman numerals indicate the spectroscopic features that were studied. Different colors indicate different transitions; different brightness indicates the number of photons participating in a transition.

Rubidium magneto-optical trap based on a grating chip

Darya Bykova[1,2], Alexandra Idrisova[1,2*], Aleksei Kalmykov[1], Anton Afanasiev[1], Victor Balykin[1]

[1] *Institute of Spectroscopy, Russian Academy of Sciences, Troitsk, Moscow, Russia*
[2] *National Research University Higher School of Economics, Moscow, Russia*
*E-mail: aaidrisova@edu.hse.ru

Аннотация

The use of planar structures, such as atom chips and grating chips, for forming a source of ultracold atoms allows for a significant increase in the compactness and stability of devices based on atom interferometry. We present the results of the experimental work during which Doppler cooling and localization of rubidium-87 atoms in a magneto-optical trap were demonstrated using a grating chip.

Laser cooling of atoms is actively used in many areas of modern physics to solve both fundamental and applied problems. One of the most advanced directions is atom interferometry using ultracold atoms. Atom interferometers enable the implementation of a wide class of precision devices: gravimeters, gyroscopes, frequency standards.

The accuracy and stability of atom interferometers are determined by the number of atoms in the ensemble, so a reliable and efficient source of cold atoms is a key element of the setup. Additionally, the potential to miniaturize the apparatus is of great importance. These factors necessitate the development of new methods for obtaining ensembles of ultracold atoms.

One promising approach for optimizing the source of ultracold atoms involves using an atom chip — a planar structure that forms the required spatial distribution of the magnetic field for cooling and localization of atoms [1]. The atom chip enables the creation of the quadrupole magnetic field for the magneto-optical trap (MOT) near its surface with low power consumption.

To cool and localize atoms in the MOT, in addition to the magnetic field, a specific configuration of laser beams that ensures effective slowing of atoms in all directions in three-dimensional space is required. One way to increase the stability and compactness of the system is to replace the traditional six-beam MOT with a scheme that uses fewer optical elements. The pyramidal MOT, where the laser beam is reflected from a pyramidal structure, is an example of such a configuration [2]. Another approach is based on the implementation of planar technologies like diffractive grating chips [3]. In this approach the light field distribution is generated by diffraction of the single incident beam on three diffraction gratings. The use of planar technologies allows integration of the atom chip and the grating chip into a single platform, opening paths to further miniaturization of devices based on ultracold atoms.

At the Institute of Spectroscopy of the Russian Academy of Sciences, a magneto-optical trap on a grating chip has been obtained. Work is currently progressing to optimize its parameters. The grating chip will then be combined with the atom chip in order to create a power-efficient and compact source of ultracold atoms for quantum sensing based on atom interferometry.

Список литературы

[1] *А.Е. Афанасьев, П.И. Скакуненко, Д.В. Быкова, А.С. Калмыков, В.И. Балыкин*, “Атомный чип”, УФН, 194, 1146 (2024).

[2] *K.I. Lee, J.A. Kim, H.R. Noh, W. Jhe*, “Single-beam atom trap in a pyramidal and conical hollow mirror”, Optics letters, 21, 1177 (1996).

[3] *J.P. Cotter, et al.*, “Design and fabrication of diffractive atom chips for laser cooling and trapping”, Applied Physics B, 122, 172 (2016).

Atomic magnetometry based on the ground state Hanle effect in alkali metal atoms in elliptically polarized light wave

Katerina Kozlova[1,2*], Anton Makarov[1,2], Denis Brazhnikov[1,2], Andrey Goncharov[1,2,3]

[1] *Novosibirsk State University, Novosibirsk, Russia*
[2] *Institute of Laser Physics SB RAS, Novosibirsk, Russia*
[3] *Novosibirsk State Technical University, Novosibirsk, Russia*
*E-mail: k.kozlova1@g.nsu.ru

Аннотация

Two registration methods for the Hanle type magneto-optical resonances in vapor cells with 133Cs are investigated and compared: counterpropagating waves configuration and scheme with one elliptically polarized wave. Sensitivities are estimated. Results can be used to create a magnetic sensor for biomedical applications.

One of the rapidly developing areas of quantum sensors is the optical magnetometry. Optically pumped magnetometers are currently used in many areas of science and technology from medicine (MEG, MCG, etc.) to navigation and space exploration. The reason for this is that optical magnetometers have a number of advantages over SQUID-magnetometers: high sensitivity, small size and power consumption, work at near room temperatures, lower cost in comparison to SQUID-magnetometers.

In the first part of current work magneto-optical resonances were observed in a miniature cubic cell (5x5x5 mm) filled with 133Cs vapor and 200 Torr Ar+N2 buffer gas. The recording method was based on the Hanle scheme [1, 2] with circularly polarized light and modulation of the transverse component of the magnetic field. The setup was modified with using elliptically polarized light, which circular components were considered as a pump and probe waves. Polarization components have different absorption coefficient in media due to circular dichroism and were registered with polarimetric method (similar to [3]). This method of registration allows one to subtract the noise of the radiation intensity at the balanced output of the balanced photodetector (BPD), which is predominant in each of its channels separately (see Fig. 1.(a)). Sensitivities of the setup were estimated with different parameters: cell temperature, optical power, polarization ellipticity (example is demonstrated on Fig. 1.(b)). In this scheme, the best estimated sensitivity was $\cong 200 fT/\sqrt{Hz}$.

In the second part of current work magneto-optical rotation resonances were registered in cylindrical vapor cell (length 22 mm, diameter 27 mm) filled with 133Cs and 20 Torr Ne buffer gas. In the experimental setup a configuration of counterpropagating waves was used, the probe wave and the pump wave had linear polarizations, the angle between which was 45 degrees [4]. A pump wave with high optical power induced dichroism in the medium, which caused a rotation of the polarization of the weak probe wave. The rotation angle is determined by the equation (1):

$$\phi = \frac{1}{2}\left| arcsin \frac{P_1 - P_2}{P_1 + P_2} \right|, \tag{1}$$

where P_1 and P_2 are signals from different BPD channels, and $P_1 - P_2$ is signal from differential channel of BPD.

In this scheme relatively strong magneto-optical rotation with angle more than 10 degrees was observed (see Fig . 2.(a)). For this configuration also sensitivities with different optical powes and cell temperature were estimated (see Fig. 2.(b)). In this scheme, the best estimated sensitivity was $\cong 300 fT/\sqrt{Hz}$.

This work was supported by the Russian Science Foundation (grant number 23-12-00195).

]

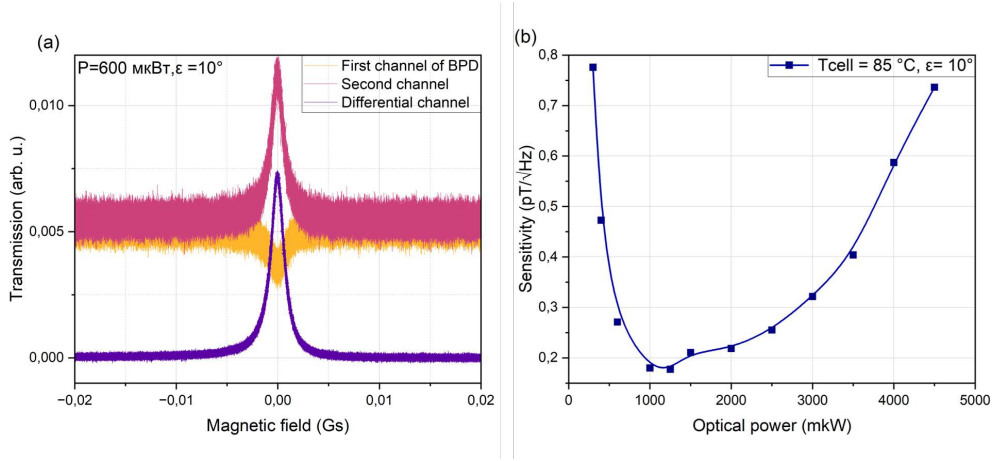

Рис. 1: (a)Example of the magneto-optical resonance in modified Hanle scheme; (b) Sensitivity estimation depending on optical power

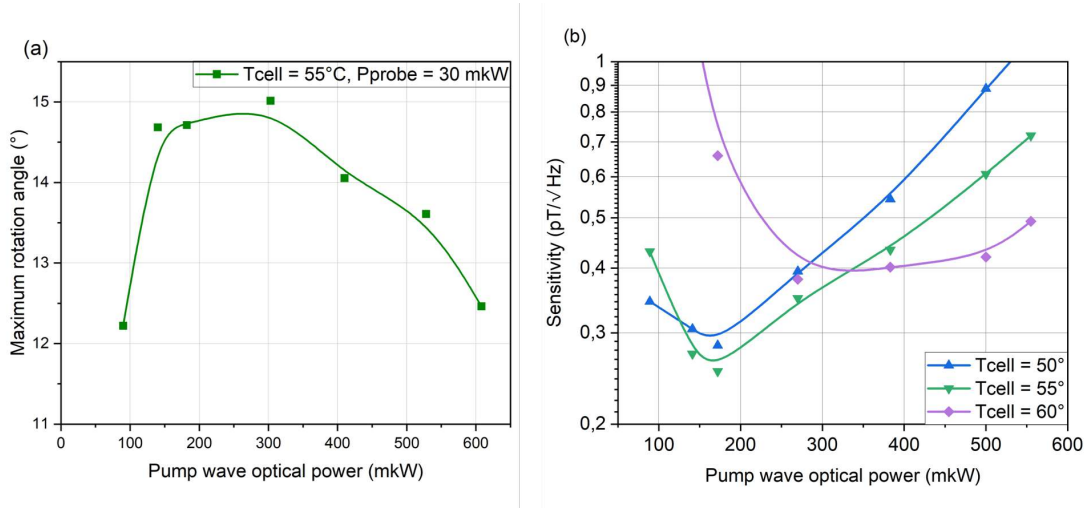

Рис. 2: (a)Maximum ratation angle depending on pump wave optical power; (b) Sensitivity estimation with different cell temperatures depending on pump wave optical power

Список литературы

[1] *W. Hanle*, Uber magnetishe Beeinflussung der Polarisation der Resonanzfluoreszenz. Zs. Phys. **30**, 93 (1924).

[2] *Е.Б. Александров, А.М. Бонч-Бруевич и В.А. Ходовой*, Возможности измерения малых магнитных полей методами ориентации атомов. Опт. Спектр. **28**, 282 (1967).

[3] *A. Makarov, K. Kozlova, D. Brazhnikov, V. Vishnyakov. and A. Goncharov*, All-optical atomic magnetometry using an elliptically polarized amplitude-modulated light wave. Opt. Commun. **577**, 131369 (2025).

[4] *A.O. Makarov, D.V. Brazhnikov and A.N. Goncharov*, Optical Rotation of the Polarization of Light in Rubidium Vapor for Applications in Atomic Magnetometry. Jept Lett. **117**, 509 (2023).

Krasnaya Polyana, Sochi, Russia March 1 – March 7, 2026
9th International School on Quantum Technologies

Nontrivial topological phases in "Zig-Zag" arrays of polarization transmons

Ekaterina Konopleva1[1,2*], **Gleb Fedorov**[2], **Oleg Astafiev**[1,2]

[1] *Skolkovo Institute of Science and Technology, 30 Bolshoy Boulevard, building 1, Skolkovo Innovation Center territory, Moscow, 121205, Russia*
[2] *Moscow Institute of Physics and Technology, Institutskiy Pereulok 9, Dolgoprudny, 141701, Russia*
*E-mail: Ekaterina.Konopleva@skoltech.ru

Аннотация

In recent years, quantum simulators of topological models have been extensively studied across a variety of platforms and regimes. A new promising research direction makes use of meta-atoms with multiple intrinsic degrees of freedom, which to date have been predominantly studied in the classical regime. Here, we propose a superconducting quantum simulator to study an extension of the well-known "Zig-Zag" model with long-range cross-polarization couplings using polarization transmons hosting degenerate dipole orbitals.

The study of topological phenomena and the consequent work on the development of supporting formalism was set in motion in the 1980's on the back of the discovery of the Quantum Hall Effect by Klitzing et al. [1]. The work that followed highlighted the limitations of natural materials and the complexities of classical simulation of large quantum systems lead researchers to employ analogue simulation in order to study these exotic condensed matter phases. The use of controllable classical and quantum simulators enables precise tuning of system parameters, engineering of previously inaccessible physical regimes, and direct reconstruction of wavefunctions.

A particularly interesting new direction of recent studies explores artificial topological structures, the elementary cells of which have multiple intrinsic degrees of freedom (DOF), for instance, degenerate orbitals or oscillatory eigenmodes [2]. In the quantum regime, they are promising candidates for scaling towards classically intractable sizes, which would enable practical quantum simulation.

In this work, we propose and study a superconducting circuit architecture to simulate the extended "Zig-Zag" model in the quantum regime, leveraging the inherent scalability of mesoscopic superconducting circuits, the individual addressability of artificial atoms, and a diversity in the choice of topologies.

0.1 Extended "Zig-Zag" model

"Zig-Zag" model with both $\theta = 90$ and only NN couplings has a special symmetry, owing to which the dipole interactions lead to the formation of two independent polarization subspaces $p_{x,y}$ that are described by separate SSH chains with opposite staggering patterns. However, in our system, long-range dipole-dipole interactions manifest in the non-negligible cross-polarization NNN (next-nearest-neighbor) couplings with strength g, shown in Fig. 1 c) alongside the σ- and π-type NN couplings.

To take this effect into account, we introduce a modified bulk Hamiltonian with NNN couplings where a total of 4 sites (A_x, B_x, A_y, B_y) per unit cell (2 per polarization subspace) is contained:

$$\begin{aligned}\mathcal{H}(K) = \mathrm{Re}[d_+]\tau_0\sigma_x + \mathrm{Im}[d_+]\tau_0\sigma_y + \mathrm{Re}[d_-]\tau_z\sigma_x + \\ \mathrm{Im}[d_-]\tau_z\sigma_y + 2g\cos(K)\tau_x\sigma_0,\end{aligned} \tag{1}$$

where $d_\pm = (d(K) \pm d'(K))/2$, τ_i are Pauli matrices acting on the polarization subspace (x, y) and σ_i are Pauli matrices acting on the SSH sublattice space (A, B).

0.2 FEM Modelling

To demonstrate the experimental feasibility of a polarization-transmon-based "Zig-Zag" simulator, we study arrays of polarization transmons in the linear limit (with the Josephson junctions replaced by linear inductors of comparable inductance) using finite element method (FEM) modelling. To verify the

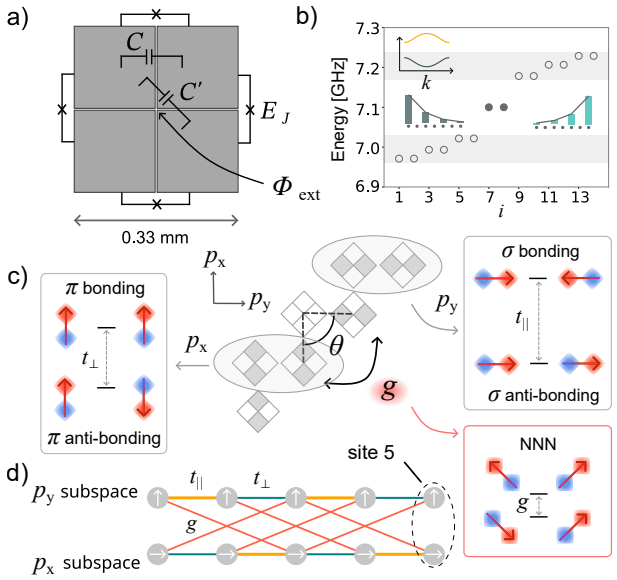

Рис. 1: **a)** A realistic geometry for an electrical circuit of the polarization transmon. **b)** The doubly degenerate energy spectrum of a 7-site "Zig-Zag" chain with $\theta = 90$ and only nearest-neighbour couplings ($g = 0$). **c)** The nearest-neighbour π-type coupling ($t_\perp$) and σ-type coupling ($t_{||}$). **d)** Superconducting "Zig-Zag" model visualized

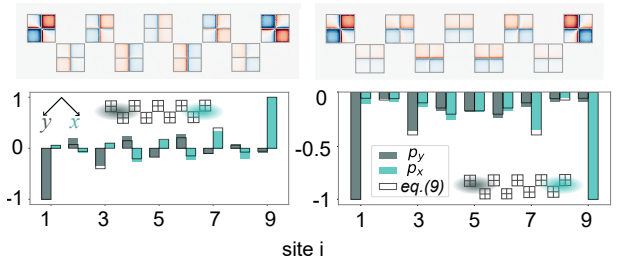

Рис. 2: A quantitative comparison between electromagnetic edge modes and single-excitation wavefunctions calculated from the second quantization formalism for the proposed architecture, $N = 9$.

proposed implementation, we compare the results obtained via FEM and the numerical diagonalization of finite model Hamiltonian.

Fig. 2 shows the edge modes, in which, as predicted, the excitations localize at both ends in symmetric and anti-symmetric superpositions, with non-zero wavefunction components on each site of the chain. The relative amplitudes and phases (bars) are in good correspondence with the proposed theory (black outline). The findings demonstrate that the proposed design is experimentally viable and effectively captures the extended "Zig-Zag" model.

References

We wish to acknowledge the RSF grant no. 25-22-00280.

Список литературы

[1] *Klitzing, K. v., Dorda, G. and Pepper, M.*, New Method for High-Accuracy Determination of the Fine-Structure Constant Based on Quantized Hall Resistance. Phys. Rev. Lett., (1980).

[2] *G. Feng, X. Xiao, P. Yu-Gui, N. Xiang, S. Qi-Li, Y. Simon, Z. Xue-Feng and A. Andrea*, Orbital topological edge states and phase transitions in one-dimensional acoustic resonator chains. Nature Communications (2023).

Two Dimensional Magneto Optical Trap as an Efficient Source of Cold Rb Atoms for Neutral Atom Quantum Computing

Diana Kuzmenok[1*], **Ilia Iukhnovets**[2,3], **Denis Mishin**[2], **Robert Beglaryan**[1], **Ivan Bobrov**[1]

[1] *Faculty of Physics, M.V. Lomonosov Moscow State University*
[2] *P.N. Lebedev Physical Institute of the Russian Academy of Sciences*
[3] *Russian Quantum Center Moscow Institute of Physics and Technology*
*E-mail: kuzmenok.da19@physics.msu.ru

Abstract

We report on the realization of a two-dimensional magneto-optical trap (2D-MOT) for ^{87}Rb atoms based on a compact permanent-magnet quadrupole field configuration. The system provides transverse laser cooling and magneto-optical confinement in a two-dimensional geometry and is developed as the first stage of a trapping architecture intended for further loading of a three-dimensional MOT (3D-MOT). Fluorescence imaging shows a longitudinally elongated atomic cloud with an axial size of approximately 5 mm, consistent with the expected geometry of a 2D-MOT. The demonstrated implementation is an initial experimental step toward scalable cold atom platforms, including neutral atom quantum computing.

Two-dimensional magneto-optical traps can be used as an initial stage in multi-step cold-atom trapping architectures, providing transverse laser cooling while allowing atomic motion along a longitudinal direction. Separation of the 2D and 3D trapping regions enables differential pumping, allowing independent optimization of vapor pressure for efficient atom capture and ultra-high vacuum conditions for long trap lifetimes [1, 2, 3]. In this work, we focus on the realization of a 2D-MOT for ^{87}Rb atoms in which the quadrupole magnetic field is generated entirely by permanent magnets.

Two pairs of permanent magnets (N750-RB) are arranged to produce a quadrupole magnetic field with a zero-field line oriented along the longitudinal axis of the trap. This configuration provides transverse magneto-optical confinement while leaving atoms free to move longitudinally. The resulting transverse magnetic field gradient is measured to be approximately 15 G/cm in the trapping region. The use of permanent magnets instead of anti-Helmholtz coils eliminates current noise sources and resistive coil heating.

The trap is formed in the glass vacuum cell containing rubidium vapor supplied by an alkali metal dispenser. Transverse laser cooling is provided by two orthogonal pairs of counter-propagating circularly polarized laser beams tuned a few natural linewidths below the D_2 cycling transition of ^{87}Rb. An additional repumping beam prevents population trapping in dark hyperfine ground states. The overlap of the cooling beams and the magnetic field zero line is optimized to maximize fluorescence from the trapped atomic ensemble.

Stable atomic fluorescence is observed over extended periods, confirming reliable two-dimensional magneto-optical confinement. Fluorescence imaging reveals a longitudinally elongated atomic cloud with strong transverse confinement and an axial size of approximately 5 mm. This spatial distribution is consistent with the expected geometry of a 2D-MOT. Representative fluorescence images and a schematic of the experimental setup are shown in Fig. 1.

The setup also includes an additional laser beam aligned along the longitudinal axis of the two-dimensional trapping region, which is intended to provide control over directed atomic motion toward a spatially separated three-dimensional trapping region in future experiments.

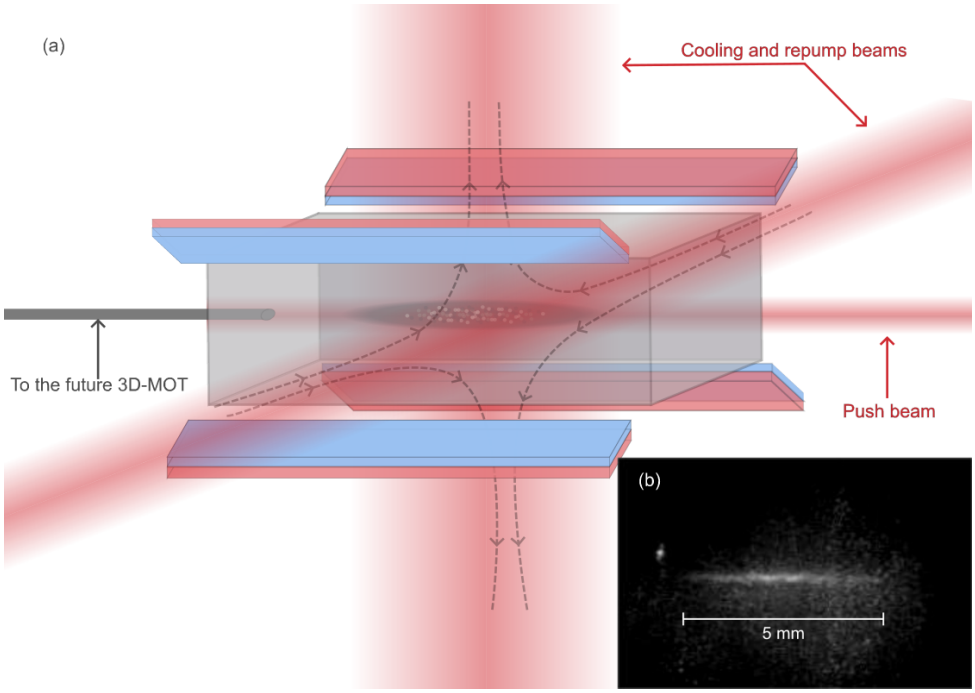

Figure 1: (a) Schematic of the two-dimensional magneto-optical trap based on permanent magnets. Two orthogonal pairs of counter-propagating laser beams provide transverse magneto-optical confinement in the presence of a quadrupole magnetic field. (b) Fluorescence image of the 2D-MOT, showing a longitudinally elongated atomic cloud with an axial size of 5 mm.

References

[1] *Chaudhuri, Saptarishi and Roy, Sanjukta and Unnikrishnan, C. S*, Realization of an intense cold Rb atomic beam based on a two-dimensional magneto-optical trap: Experiments and comparison with simulations. Phys. Rev. A. **74**, 023406 (2006).

[2] *Dieckmann, K., Spreeuw, R. J. C., Weidemüller, M.and Walraven, J. T. M.*, Two-dimensional magneto-optical trap as a source of slow atoms. Phys. Rev. A. **58**, 3891 (1998).

[3] *H. Crepaz*, Trapping and cooling rubidium atoms for quantum information.(2006).

Features of the transmon spectrum at high cavity photon number in the straddling regime

Ekaterina Lavrina[1,2], **Julia Zotova**[2], **Gleb Fedorov**[2], **Oleg Astafiev**[1,2]

[1] *Skolkovo Institute of Science and Technology, 121205 Moscow, Russia*
[2] *Moscow Institute of Physics and Technology, Institutskiy Pereulok 9, Dolgoprudny 141701, Russia*

Abstract

When performing a dispersive readout of a superconducting transmon qubit, the resonator must be populated with roughly 10–100 photons to improve signal-to-noise ratio. This work studies the system under such conditions in the straddling regime, where the resonator frequency lies between the qubit's $e \to g$ and $f \to e$ transition frequencies. At elevated photon numbers, we observe complex spectral shifts: nonlinear, non-monotonic frequency deviations from the ac-Stark effect, linear and resonant splitting of transitions involving different Fock states, and changing anharmonicity. As the absolute value of anharmonicity defines the state leakage rate out of the computational two-level subspace, its behavior is important to predict. Moreover, we show numerically the straddling regime can suppress state leakage, potentially enhancing qubit stability during measurement.

To implement quantum non-demolition measurement of a superconductive transmon qubit, dispersive readout is widely used. Within this method, transmon is coupled to the resonator, e.g. capacitively, and transmon state is measured indirectly by its effect on the resonator transition frequency called dispersive shift, $\chi = (\omega_r^{|e\rangle} - \omega_r^{|g\rangle})/2$. The straddling defined as $\omega_{fe} < \omega_r < \omega_{eg}$ demonstrates increased resonator dispersive shift [1] and suppressed ZZ-interaction [2] in two-qubit gates. Therefore, it improves the fidelity of the dispersive readout and implemented in quantum circuits.

Although significant attention was devoted to implementing the straddling regime for two-qubit gates, certain phenomena in the single transmon-resonator system have remained unexplored. For example, the behavior of a transmon under increasing readout power – a technique widely used to improve the signal-to-noise ratio and operation of single- and two-qubit gates [3, 4] – has not been investigated within the straddling regime. Addressing this issue, we have conducted the spectroscopy of the transmon increasing the resonator population and analyzed the state leakage mechanisms in the straddling regime numerically.

The system we studied consisted of a superconducting transmon qubit capacitively coupled to a $\lambda/4$ coplanar resonator (see Fig.1(a)). This system is described by the Hamiltonian:

$$\hat{\mathcal{H}} = \hat{\mathcal{H}}_t + \hat{\mathcal{H}}_r + \hat{\mathcal{H}}_{int}, \tag{1}$$

where transmon $\hat{\mathcal{H}}_t$, resonator $\hat{\mathcal{H}}_r$ and interaction $\hat{\mathcal{H}}_{int}$ parts are expressed as:

$$\begin{aligned} \hat{\mathcal{H}}_t &= 4E_C\hat{n}^2 - \frac{E_J(\Phi)}{2}\sum_n |n\rangle\langle n+1| + |n+1\rangle\langle n|, \\ \hat{\mathcal{H}}_r &= \hbar\omega_{r,bare}\left(\hat{a}^\dagger\hat{a} + \frac{1}{2}\right), \\ \hat{\mathcal{H}}_{int} &= \hbar g \cdot i(\hat{a}^\dagger - \hat{a}) \otimes \hat{n}. \end{aligned} \tag{2}$$

Here $\hat{n}$ denotes the transmon charge operator and n represents its eigenvalues, which correspond to the charge states. The transmon frequencies $\omega_{ij}(\Phi)$ are tuned by an external magnetic flux Φ that modulates the Josephson energy $E_J(\Phi)$ of its SQUID. For the numerical analysis of the spectra described in the following chapters, we calculated the transition frequencies between the charge states of the transmon-resonator system as functions of the resonator population $\bar{n}_r$ at corresponding Φ-s.

The device was measured in a dilution refrigerator at a base temperature of approximately 20 mK. An external magnetic flux Φ was applied using a coil wound around the sample holder. The measurements were performed using cross-Kerr two-tone spectroscopy: the readout tone is fixed at the resonator frequency $f_r = \omega_r/(2\pi)$, while the frequency of the second tone is swept to excite transitions between the transmon eigenstates. Transitions therefore are detected via dispersive shift causing change in the transmission of the first tone. The power of this readout tone sets the resonator average photon population $\bar{n}_r$.

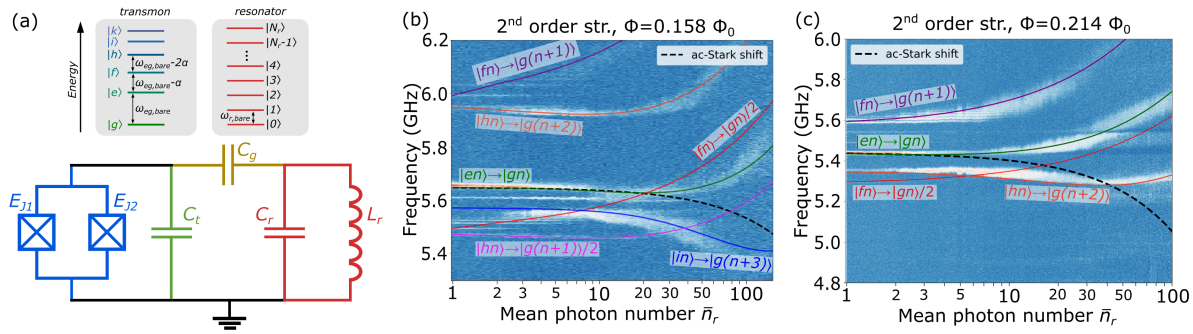

Figure 1: (a) Circuit diagram of the system, consisting of a transmon (formed by a tunable dc-SQUID in blue and a transmon capacitor in green) capacitively coupled to a readout resonator (red) via a mutual capacitor (yellow). (b),(c) Transitions spectra at different magnetic fluxes.

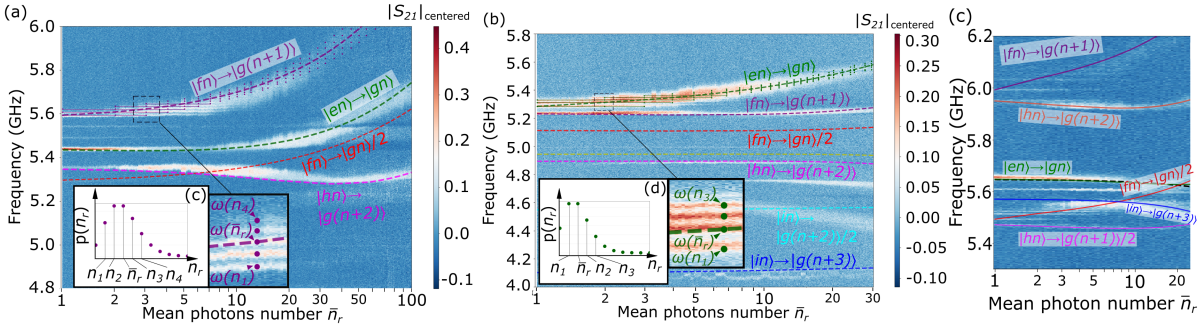

Figure 2: The resonator number splitting. (a) Uniform splitting in the sideband transition $|f0\rangle \to |g1\rangle$. (b) Uniform splitting in the $|e\rangle \to |g\rangle$ sideband transition. (c) The number splitting near sidebands $|f0\rangle \to |g1\rangle$ and $|h0\rangle \to |g2\rangle$ resonance.

The obtained spectra demonstrate the nonlinear and even non-monotonous shifts of the transmon and sidebands transition frequencies. In particular, there is a deviation of the ω_{eg} frequency shift from the linear dependence caused by ac-Stark shift: $\Delta_{\text{Stark}} = 2\chi\eta \cdot \bar{n}_r$, where $\chi = -g^2 E_C/(\Delta(\Delta + E_C))$, $\eta = \kappa^2/(\kappa^2 + 4\chi^2)$, where κ is the resonator decay rate [5]. The exact numerical values of ω_{eg} are presented in Fig.1(a),(b) by solid green curves, and ac-Stark shift is shown by dashed black curves.

Another effect observed in the straddling regime is a resonator photon number splitting [6], presented in Fig.2. Since for each mean resonator population $\bar{n}_r$ there is a photon number distribution of width $\sqrt{\bar{n}_r}$, several Fock states are involved simultaneously, and multiple transitions are visible. The frequency splitting between them is uniform while split transition is far from the resonances with other transitions Fig.2(a),(b). In contrast, near the resonance splitting decreases with n_r growth Fig.2(c) [7].

A key feature observed is an anharmonicity $\alpha = \omega_{fe} - \omega_{eg}$ changing. It is equal to the twice frequency gap between red and green curves in Fig.1, $\alpha = 2(\omega_{fg/2} - \omega_{eg})$. Since $|\alpha|$ defines the state leakage rate [8], its behavior is important to predict. To analyze it in the whole interval $\Phi/\Phi_0 \in [0.0, 0.5]$, we numerically calculate $\alpha(\bar{n}_r)$ function, treating Φ as a parameter. Depending on the system regime, anharmonicity can increase, decrease or even change non-monotonously with $\bar{n}_r$ (see Fig.3(a)). While in the regime called first-order straddling regime, $\omega_{fe} < \omega_r < \omega_{eg}$, $|\alpha|$ increases, this regime is subject to strong transmon ionization [9] according to our numerical analysis shown in Fig.3(b). However, third-order straddling regime, $\omega_{ih} < \omega_r < \omega_{hf}$, observed in the top sweetspot shows suppressed ionization of $|g\rangle$ and $|e\rangle$ states up to 300 photons in the resonator (see Fig.3(c)), which is sufficient for the dispersive readout implementation.

The authors are grateful to the Russian Science Foundation Project No. 25-72-00088 for financial support. The authors acknowledge Alexei Bolgar, Victor Lubsanov, Daria Kalacheva, and Eugene Korostylev for the sample fabrication.

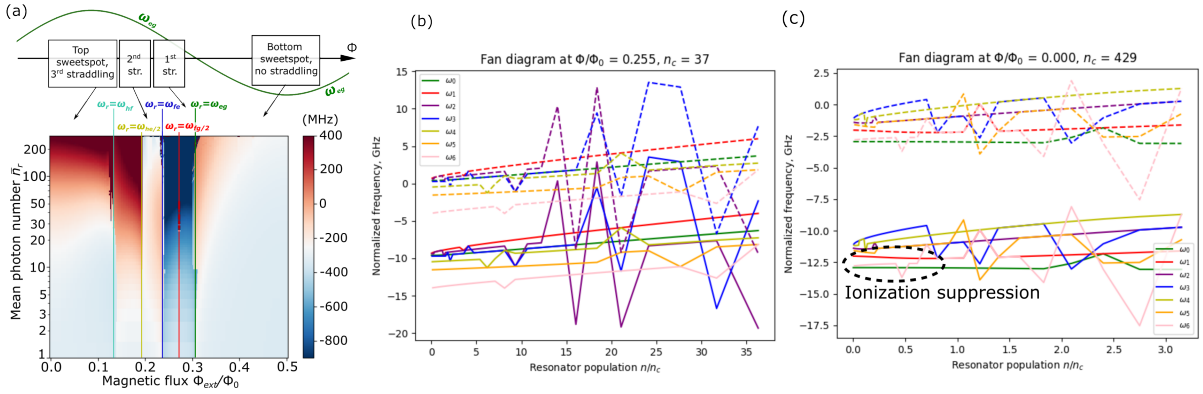

Figure 3: (a) Numerically obtained values of the anharmonicity depending on the resonator population at different magnetic fluxes. (b),(c) Transmon dressed states fan-diagrams [10]. Sharp jumps correspond to ionization of the corresponding level, leading to leakage of states from it.

References

[1] *Koch, J., Yu, T. M., Gambetta, J., Houck, A. A., Schuster, D. I., Majer, J., ... & Schoelkopf, R. J.* , Charge-insensitive qubit design derived from the Cooper pair box. Physical Review A—Atomic, Molecular, and Optical Physics, 76(4), 042319 (2007).

[2] *Stehlik, J., Zajac, D. M., Underwood, D. L., Phung, T., Blair, J., Carnevale, S., ... & Dial, O. E.* , Tunable coupling architecture for fixed-frequency transmon superconducting qubits. Physical review letters, 127(8), 080505 (2021).

[3] *Johnson, J. E., Macklin, C., Slichter, D. H., Vijay, R., Weingarten, E. B., Clarke, J., & Siddiqi, I.*, Heralded state preparation in a superconducting qubit. Physical review letters, 109(5), 050506 **94**, 017402 (2012).

[4] *Rigetti, C., & Devoret, M.* , Fully microwave-tunable universal gates in superconducting qubits with linear couplings and fixed transition frequencies. Physical Review B—Condensed Matter and Materials Physics, 81(13), 134507 (2010).

[5] *Yan, F., Gustavsson, S., Kamal, A., Birenbaum, J., Sears, A. P., Hover, D., ... & Oliver, W. D.*, The flux qubit revisited to enhance coherence and reproducibility. Nature communications, 7(1), 12964 (2016).

[6] *Schuster, D. I., Houck, A. A., Schreier, J. A., Wallraff, A., Gambetta, J. M., Blais, A., ... & Schoelkopf, R. J.*, Resolving photon number states in a superconducting circuit. Nature, 445(7127), 515-518 (2007).

[7] *Zeng, G. H., Zhang, Y., Bolgar, A. N., He, D., Li, B., Ruan, X. H., ... & Peng, Z. H.*, Quantum versus classical regime in circuit quantum acoustodynamics. New Journal of Physics, 23(12), 123001 (2021).

[8] *Babu, A. P., Tuorila, J., & Ala-Nissila, T.* , State leakage during fast decay and control of a superconducting transmon qubit. npj Quantum Information, 7(1), 30 (2021).

[9] *Dai, W., Hazra, S., Weiss, D. K., Kurilovich, P. D., Connolly, T., Babla, H. K., ... & Devoret, M. H.*, Spectroscopy of drive-induced unwanted state transitions in superconducting circuits. arXiv preprint arXiv:2506.24070 (2025).

[10] *Sank, D., Chen, Z., Khezri, M., Kelly, J., Barends, R., Campbell, B., ... & Martinis, J. M.* , Measurement-induced state transitions in a superconducting qubit: Beyond the rotating wave approximation. Physical review letters, 117(19), 190503 (2016).

Heteroatomic MOT based on Tm and Yb atoms

Khristina Smaznova[1,2*], **Denis Mishin**[1],
Daniil Provorchenko[1], **Dmitry Tregubov**[1],
Nikolay Kolachevskiy[1,2], **Artem Golovizin**[1,2]

[1] *P.N. Lebedev Physical Institute, Leninsky prospekt 53, 119991 Moscow, Russia*
[2] *Russian Quantum Center, Bolshoy Bulvar 30,bld.1, Skolkovo IC, 121205 Moscow, Russia*
*E-mail: h.smaznova@lebedev.ru

Аннотация

Over the past two decades, ensembles of ultracold atoms of rare earth metals have become a promising platform for quantum computing, quantum information processing, and optical atomic clocks [1, 2, 3]. The schemes of two-dimensional magneto-optical traps (2D-moles) have a number of advantages: the compact architecture of the installation allows the source of hot atoms to be located close to the center of the formation of 2D-moles; the spatial separation of the 2D and 3D-MOLES chambers allows to achieve high vacuum conditions in the scientific chamber. Heteroatomic arrays based on Tm and Yb atoms will make it possible to implement and describe systems based on the Fermi- and Bose-Hubbard models.

The present work is devoted to the creation of 2D and 3D moles with a continuous source of 171Yb and 169Tm cold atoms. The experimental setup consists of two vacuum chambers see Fig. 1. In the first vacuum chamber, ensembles of ultracold atoms are formed and, by shutting off the reverse stroke of the horizontal cooling beam, a continuous stream of cold atoms is formed.

Figures

Список литературы

[1] *Ma, Shuo and Burgers, Alex P and Liu, Genyue and Wilson, Jack and Zhang, Bichen and Thompson, Jeff D*, Universal gate operations on nuclear spin qubits in an optical tweezer array of Yb 171 atoms. Physical Review X **7**, 021028 (2022).

[2] *Bluvstein, Dolev and Evered, Simon J and Geim, Alexandra A and Li, Sophie H and Zhou, Hengyun and Manovitz, Tom and Ebadi, Sepehr and Cain, Madelyn and Kalinowski, Marcin and Hangleiter, Dominik and others*, Logical quantum processor based on reconfigurable atom arrays. Nature **95**, 7997 (2024).

[3] *D. Mishin, D. Provorchenko, D. Tregubov, N. Kolachevsky, and A. Golovizin*, Continuous operation of a bicolor thulium optical lattice clock. Applied Physics Express 14 **94**, 112006 (2021).

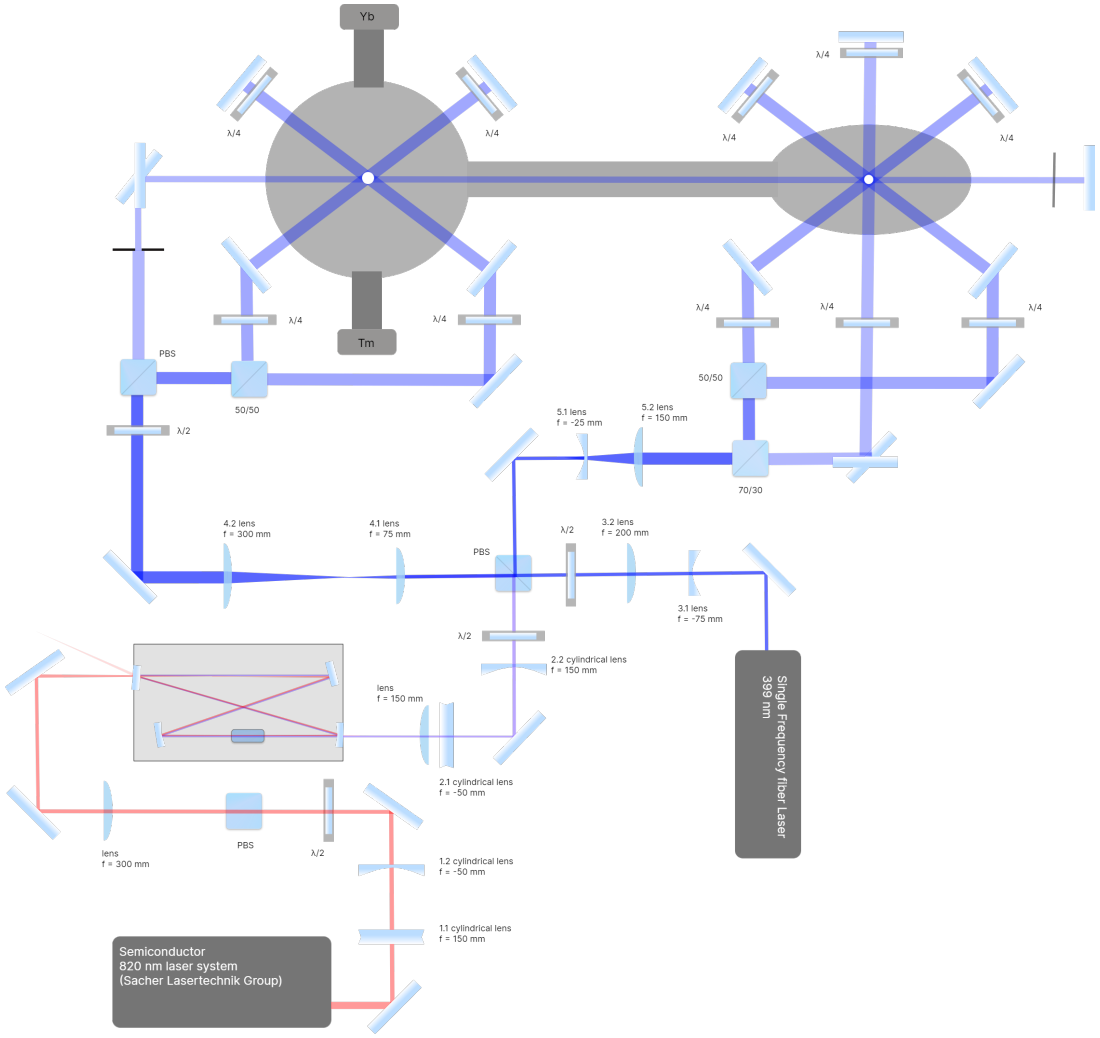

Рис. 1: Entire caption for figure centered and below the illustration

Quantum applications of the universal integrated optical chip fabricated by femtosecond laser writing

Kseniia Urusova[1*], Ilya Kondratyev[1], Artem Argenchiev[1], Yuri Biriukov[1], Nikolay Skryabin[2], Ivan Dyakonov[1,2], Stanislav Straupe[1,2] and Sergey Kulik[1] ,

[1] *Quantum Technology Centre and Faculty of Physics, M.V. Lomonosov Moscow State University, 1 Leninskie Gory Street, Moscow 119991, Russian Federation*
[2] *Russian Quantum Center, Russia, Moscow, 121205, Bol'shoy bul'var 30 building 1*
*E-mail: urusova.kn21@physics.msu.ru

Abstract

We experimentally characterize a universal six-port integrated optical interferometer and demonstrate its potential in the quantum applications. Two quantum experiments were implemented: post-selected generation and full quantum state tomography of a three-qubit GHZ state, and heralded teleportation and tomography of a single-qubit state. Both the required unitary transformations and projective measurements in arbitrary bases were implemented using a single reconfigurable interferometric structure, without additional interferometric elements. In the GHZ-state experiment, the reconstructed density matrix reaches a fidelity of 0.89 with respect to the ideal target state. In the teleportation experiment, the logical states $|0\rangle$ and $|1\rangle$ were successfully teleported with fidelities of 0.91 and 0.97, respectively. The experimental results are in excellent agreement with the theoretical model and confirm the suitability of the platform for implementing complex quantum operations in an integrated photonic chip.

Integrated photonics enables compact, reconfigurable devices for linear optical transformations. Unlike electronic circuits, these devices manipulate light, allowing processing of both classical and quantum states. Universal multiport interferometers are of great interest, as they have the potential to implement arbitrary unitary operations and could serve as components in quantum computers [1]. However, the current architectures of these interferometers are susceptible to fabrication imperfections, which limits their practicality.

Here, we experimentally study a more robust interferometric waveguide structure proposed in [2] (Fig. 1a), consisting of alternating multiport beam splitters and phase shifters.

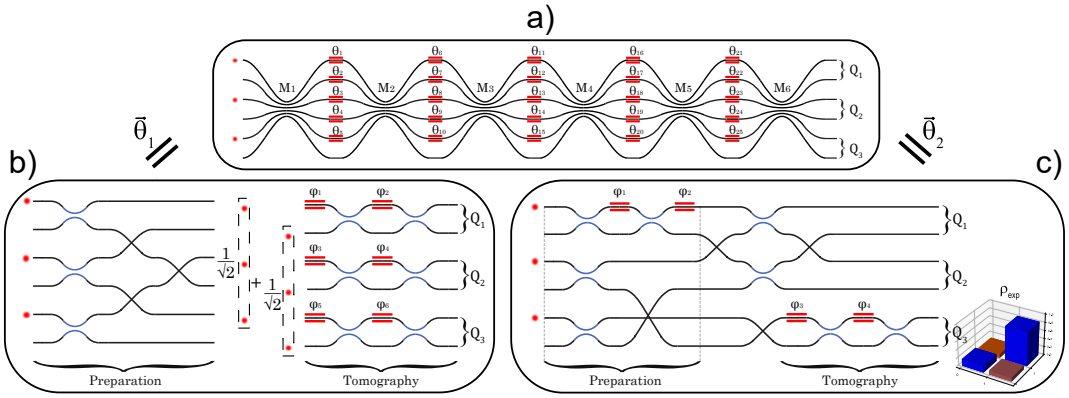

Figure 1: (A) Studied waveguide structure. (B) Scheme for generating the GHZ state through post-selection. Since the studied scheme is universal, it allows for the implementation of the transformation of this scheme by setting phase vector $\vec{\theta_1}$. (C) Scheme for heralded teleportation of a single-qubit state. Since the studied scheme is universal, it allows for the implementation of the transformation of this scheme by setting phase vector $\vec{\theta_2}$.

We fabricated a six-port integrated optical chip based on the architecture described in [2], using femtosecond laser writing, and developed an analytical model for it. We experimentally determined all the chip's parameters, with correlation coefficients of 0.99+.

To demonstrate the universality of the fabricated interferometer, two quantum experiments were implemented: the generation and tomography of a three-qubit GHZ state (eq. 1) using post-selection, and the heralded teleportation and tomography of a single-qubit state. We used a dual-rail encoding of single photons as qubits, where logical states 0 and 1 corresponded to the photon's presence in one of two waveguides on the chip (thus, a six-port chip encodes three qubits). A quantum dot was used as a source of single photons, and a spatial demultiplexer was employed to deliver photon triplets.

$$|GHZ\rangle = \frac{|000\rangle_L + |111\rangle_L}{\sqrt{2}} = \frac{|101010\rangle_{Fock} + |010101\rangle_{Fock}}{\sqrt{2}} \tag{1}$$

Importantly, due to the universality of the circuit, in both experiments both the main operation (entanglement generation or state preparation and its teleportation) and the projective measurements in the required bases were implemented using only a single structure, without any additional interferometric elements. The scheme used for GHZ state generation is shown in Fig. 1b (equivalent to the structure in [3]), the teleportation scheme is also presented in Fig. 1c.

As a result of the experiments, a quantum state was obtained whose density matrix matches that of the GHZ state with a fidelity of 0.89 (Fig. 2a), and the logical states $|0\rangle_L = |10\rangle_{Fock}$ and $|1\rangle = |01\rangle_{Fock}$ were successfully teleported with a fidelity of 0.91 and 0.97 (Fig. 2b). Fidelity was calculated using the following formula:

$$F_{ampl} = \frac{\sum_{i,j} |u_{ij} v_{ij}|}{\sqrt{\sum_{i,j} |u_{ij} u_{ij}| \cdot \sum_{ij} |v_{ij} v_{ij}|}} \tag{2}$$

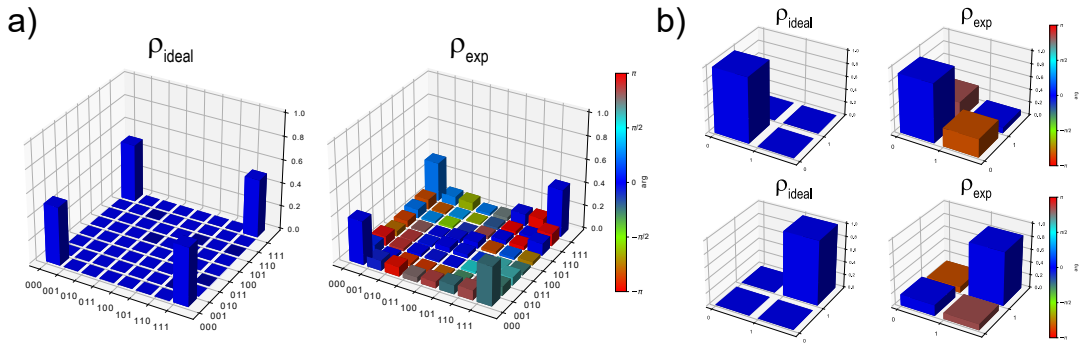

Figure 2: (A) The density matrix of the ideal GHZ state and the density matrix of the experimentally prepared state. The fidelity is 0.89. (B) The density matrices of the ideal states $|0\rangle$, $|1\rangle$ and the density matrices of the experimentally prepared and teleported states. The fidelity is 0.91 for $|0\rangle$ and 0.97 for $|1\rangle$

.

In future work, we plan to improve the accuracy of the experimental preparation of the GHZ state as well as the fidelity of quantum teleportation

The research is carried out with the support of Russian Science Foundation project №22-12-00353-P, https://rscf.ru/en/project/22-12-00353/.

References

[1] *PsiQuantum team*, A manufacturable platform for photonic quantum computing. Nature. **641**, 876 (2025).

[2] *I. V. Kondratyev, I. V. Dyakonov, M. Yu. Saygin, S. S. Straupe, S. P. Kulik*, Multiport universal unitary interferometer design. AIP Conf. Proc. **2241 (1)**, 020022 (2020).

[3] *Pont, M., Corrielli, G., Fyrillas, A. et al.*, High-fidelity four-photon GHZ states on chip. npj Quantum Inf. **10**, 50 (2024).

An efficient source of single photons based on a charged quantum dot in the Coulomb blockade regime

Aidar Galimov[1*], Maxim Rakhlin[1], Yuriy Serov[1], Grigory Klimko [1], Marina Kulagina[1], Yuriy Zadiranov[1], Alexey Toropov[1]

[1] *Laboratory of Quantum Photonics, Ioffe Institute, St. Petersburg, Russia*
*E-mail: aidar-34-dom34@yandex.ru

Abstract

We present a relatively simple method for achieving Coulomb blockade regime in single-photon sources based on microcavity heterostructures with a semiconductor quantum dot (QD) by implementing a p-n-p doping profile during epitaxy and using weak above-band optical illumination. This approach allows stabilization of the specified singly charged state of the QD with 98% fidelity and fabrication of a photon source with a record-high 34% fiber-coupled efficiency, 96.3% single-photon purity, and 94% photon indistinguishability.

The development of efficient sources of indistinguishable single photons is an increasingly important topic for quantum technologies [1, 2]. A highly promising approach utilizes resonantly excited, epitaxially grown semiconductor quantum dots (QDs) embedded within optical microresonators. Among monolithic sources, elliptical micropillars currently offer the highest reported end-to-end efficiency, reaching 28% [3]. To further improve efficiency, full charge-state stabilization of the emitting QD is essential. The most effective technique to date employs the Coulomb blockade effect in a doped microcavity with a QD located within a tunneling p-n junction [4]. However, implementing this method is exceptionally challenging, as it requires fabricating a high-Q microresonator containing a heavily doped active region, which introduces significant free-carrier absorption at the QD emission wavelength. In this paper, we present a simpler alternative method for implementing Coulomb blockade in QDs, which enabled us to increase the single-photon emission efficiency in elliptical micropillars up to 34%.

The presented single-photon source is an elliptical micropillar made from a heterostructure grown by molecular beam epitaxy and containing self-organized InAs/GaAs QDs sandwiched between the lower (30 layer pairs) and upper (18 layer pairs) distributed Bragg reflector [5]. The optimized reactive ion etching method was used to obtain strictly vertical sidewalls with minimal roughness. The asymmetry of the resonator induced a polarization degree of 86% for the single-photon emission, which significantly reduced the losses associated with cross-polarization filtering during resonant excitation.

During the epitaxial growth process, a p-n-p doping profile was achieved in the microcavity heterostructure due to the intrinsic background doping of p-type GaAs and an intentionally grown thin layer of n-type GaAs [6]. By varying the n-layer doping concentration and its distance from the QDs, the position of the Fermi level relative to the QD ground-state energy can be controlled, enabling the creation of structures with a predominant number of positively charged, negatively charged, or neutral QDs. The magnitude and sign of the QD charge were determined experimentally through correlation studies of spin dynamics and photoluminescence (PL) decay times under resonant and quasi-resonant excitation. The measured values show good agreement with the theoretical model obtained from an analytical solution of the Poisson equation for the one-dimensional p-n-p structure.

Further fine-tuning of the QD energy level relative to the Fermi level can be achieved by applying weak optical illumination with photon energies above the GaAs bandgap. This lowers the potential barrier in the p-n-p structure and, in particular, enables the realization of a stable singly positively charged state X^{+1} of the QD being in the Coulomb blockade regime. Photon correlation statistics measured in a representative structure revealed strong charge-state blinking at low illumination powers (Fig. 1a), while with increasing power, the hole-level energy crosses the Fermi level, stabilizing the singly charged state within the Coulomb blockade energy range ($\approx$ 20 meV) with a fidelity of 98%. Thus, using only weak optical illumination, we achieve a Coulomb blockade of the singly charged state without applying any external electric fields, significantly simplifying the technological implementation. Notably, the optical power used is sufficiently low to preserve high-quality single-photon emission characteristics.

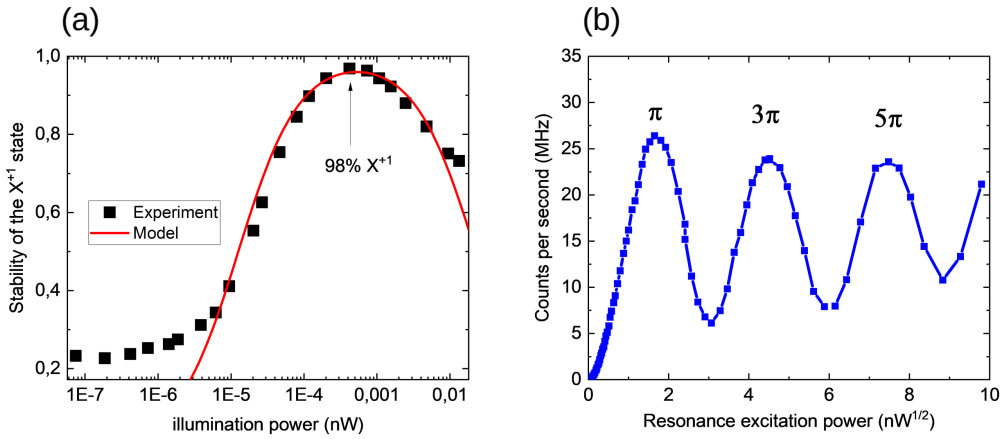

Figure 1: (a) Stability of the X^{+1} state depending on the optical illumination power. (b) Rabi oscillations of the QD in the Coulomb blockade regime

Under resonant coherent excitation, the photon source with a singly positively charged QD exhibits a single-photon intensity of 26.4 MHz under π-pulse conditions (Fig. 1b) at an excitation laser repetition rate of 78.3 MHz. The corresponding single-photon emission efficiency into a single-mode fiber is 34%, which is one of the highest values recorded for monolithic photon sources. The generated single photons exhibit a purity of 96.3% [$g^{(2)}(0) = 0.037$] and an indistinguishability of 94%.

The work was supported by Rosatom in the framework of the Roadmap for Quantum computing (Contract №. 868/1734-D dated 22 September 2025)

References

[1] *N. Skryabin, Yu. Biriukov, M. Dryazgov et al.*, Heralded generation of programmable two-qubit entangled states on a linear-optical platform. Optica Quantum **3**, 2 (2025).

[2] *M. Dryazgov, Yu. Biriukov, I. Dyakonov, K. Taratorin, A. Korneev, M. Rakhlin, A. Galimov et al.*, Resource-efficient low-loss four-channel active demultiplexer for single photons. Optica Quantum **1**, 1 (2023).

[3] *H. Wang, Y.-M. He, T.-H. Chung et al.*, Towards optimal single-photon sources from polarized microcavities. Nat. Photonics **13**, 770–775 (2019).

[4] *R. Warburton, B. Miller, C. Dürr et al.*, Coulomb interactions in small charge-tunable quantum dots: A simple model. Phys. Rev. B. **58**, 16221 (1998).

[5] *A. Galimov, M. Bobrov, M. Rakhlin et al.*, Towards Bright Single-Photon Emission in Elliptical Micropillars. Nanomaterials **13**, 9 (2023).

[6] *A. Galimov, Yu. Serov, M. Rakhkin et al.*, Charge States of Single Quantum Dots in a Microcavity p–n–p Heterostructure with the Built-in Coulomb Blockade. Jetp Lett **121**, 5 (2025).

Krasnaya Polyana, Sochi, Russia March 1 – March 7, 2026
9th International School on Quantum Technologies

Second-harmonic generation in a "nonlinear crystal-metasurface" structure

Egor S. Vyatkin*, **Segey A. Tarasenko**

Ioffe Institute, St. Petersburg, Russia
*E-mail: vyatkin.egor@mail.ioffe.ru

Abstract

We present an analytical theory of second harmonic generation (SHG) in hybrid structures combining a nonlinear 2D crystal with a dielectric metasurface. The theory describes the excitation spectrum and enhancement of SHG at both leaky and quasi-bound state in the continuum (quasi-BIC) resonances in terms of the material parameters. For low-loss systems, the SHG efficiency at leaky resonances is determined by their radiative broadening, governed by the relevant Fourier harmonics of the metasurface polarizability, whereas the SHG enhancement at quasi-BIC resonances is ultimately limited by inhomogeneous broadening and absorption in the system. The developed framework provides a systematic theoretical basis for optimizing the resonant nonlinear frequency conversion in hybrid 2D-material-metasurface platforms and identifies the fundamental limitations of the SHG efficiency.

Hybrid structures based on low-dimensional semiconductor and dielectric metamaterials are at the core of modern research in the field of nonlinear nanophotonics [1, 2]. Such a platform combines the advantages of strong nonlinear response of semiconductors [3] with the control of optical resonances in metasurfaces [4]. The resonant enhancement of the near field leads to a dramatic increase in nonlinear optical phenomena such as second harmonic generation (SHG), which is actively studied both experimentally and theoretically. However, theoretical works are primarily focused on modeling the electric field distribution and determining the parameters of Fano optical resonances from numerical calculations.

In this work, we present an analytical theory of SHG in a hybrid structure consisting of a nonlinear two-dimensional crystal and a dielectric metasurface, Fig. 1 (a). Under resonant conditions, the incident electromagnetic wave excites high Q factor photonic modes in the metasurface, which leads to a substantial enhancement of the SHG in the two-dimensional crystal.

Figure 1 (b) shows the calculated intensity of the forward emitted second harmonic radiation as a function of the fundamental frequency and the angle of incidence. At the normal incidence of radiation ($\theta = 0$), the SHG signal exhibits a single resonance. This resonance is associated with the excitation of the symmetric standing wave (leaky mode) in the metasurface. A slight deviation of the light incidence from the normal leads also to the excitation of the antisymmetric quasi-BIC mode. This gives rise to

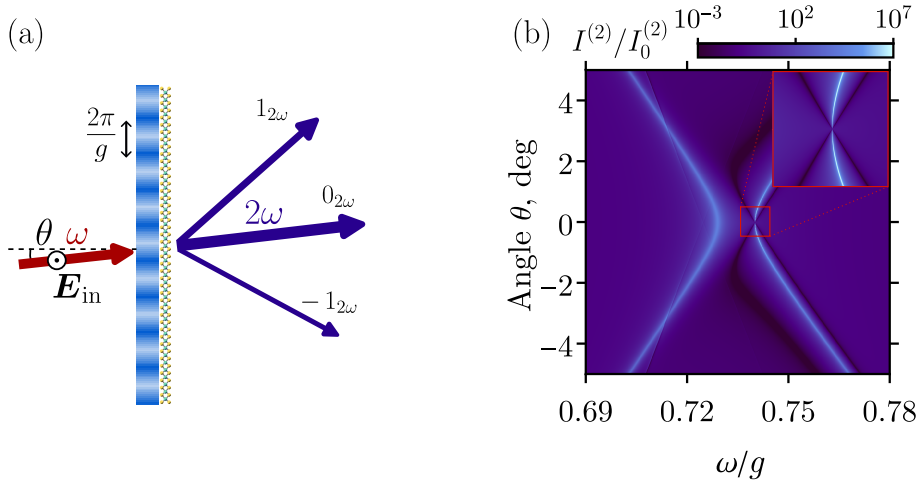

Figure 1: (a) Second harmonic generation (SHG) in 2D nonlinear crystal integrated with dielectric metasurface. (b) SHG enhancement as a function of the light frequency and the angle of incidence.

an additional, exceptionally narrow and high, peak in the SHG excitation spectrum at slightly higher frequency. With a further increase of the incidence angle, the two peaks get spectrally separated and acquire comparable radiative broadening.

The developed analytical theory captures the resonant contributions to the second harmonic emission, accurately describing the amplitudes, widths, and spectral positions of the resonances in terms of the Fourier harmonics of the metasurface polarizability α_n and nonlinear susceptibility of the 2D crystal [5]. For low-contrast gratings ($|\alpha_n| \ll |\alpha_0|$ for $n \neq 0$), the full harmonic description can be reduced to an effective model involving two coupled electromagnetic modes, where the interaction with higher-order harmonics result in a renormalization of the model parameters. The effective model describes qualitatively both the leaky and quasi-BIC modes as well as their interaction and interconversion. In low-loss structures, the enhancement factor of the second harmonic emission intensity at leaky resonances is governed by radiative broadening. For the low-energy leaky resonance at the normal incidence of light, the factor can be estimated as $\sim (\mathrm{Re}\,\alpha_0/\alpha_1)^4$, where α_0 is the mean polarizability and α_1 is the first Fourier harmonic. Symmetry breaking due to deviation of the incident light from normal or asymmetry in the metasurface enables the excitation of the complementary quasi-BIC mode. The radiative broadening of the quasi-BIC mode can be vanishingly small, such that the enhancement of SHG is ultimately limited by inhomogeneous broadening and absorption in the system. The maximal enhancement factor at the quasi-BIC resonance reaches $\sim (\mathrm{Re}\,\alpha_0/\,\mathrm{Im}\,\alpha_0)^4$.

In addition to SHG arising from the conventional second order nonlinear susceptibility, we describe a nonlocal SHG mechanism in hybrid structures that originating from the in-plane inhomogeneity of the near field. This mechanism gives rise to diffracted beams at the doubled frequency, even when both the two-dimensional crystal and the metasurface possess a center of spatial inversion.

This work was supported by the Russian Science Foundation (Project No. 22-12-00211-П).

References

[1] *N. Bernhardt, K. Koshelev, S.J.U. White, K.W.C. Meng, J.E. Fröch, S. Kim, T.T. Tran, D.-Y. Choi, Y. Kivshar, and A.S. Solntsev*, Quasi-BIC resonant enhancement of second-harmonic generation in WS_2 monolayers. Nano Lett. **20**, 5309 (2020).

[2] *T. Ning, L. Zhao, Y. Huo, Y. Cai, and Y. Ren*, Giant enhancement of second harmonic generation from monolayer 2D materials placed on photonic moiré superlattice. Nanophotonics **12**, 4009 (2023).

[3] *L. Zhou, H. Fu, T. Lv, C. Wang, H. Gao, D. Li, L. Deng, and W. Xiong*, Nonlinear optical characterization of 2D materials. Nanomaterials **10**, 2263 (2020).

[4] *E.S. Vyatkin, A.V. Poshakinskiy, and S.A. Tarasenko*, Emergent spin and orbital angular momentum of light in twisted photonic bilayer. Phys. Rev. B **111**, 125303 (2025).

[5] *E.S. Vyatkin and S.A. Tarasenko*, Resonant enhancement of second harmonic generation in 2D nonlinear crystal integrated with meta-waveguide: analytical vs numerical approaches. arXiv:2511.04325 (2025).

Optical nonlinearity of an atomic ensemble driven by a saturating coherent field

Arseniy Usoltsev[1,2*], Leonid Gerasimov[1,2], Alisa Manukhova[3], Sergei Kulik[1] and Dmitriy Kupriyanov[1,2,4]

[1] *Quantum Technology Centre, M.V. Lomonosov Moscow State University, Leninskiye Gory 1-35, 119991 Moscow, Russian Federation*
[2] *Centre for Interdisciplinary Basic Research, HSE University, St. Petersburg 190008, Russian Federation*
[3] *Department of Optics, Palacký University, 17 Listopadu 12, 771 46 Olomouc, Czech Republic*
[4] *Department of Physics, Old Dominion University, 4600 Elkhorn Avenue, Norfolk, Virginia 23529, USA*
*E-mail: usoltcev.as21@physics.msu.ru

Abstract

We present a microscopic analysis and evaluation of the dielectric susceptibility of a dielectric medium consisting of vector-type two-energy-level atoms responding on a weak probe mode when the atoms are driven by a strong coherent field. Each atom, in an environment of others, exists as a quasiparticle further structuring a bulk medium. In a limit of dilute atomic gas, the dynamics of each atom follows the Mollow-type nonlinear excitation regime, and the medium susceptibility collectivizes the individual atomic responses to the probe mode. We outline how the collective dynamics can be interpolated up to a dense medium, and we argue from general positions that in such a medium the optical nonlinearity and, in particular, its parametric part could not be significantly magnified by manipulating both the coherent pump and the sample density. That indicates certain limitations for potential capabilities of quantum communication protocols utilizing the entangled photons, created by a parametric process, as a main resource of quantum correlations.

Consider an example of a four-wave mixing process developing in a dielectric medium consisting of cold atoms having a closed optical transition (Fig. 1). It is driven by a strong quasi-resonance coherent field and, in a steady-state regime, has a nonlinear fluorescence response in three resonance lines known as Mollow triplet. The ensemble of such atoms constructs a disordered atomic medium, where a weak probe light can propagate along an arbitrary direction and with an arbitrary polarization.

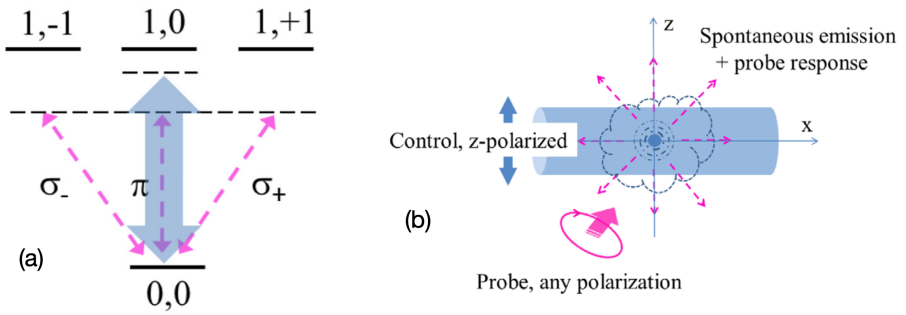

Figure 1: (a) Energy structure of a medium atom which has a single non-degenerate ground state and three excited Zeeman sublevels. The three dashed arrows belong to a weak probe impinging on the atom from an arbitrary direction, the shaded arrow belongs to a strong coherent field. (b) Excitation geometry of an isolated atom, thinkable as an elementary scatterer inside a dilute atomic cloud, and driven by two modes of the strong control and weak probe. The responding field contains both the spontaneous emission and scattered part of the probe mode

For a dilute gas under nonlinear excitation by a strong coherent field, the linear response of the dipole polarization to a weak probe mode is given by the following Kubo formula:

$$\chi_{ij}(\mathbf{R};t,t') = \frac{i}{\hbar}\left\langle\left[\hat{d}_i^{(\mathbf{R})}(t),\hat{d}_j^{(\mathbf{R})}(t')\right]\right\rangle n(\mathbf{R}), \tag{1}$$

where $n = n(\mathbf{R})$ is a smoothed density distribution described by a uniform spatial profile at the point $\mathbf{R}$. The dipole $\hat{d}^{(\mathbf{R})}(t)$ is driven by a strong coherent field as well as by all other modes (excluding the probe mode), thus its dynamics is governed by Mollow-type Heisenberg-Langevin equations, see [1].

In the steady-state regime for the positive frequency response of an atomic dipole to the probe, polarized along the principal axes x and y, see Fig. 1, the susceptibility component depends only on the time delay as $\chi^{(+)}_{xx}(t,t') = \chi^{(+)}_{xx}(t-t')$. But the susceptibility component responding to a probe, polarized along the z-direction (coinciding with the polarization of the driving field), depends on its time arguments independently and consists of two contributions:

$$\chi^{(+)}_{zz}(t,t') = \chi^{(+-)}_{zz}(t-t') + \chi^{(++)}_{zz}(t,t')e^{+2i\mathbf{k}_c\cdot\mathbf{R}}. \tag{2}$$

The susceptibilities $\chi^{(+)}_{xx}$ and $\chi^{(+-)}_{zz}$ respond to the probe mode, involved in the Rayleigh or stimulated quasi-Raman processes (Kerr-type optical nonlinearity). The susceptibility $\chi^{(++)}_{zz}$ mixes the different frequency components and expresses the parametric conversion of the signal probe mode $\omega = \omega_s = \omega_c + \Omega$ to the conjugated idler probe mode $\omega_i = \omega_c - \Omega$.

Results

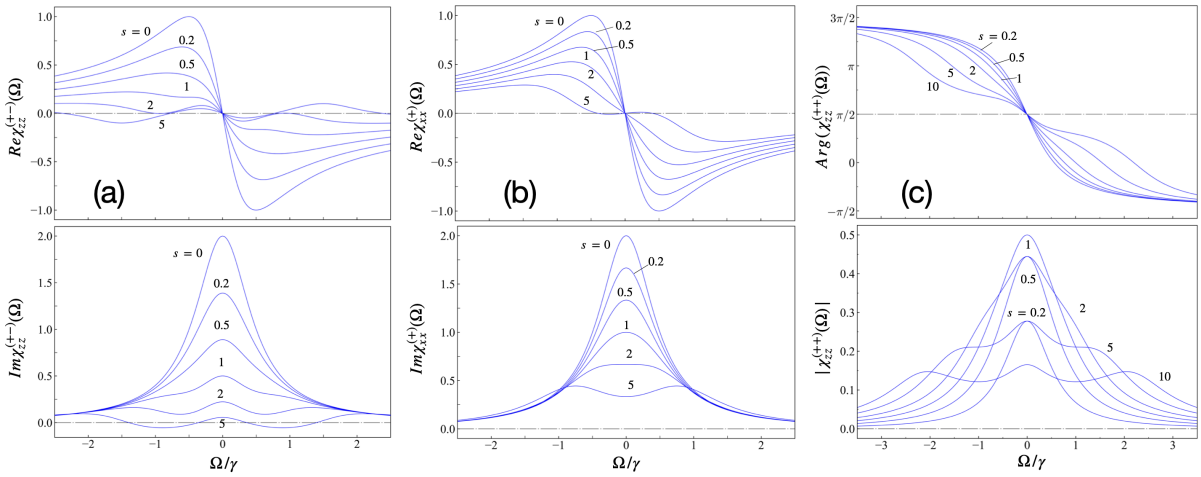

Figure 2: (a) Kerr-type nonlinear susceptibility for z-polarized probe, calculated for the control field resonant to the atomic transition, and for different saturation parameters s. (b) Same as in (a) but for the x-polarized probe. (c) Parametric nonlinear susceptibility, calculated for the control field resonant to the atomic transition, and for different saturation parameters s.

As follows from the dependencies of Fig. 2[a, b], in the saturation limit for a large saturation parameter s, defined in [2], both the susceptibilities of the z-polarized probe vanish, see calculation details in [1]. However, the susceptibility component for the x-polarized probe does not vanish with enhancing s but transforms to a doublet resonance structure, where the resonance maxima indicate the ac-Stark splitting of the ground state.

The behavior of the parametric part, reproduced in Fig. 2[c], show that there is an optimal regime when the coupling of the signal light with the atomic matter is maximized near a non-saturating value of $s \sim 1$. For higher s the spectrum becomes broader with the Mollow sidebands manifested, and a local enhancement of the parametric coupling is observed near these sidebands.

If the atomic medium is considered to be dense and excited by a strong saturating external coherent field, the Mollow nonlinear fluorescence would be emitted by the medium atoms in arbitrary directions and would interfere with an incident probe light and create large fluctuations of the local field amplitude. The damaging role of fluctuations on coherent processes of light propagation through a disordered ultracold atomic gas has been observed in experiments [3]. Apparently, in such a medium, the parametric process could be initiated by a non-saturating control field and evolve in the spectral domain, where the medium

is transparent and possesses ideal dielectric properties with a real-valued dielectric constant $\varepsilon \sim \varepsilon' > 1$, having a vanishing imaginary part $\varepsilon'' \to 0$. As shown in [4], in the spectral domain of transparency, the radiation decay should be renormalized as $\gamma \to \gamma_\varepsilon = \sqrt{\varepsilon}\,\gamma$. Any atomic dipole, existing as an exciton-type quasiparticle, would obey the dynamics similar to the case of a dilute gas, where the transverse electric field of the probe light, acting on the dipole, would be displaced by the Lorentz–Lorenz correction to the local field.

Finally, we can point out that the internal interactions and the excitation by a strong control field, taken as a joint effect, mainly modify the quasi-energy structure of the atomic medium and cannot significantly magnify the coherent response of the polarization current to the driving fields. This can limit potential capabilities of quantum communication protocols, utilizing entangled photon pairs created by a parametric process as a main resource of quantum correlations.

Acknowledgements

This work was supported by the Russian Science Foundation under Grant No. 23-72-10012.

References

[1] *A. S. Usoltsev, L. V. Gerasimov, A. D. Manukhova, S. P. Kulik, and D. V. Kupriyanov*, Optical nonlinearity of a cold atomic ensemble driven by a strong coherent field in a saturation regime, J. Opt. Soc. Am. B **43**, 159-170 (2026)

[2] *C. Cohen-Tannoudji, J. Dupont-Roc, and G. Grynberg*, Atom-Photon Interactions (Wiley & Sons, Inc., 1993).

[3] *D. V. Kupriyanov, I. M. Sokolov, and M. D. Havey*, Mesoscopic coherence in light scattering from cold, optically dense and disordered atomic systems. Phys. Rep. **671**, 1–60 (2017).

[4] *I. M. Sokolov, M. D. Kupriyanova, D. V. Kupriyanov, et al.*, Light scattering from a dense and ultracold atomic gas Phys. Rev. A **79**, 897 053405 (2009).

Wave mixing on a superconducting artificial atom: single-photon and two-photon cases

Timur Sabirov[1,2*], **Alexey Dmitriev**[1], **Andrey Vasenin**[1], **Sergey Gunin**[1], **Oleg Astafiev**[2,1]

[1] *Laboratory of Artificial Quantum Systems, Moscow Institute of Physics and Technology, 141700 Dolgoprudny, Russia*
[2] *Skolkovo Institute of Science and Technology, Nobel St. 3, 143026 Moscow, Russia*
*E-mail: sabirov.tr@phystech.edu

Abstract

This experimental study investigates a nonlinear optics effect—wave mixing—on a superconducting two-level artificial atom, a transmon. The low efficiency of single-photon detectors in the microwave range complicates the study of photon statistics. Due to intermodulation, wave mixing allows us to separate various processes into individual spectral components and associate probabilities with their amplitudes, which can be measured using an ADC. This study demonstrates the sensitivity of the wave mixing spectrum to photon statistics using a coherent signal and photon-vacuum superposition as examples. Using this method, single-photon and two-photon generation of a single qubit under the action of a pulse were experimentally demonstrated.

In this paper, we experimentally investigate a nonlinear quantum-optical effect—wave mixing of propagating wave packets (anti-bunched and coherent signals) in a cascade system of superconducting atoms—qubits. The experimental platform utilizes transmon qubits interacting with a waveguide in strong coupling, allowing us to study scattering in the cascade system at the level of single quanta of electromagnetic radiation.

It was demonstrated that wave mixing can be used to obtain information about the photon statistics of the scattered field, which is of great interest for quantum communications [1].

A cascade system of superconducting qubits is designed as follows: a microwave signal excites a source qubit, then the wave packet, after spontaneous emission, propagates through a cryogenic circulator to a scatterer qubit, to which a continuous microwave signal is fed through a separate channel using a directional coupler. Due to the presence of a cryogenic microwave circulator, the signal propagates only from the source qubit to the scatterer qubit 1..

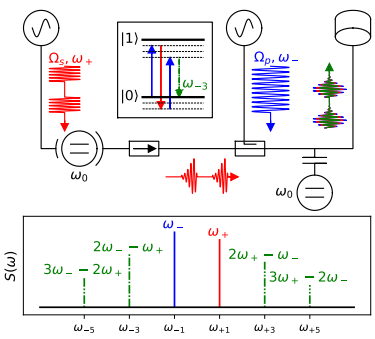

Figure 1: Scheme of the cascade and example of spectrum

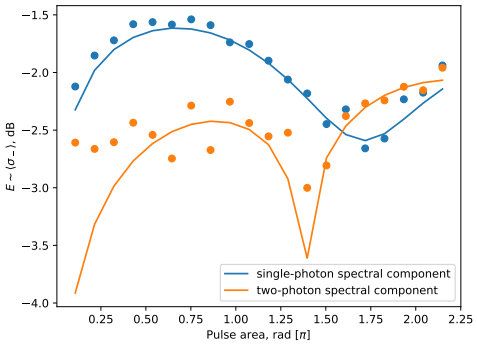

Figure 2: Dependency of spectral components on the pulse area

The simulation was carried out based on a theoretical model of the experimental system, constructed using the theory of open quantum systems [2, 3].

Wave-mixing spectra for single-photon case was obtained and brought into quantitative agreement with simulations. That case further used as a benchmark to observe other cases of photon compositions.

The dependence of the discussed effect on the excitation signal amplitudes were experimentally obtained at points corresponding to pulses of different amplitudes and durations to demonstrate control of

single qubit as a source of single-photons and two-photons. The difference between generation regimes was described with correlation functions of first and second order.

Author thanks colleagues from Laboratory of Artificial Quantum Systems and MIPT Shared Facilities Center.

References

[1] Dmitriev A. Y. et al. Quantum wave mixing and visualisation of coherent and superposed photonic states in a waveguide //Nature communications. – 2017. – Т. 8. – №. 1. – С. 1352.

[2] Pogosov W. V., Dmitriev A. Y., Astafiev O. V. Effects of photon statistics in wave mixing on a single qubit //Physical Review A. – 2021. – Т. 104. – №. 2. – С. 023703.

[3] Gardiner C. W., Parkins A. S. Driving atoms with light of arbitrary statistics //Physical Review A. – 1994. – Т. 50. – №. 2. – С. 1792.

Microwave single-photon source with relaxation rate controlled by a dc-squid

Andrei Vasenin[1*], Vladimir Voskresenskii[1], Aleksei Dmitriev[1], Daria Kalacheva[1], Viktor Lubsanov[1], Evgenia Alekseeva[1], Aleksei Bolgar[1], Ming-Tang Deng[2], Oleg Astafiev[3,1]

[1] *Laboratory of Artificial Quantum Systems, Moscow Institute of Physics and Technology, Moscow, Russia*
[2] *National University of Defense Technology, Changsha, China*
[3] *Skolkovo Institute of Science and Technology, Moscow Russia*
*E-mail: vasenin.av@phystech.edu

Abstract

By temporal shaping of single-photons, one can increase their absorption probability by other single-atoms. Microwave single-photon sources in the frequency range up to 10 GHz can be produced from superconducting quantum circuits. The temporal shaping can be achieved by modulating the radiative coupling between a superconducting artificial atom and a waveguide. This work present a real-world example of such a microwave single-photon source demonstrating tunability of the relaxation rate from 50 MHz down to several kHz.

Superconducting artificial atoms offer a unique advantage for quantum optics experiments, as they easily achieve strong coupling with electromagnetic waves [1]. This property enables exploration of light-matter interactions at the single-photon and single-atom level [2]. A wide range of quantum optic phenomena depends on the time-domain shape of single photons, which can be controlled by adjusting the coupling strength of an atom to the emission line. One of the many ways to do so is by controlling the density of vacuum modes in the waveguide.

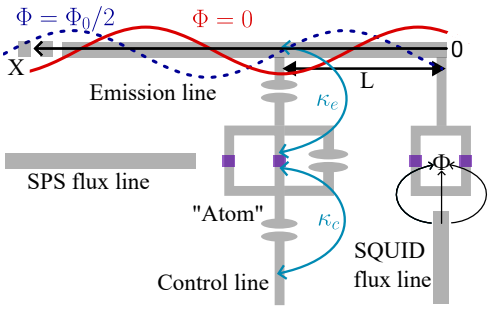

Figure 1: Scheme of the artificial atom coupled to a waveguide with a tunable dc-squid "mirror"

In this work, we designed, theoretically investigated, and experimentally examined a superconducting single-photon source (SPS) with tunable coupling strength (Fig. 1). A superconducting transmon qubit is used as the artificial atom in our device. The tunable coupling operation is based on the dependence of the spectral density distribution of vacuum modes $S(\omega)$ in the waveguide on the boundary condition. $S(\omega)$, in turn, is linearly related to the decay rate Γ_1, which determines the spectral linewidth of the emitted photons

$$\Gamma_1 = Z_0 \frac{|A|^2}{\hbar^2} \kappa^2 S(\omega), \tag{1}$$

where $A = 1\hat{Q}0$ is the matrix element of the charge operator, Z_0 is the impedance of the emission line, and κ is the atom-line voltage coupling coefficient.

To control the boundary conditions, a SQUID is placed at the end of the emission line, which acts as a mismatched load with impedance modulated by the external magnetic flux Φ threading the SQUID loop [3]. For example, if the distance L between the artificial atom and the SQUID equals a quarter of a certain wavelength λ, then at $\Phi = 0$ the spectral density $S(\omega)$ at the atom-line coupling point is maximal, while at $\Phi = \Phi_0/2$ it is minimal, where Φ_0 is the flux quantum.

Based on numerical and analytical studies, we selected device parameters such that for the transition frequency $f = 6.0\,\mathrm{GHz}$, the decay rate $\Gamma_1/(2\pi)$ for the emission line can be varied from 50 MHz down to zero, while the coupling to the control line is constant and equals 45 kHz.

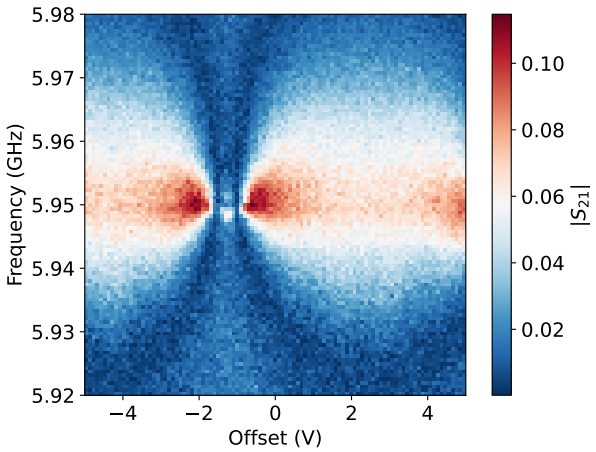

Figure 2: Results of single-tone spectroscopy of the single-photon source with the tunable relaxation rate controlled by applied voltage to end of the flux line

We experimentally validated the device by performing a single-tone spectroscopy (Fig. 2). The transmission through the SPS was measured as a function of frequency and the control voltage applied to the SQUID flux line. As shown in the figure, magnetic flux tuning modulates the SPS linewidth, which reflects the change of the relaxation rate Γ_1. The experiments are ongoing and more results will appear later.

This research was supported by the Program of Strategic Academic Leadership “Priority 2030”.

References

[1] *A. Wallraff, D. I. Schuster, A. Blais, L. Frunzio, R.-S. Huang, J. Majer, S. Kumar, S. M. Girvin, and R. J. Schoelkopf*, Strong coupling of a single photon to a superconducting qubit using circuit quantum electrodynamics. Nature **431**, 162 (2004).

[2] *A. Yu. Dmitriev, A. V. Vasenin, S. A. Gunin, S. V. Remizov, A. A. Elistratov, W. V. Pogosov and O. V. Astafiev*, Direct experimental observation of sub-Poissonian photon statistics by means of multiphoton scattering on a two-level system. Phys. Rev. A **111**, 043715 (2025).

[3] *P. Forn-Díaz, C. W. Warren, C. W. S. Chang, A. M. Vadiraj, and C. M. Wilson*, On-demand microwave generator of shaped single photons. Phys. Rev. Applied **8**, 054015 (2017).

Nonlinear interferometry in the mid-infrared range

Artem Sabanin[1*], **Sergey Kulik**[1,2], **Anna Paterova**[1]

[1] *South Ural State University, Quantum Engineering of Light Laboratory, Chelyabinsk, Russia*
[2] *Center for Quantum Technologies, Faculty of Physics, Lomonosov Moscow State University, Moscow, Russia*
*E-mail: artem.sabanin@mail.ru

Аннотация

Nonlinear interferometry may become a promising alternative to classical infrared metrology methods. It is based on the interferometry of biphoton fields generated by spontaneous parametric down conversion. This paper examines nonlinear interferometry in the mid-infrared range up to 12 mcm.

Nonlinear interferometry is a promising approach in infrared (IR) metrology [1,2]. Classical IR metrology methods have several drawbacks: low quantum efficiency of the IR detectors used, a narrow spectral tuning range, and a low signal-to-noise ratio. Nonlinear interferometry can overcome these limitations inherent in classical approaches.

Nonlinear interferometry is based on the process of spontaneous parametric down conversion (SPDC) [3] in two or more nonlinear crystals. As a result, a laser pump photon decays in a medium with nonlinear susceptibility into a pair of correlated photons, one of which is called the signal photon and the other an idler photon. In a highly nondegenerate SPDC photon generation regime, a signal photon can be generated in the optical or near-IR range, and the corresponding idler photon will be in the mid-IR range. Interference between pairs of photons in a SPDC, initially separated in time or space, occurs due to the fulfillment of the photon indistinguishability condition [4,5]. Nonlinear interferometry makes it possible to perform sample metrology in a wide IR range by recording correlated photons in the visible or near-IR range. This method does not require the use of IR detectors, significantly increasing detection efficiency and enabling research in the longer wavelength range of the electromagnetic spectrum.

This paper demonstrates a nonlinear interferometry method for metrology in the mid-IR range, using silver thiogallate ($AgGaS_2$) as the crystal. It enables metrology down to 12 µm, while recording only signal photons up to 1 µm.

Список литературы

[1] *D.A. Kalashnikov, A.V. Paterova, et al.*, Infrared spectroscopy with visible light. Nature photonics. **10**, p.98-101 (2016).

[2] *A.V. Paterova, S.M. Maniam, H. Yang, et al.*, Hyperspectral infrared microscopy with visible light. Sci. Adv. **6**, 44 (2020).

[3] *D.N. Klyshko, A.N. Penin, B.F. Polkovnikov*, Parametric luminescence and light scattering on polaritons. JETP Letters. **11**, p.11-14 (1970).

[4] *L. J. Wang, X. Y. Zou and L. Mandel*, Induced coherence without induced emission. Phys.Rev. **44**, 4614–22 (1991).

[5] *L. J. Wang, X. Y. Zou and L. Mandel*, Induced coherence and indistinguishability in optical interference Phys. Rev. Lett. **67**, 318–21 (1991)

Dispersion analysis of $AgGaS_2$ crystal in a broad mid-infrared range by spontaneous parametric down-conversion

Evgeniy Zatsepin[1*], Alexander Veselovskiy[1,2], Artem Sabanin[1], Dmitry Badikov[3], Galiya Kitaeva[1,2], Sergei Kulik[1,2], Anna Paterova[1]

[1] *Laboratory of Quantum Engineering of Light, South Ural State University, Chelyabinsk 454080, Russia*
[2] *Faculty of Physics, M. V. Lomonosov Moscow State University, Moscow, 119991, Russia*
[3] *High Technologies Laboratory, Kuban State University, Krasnodar 350040, Russia*
*E-mail: zatsepines@susu.ru

Аннотация

A method for measuring the dispersion of nonlinear crystals based on the effect of spontaneous parametric down-conversion (SPDC) is presented. The effectiveness of this method is shown using the example of an $AgGaS_2$ crystal, whose refractive index is known up to 10.6 μm and has been refined for the range of 10-22 μm. Shown that the theoretical spectra calculated taking into account the new refractive indices fully correspond to experimental spectra that had not previously been involved in calculations.

Traditional methods for measuring the dispersion characteristics of nonlinear crystals have a number of limitations related to the need for direct detection of infrared (IR) radiation and a relatively narrow operating spectral range. This imposes certain requirements on the efficiency of IR radiation detectors and the signal-to-noise ratio in measurements. We propose a method based on the effect of SPDC [[1]-[2]] and the analysis of the spectra of signal photons of SPDC, which are in the visible and near-infrared range.

The frequency-angular spectrum of SPDC contains complete information about the dispersion of a nonlinear crystal at frequencies that correspond to the conditions for generating this effect. Using several spectra of idle SPDC photons at different synchronism angles, it is possible, by composing a system of equations, to solve the inverse problem and calculate the ordinary and extraordinary refractive indices of the studied crystal in the region corresponding to idle SPDC photons in the mid- and far-IR ranges.

By analyzing several SPDC spectra corresponding to different synchronism angles, it is possible to estimate the effective refractive indices with high accuracy, as well as calculate n_e and n_e by minimizing expression (1):

$$n_{exp}(\lambda_i, \theta_j) - sqrt([\frac{cos^2(\theta_j)}{n_o^2(\lambda_i)} - \frac{sin^2(\theta_j)}{n_e^2(\lambda_i)}]^{-1}) \to 0 \quad (1)$$

where, $n_{exp}(\lambda_i, \theta_j)$ is a matrix consisting of experimentally obtained effective refractive indices.

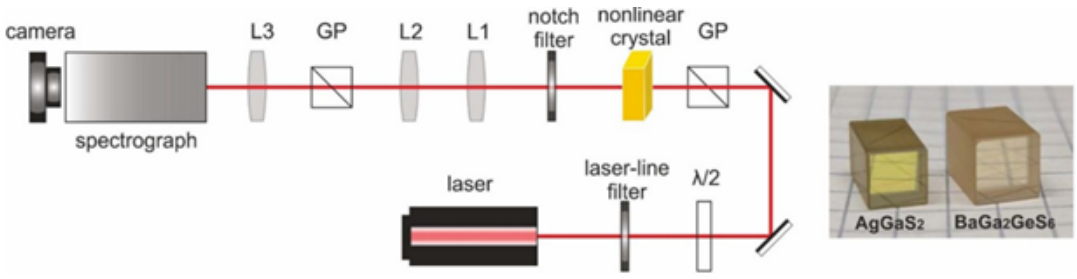

Рис. 1: Scheme of the experimental setup. A CW diode laser at 786.7 nm pumps AGS (type-I) and BGGS (type-II) nonlinear crystals configured for non-degenerate SPDC. The pump polarization is controlled using a half-wave plate ($\lambda/2$) and a Glan–Thompson (GP) prisms, and the residual pump light is suppressed by a notch filter. The SPDC signal is focused into a prism spectrograph to record its wavelength-angular spectrum with a CMOS camera. The photo at the right-hand side of the figure corresponds to $AgGaS_2$(AGS) and $BaGa_2GeS_6$(BGGS) nonlinear crystals.

Fig. 1 shows a scheme of the experimental setup employed for recording the spectra of signal SPDC photons. A continuous wave (CW) diode laser (with 786.7 ± 0.2 nm wavelength, 40 mW power) is used as a pump source for nonlinear crystals.

Next, we measured the frequency-angular spectra of AGS and BGGS crystals and compared them with the theoretical ones. Fig. 2 shows that the measured SPDC spectra extend to wavelengths corresponding up to 23 μm for idle photons, where there is no literature data on dispersion [[3]-[4]]. This means that the current Sellmeier equations for AGS and BGGS crystals have limitations and are unable to correctly describe the dispersion, and hence the SPDC spectra.

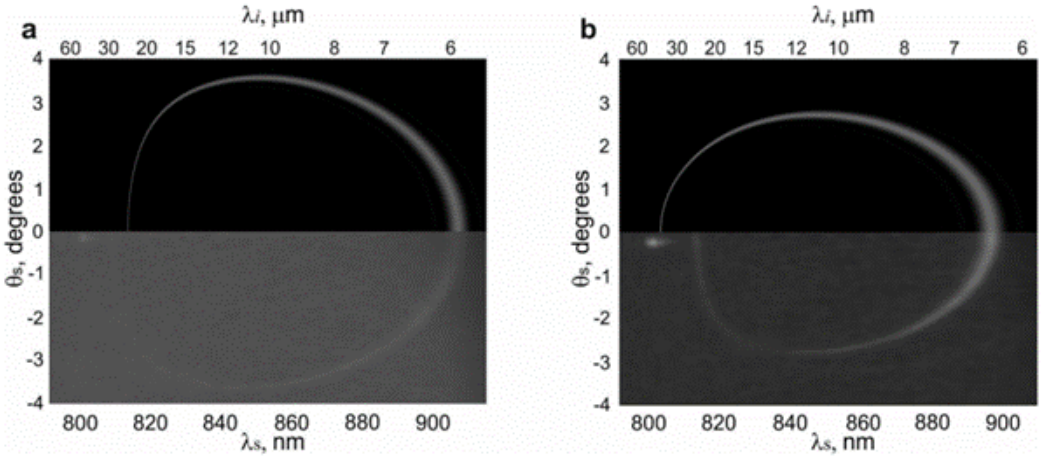

Рис. 2: Theoretical and experimental data for (a) AGS and (b) BGGS crystals. The lower halves of the graphs show the experimentally measured results, while the upper halves correspond to the theoretical spectra. The bottom x-axis in all plots corresponds to the detected signal wavelength, whereas the top x-axis indicates the conjugate idler wavelength in the mid-IR range.

Frequency-angular spectra were obtained for the AGS crystal at $\theta_c = 48.40^\circ \pm 0.04^\circ$, $51.60^\circ \pm 0.04^\circ$, and $53.40^\circ \pm 0.04^\circ$, respectively. The system of equations was compiled and the ordinary and unusual refractive indices were calculated, see Fig. 3. The new Sellmeier coefficients accurately describe the refractive indices over a wide spectral range from the visible region up to 22 μm with the exception of the regions with scattering on polaritons[[5]], that are not included in the approximation.

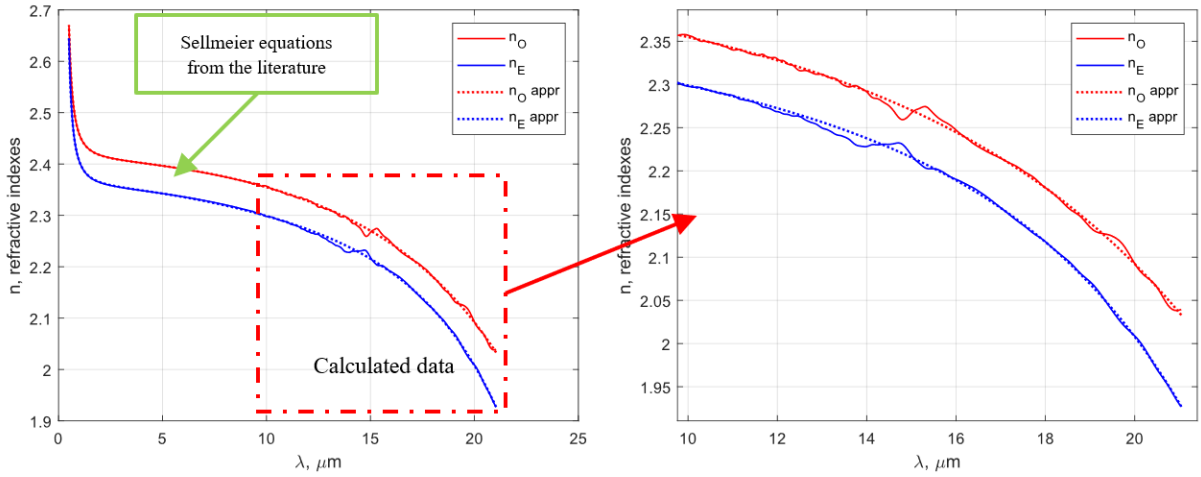

Рис. 3: Refractive indices fitted with Sellmeier equations. Solid curves before 10.6 μm correspond to Sellmeier equations from Refs. Solid curves beyond 10.6 μm show calculated ordinary and extraordinary refractive indices in our measurements. Dotted curves show the approximations with new Sellmeier coefficients.

After clarifying the refractive indices, the theoretical frequency-angular spectrum of the SPDC was constructed for the angle $\theta_c = 43.03 \pm 0.04^\circ$ and compared with the experimental one, which did not participate in the recent calculations, see Fig. 4.

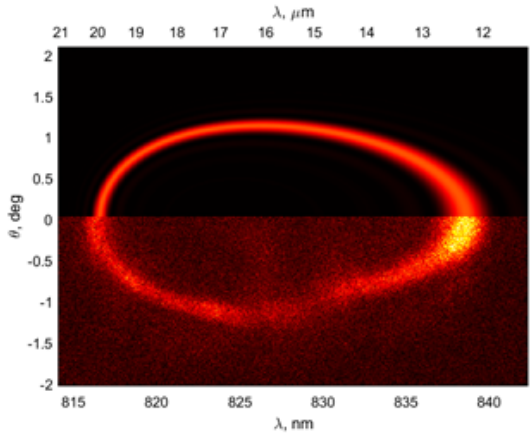

Рис. 4: Experimental and theoretical spectra of signal SPDC photons for the case $\theta_c = 43.03^\circ \pm 0.04^\circ$. The theory at the upper half of the spectrum is calculated using new Sellmeier equations. The lower half of the graph shows the experimental data. The lower x-axis shows the detected wavelengths of the signal SPDC photons, while the corresponding idler photon wavelengths are shown on the upper x-axis.

Acknowledgement

This work is supported by the Government of the Russian Federation (Grant No. 075-15-2025-018, dated 27 February 2025) and by South Ural StateUniversity, where the experimental data is collected and analytical simulations are conducted.

E Z, A S, and A P are grateful to Viktor Khristenko's grant program 'Step into the Future' for supporting the theoretical simulations of the work.

E Z, A V, G K, S K and A P also acknowledge support from the State Assignment FENU-2024-0002, which enabled the detailed analysis and interpretation of the experimental results.

Список литературы

[1] *M. H. Rubin, D. N. Klyshko, Y. H. Shih, and A. V. Sergienko*, Theory of two photon entanglement in type-II optical parametric down-conversion. Physical Review A **50(6)**, pp. 5122-5131 (1994).

[2] *L. J. Wang, X. Y. Zou, and L. Mandel*, Induced coherence without induced emission. Phys. Rev. Lett. A **44**, 4614 (1991).

[3] *K. Kato, T. Okamoto, S. Grechin, and N. Umemura*, New Sellmeier and Thermo-Optic Dispersion Formulas for $AgGaS_2$. Crystals, **9(3)**, 129 (2019).

[4] *V.V. Badikov, et al*, Crystal growth and characterization of new quaternary chalcogenide nonlinear crystals for the mid-IR: $BaGa_2GeS_6$ and $BaGa_2GeSe_6$. Opt. Mat. Exp. **6(9)**, 2933 (2016).

[5] *Y. N. Polivanov*, Raman scattering of light by polaritons. Sov. Phys. Usp. **21**, 805 (1978).

Single artificial atom sound amplification by stimulated emission radiation

Peter Shlykov[1,2*], **Sanduleanu Shtefan**[1],
Oleg Astafiev[2,1],
Bolgar Alexey[1]

[1] *Moscow Institute of Physics and Technology, Dolgoprundiy, Russia*
[2] *Skolkovo Institute of Science and Technology, Moscow, Russian Federation*
*E-mail: shlykov.piu@phystech.edu

Abstract

Lasing is a classical quantum optics effect with lots of applications. In this work we demonstrate the SASER (Sound Amplification by Stimulated Emission of Radiation) action by utilizing a surface acoustic wave (SAW) resonator on a quartz [1] coupled to a deliberately designed superconducting three-level quantum system (artificial atom), in which population inversion is realized [2]. The SASER operates at frequency above 3 GHz. Acoustic-to-electric signals are converted with piezo-electric effect and the circuit elements: the artificial atom and input/outputs are coupled via the acoustic waves. We found amplification of the waves and strong self-emission with a significant narrowing of the linewidth.

Introduction

The platform of superconducting artificial atoms enables realization of various quantum optic effects such as resonance fluorescence [3], quantum wave mixing [4] and others [5]. This success in circuit quantum electrodynamics is based on the tunable, strong light-matter interactions these systems provide [3].

Recently, several groups have demonstrated Quantum Acoustodynamics (QAD) with artificial atoms, where electromagnetic waves are replaced by acoustic ones and photons by phonons [6]. One of the key elements in the QAD experiments with surface acoustic waves is a mechanical resonator, formed by metal stripes-Bragg mirrors. These resonators can reach frequencies up to a few gigahertz and quality factors up to 10^5.

The laser is based on the universal principle of stimulated emission within an electromagnetic resonant cavity containing a gain medium, represented by a system of atoms with population inversion mechanism. In particular, the lasing effect with a single artificial atom has previously been demonstrated in superconducting systems [5]. By coupling a three-level artificial atom with adjusted parameters to an acoustic resonator lasing in the acoustic system can be established.

Device

Our device is based on the following achievements: (i) a SAW phononic crystal with resonant acoustic fields confined in a small 2D volume in both x and y directions; (ii) population-inversion mechanism in a superconducting three-level artificial atom, made in the flux-qubit geometry (a loop with a series of junctions); (iii) physically strong coupling of the artificial atom to the acoustic field of the SAW resonator; (iv) additional (strong) coupling of the artificial atom to an electric field of the transmission line – 1D open space.

Results

From notch-type transmission measurements we estimate relaxation rates $\Gamma_{eg}/2\pi = 40$ MHz, $\Gamma_{fg}/2\pi = 8$ MHz, $\Gamma_{fe}/2\pi = 80$ MHz. The resonator's fundamental mode with frequency $\omega/2\pi = 3.2104$ GHz exhibits decay rates of $\kappa_0/2\pi = 0.13$ MHz (single-phonon) and $\kappa_m/2\pi = 0.094$ MHz (multi-phonon regime).

The device was characterized near the flux bias point where vacuum Rabi splitting is observed in the resonator's transmission spectrum (Fig. 1a). The introduction of an additional microwave pump tone at

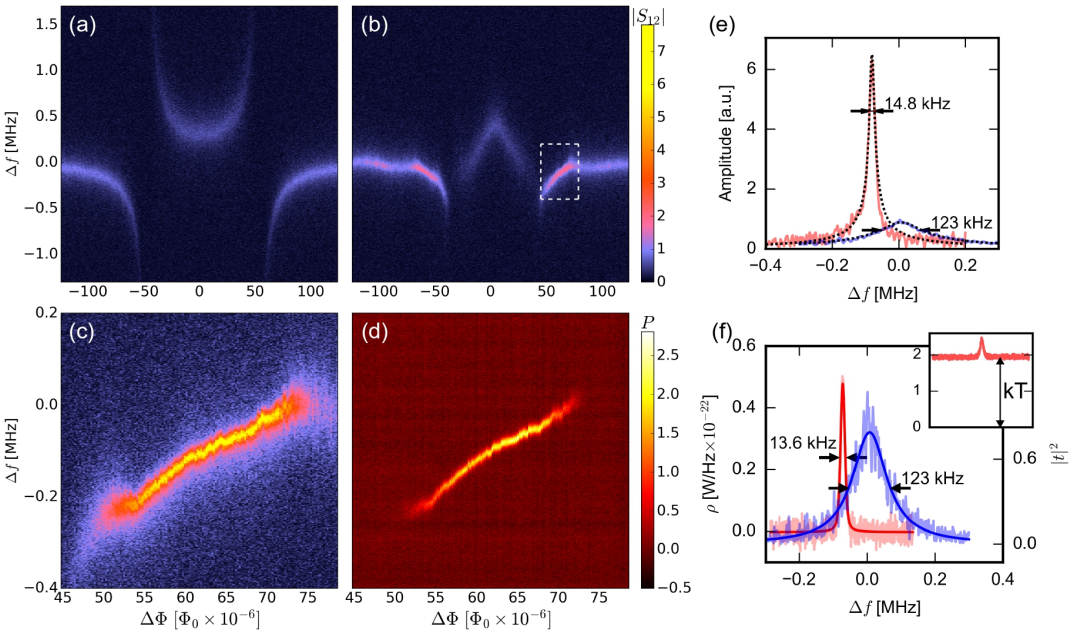

Figure 1: (a) Transmission single tone spectroscopy(STS) of the anticrossing between acoustic resonator and artificial atom from magnetic flux. (b) STS of the anticrossing with pump of the atom at transition frequency of $|f> \leftrightarrow |g>$. (c) Highlighted region of figure (b) with decreased probe tone power in STS. (d) Emission from the acoustic laser in the same region as on (c). (e) Comparison of transmission through the resonator with(red) and without(blue) pump of the atom. (f) Comparison of emission spectra of acoustic laser(red) with squared transmission through the resonator(blue)

the frequency ω_{fg} of the artificial atom dramatically changes the response: the anticrossing vanishes and is replaced by "hot-spots", where the transmission exceeds unity (Fig. 1b).

By reducing probe tone power to few photons we observe drastic change in transmission of the signal: the transmission band becomes narrower 8 times (Fig 1e) and the signal is amplified up to 7 times (Fig 1c). Measurements of the emission from the resonator also reveal narrowing of the resonator band: up to 9 times (Fig. 1f).

References

[1] *Bolgar, A. N., Sanduleanu, S. V., Strelnikov, A. Astafiev, O. V.*, High Quality Quasinormal Modes of Phononic Crystals for Quantum Acoustodynamics. J. Low Temp. Phys. 210, 366–376 (2023).

[2] *Astafiev, O. V. et al.*, Ultimate on-chip quantum amplifier. Phys. Rev. Lett. 104, 183603 (2010).

[3] *Astafiev, O. et al.*, Resonance fluorescence of a single artificial atom. Science 327, 840–843 (2010).

[4] *Dmitriev, A. Y. et al.*, Quantum wave mixing and visualisation of coherent and superposed photonic states in a waveguide. Nat. Commun. 8, 1352 (2017).

[5] *Astafiev, O. et al.*, Single artificial-atom lasing. Nature 449, 588–590 (2007).

[6] *Manenti, R. et al.*, Surface acoustic wave resonators in the quantum regime. Phys. Rev. B 93, 041411 (2016).

Multimode squeezed light generation by type-0 and type-II parametric down-conversion

Alexander Chudakov[1,2], **Vladislav Severin**[1], **Anastasia Poshevkina**[1,2], **Kirill Kuznetsov**[1,3], **Dmitry Kalashnikov**[1], **Polina Sharapova**[1,3]

[1] *Russian Quantum Center, Moscow, Russia*
[2] *Moscow Institute of Physics and Technology, Moscow Region, Russia*
[3] *Lomonosov Moscow State University, Moscow, Russia*
*E-mail: a.chudakov@rqc.ru

Аннотация

We studied both experimentally and theoretically multimode squeezed vacuum states of light generated via type-0 and type-II parametric down-conversion (PDC) in a PPKTP crystal pumped by a picosecond Ti: Sapphire laser. To characterize the multimode squeezed light, a theoretical analysis based on the Schmidt-mode theory was performed. In the experiment, a spatial light modulator was used to shape the local oscillator, characterize the modes and measure their squeezing. Using homodyne detection, squeezing and antisqueezing were measured in the first three modes of type-0 and type-II PDC. The highest squeezing values were achieved for the HG00 mode for both type-0 and type-II cases, which turned out to be 0.6 dB and 0.35 dB, respectively.

In this work, we study both theoretically and experimentally the multimode squeezed vacuum states of light generated via the type-0 and type-II parametric down-conversion (PDC) process in a PPKTP (periodically poled titanil phosphate) crystal pumped by a picosecond laser. In experiment, such states were realized using the pulsed Ti: Sapphire laser with an average output power of 0.9 W, a pulse repetition rate of 76 MHz and pulse duration of 2 ps, the central wavelength is 783 nm. This laser was applied to generate the second harmonic (the wavelength of 391.5 nm) inside the LBO (lithium triborate) crystal of 17 mm length. The second harmonic was then used to pump the 1 mm long PPKTP crystal to generate squeezed vacuum light through the type-0 and type-II PDC process, depending on the crystal used.

To measure squeezing, we realized the balanced homodyne detection scheme, where the part of the fundamental laser beam at 783 nm was used as the local oscillator (LO). The LO passed through the pulse shaper scheme based on the spatial light modulator (SLM) and dispersion grating in the folded zero-dispersion line geometry of the 4f-system. This scheme introduces the phase shift in the desired frequency component of the LO and thus sets the required frequency Schmidt mode.

This scheme makes it possible to convert the frequency spectrum to spatial before SLM, create the required spatial mode with an appropriate phase mask applied to the beam in the Fourier plane, and then transform back the spatial spectrum to frequency after reflection. Thus, the circuit allows one to form the necessary frequency Schmidt mode in the LO channel. In our work, phase masks were generated for the first three Gauss-Hermite modes in the same way as was done in [1], where depending on the displacement of the horizontal alternating gray level bands, a certain phase delay was applied to certain blocks of the SLM matrix. Examples of generated phase masks are shown in Fig. 1.

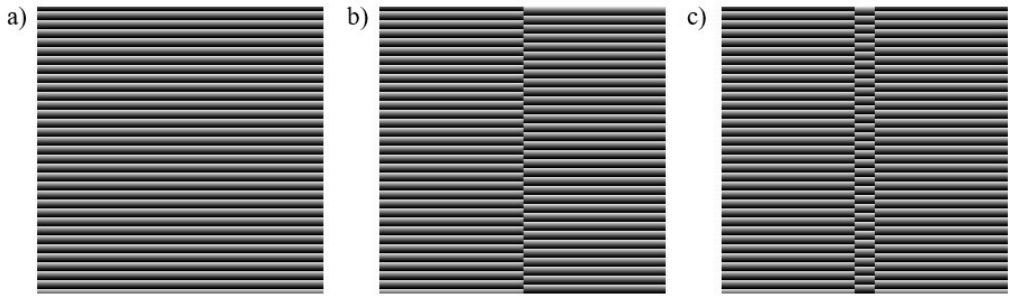

Рис. 1: Phase masks for the first three Gauss-Hermite modes: a) HG_{00}; b) HG_{01}; c) HG_{02}

To measure the squeezing parameter, the LO and the quantum light under study were mixed on a beam splitter in a 50:50 ratio to perform homodyne detection. The homodyne detector performed a procedure of subtracting signals from its two inputs, as a result, the output signal is proportional to the quadrature of the quantum light under study. After collecting statistics and processing data using an analog-to-digital converter (ADC) and the developed software, the variance V of the quadrature of squeezed light was calculated.

Taking into account the measured quadrature, the squeezing (antisqueezing) was estimated as

$$\eta = 10 \times log_{10}\left(\frac{V_m}{V_{vac}}\right), \tag{1}$$

where V_{vac} is the variance of the vacuum state quadrature, V_m is the minimal (maximal) variance of the multimode squeezed light quadrature under the study. Note that the shaped LO interacts only with the Schmidt mode of the same form, acting therefore as the filter.

The statistics collected during homodyne detection made it possible to plot the dependence of squeezing on time, which in this case is equivalent to a change in the LO phase. These graphs are shown in Fig. 2 for PDC type-0 (a) and PR mod type-II (b).

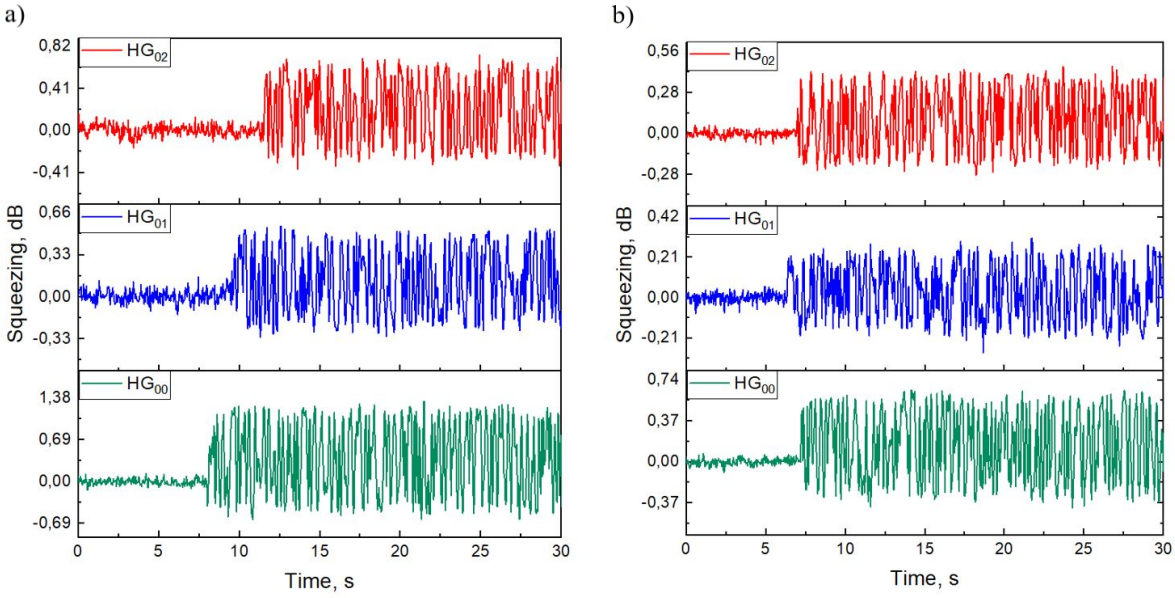

Рис. 2: Experimental squeezing in the first three modes of PDC: a) type-0; b) type-II

Also, we measured and analyzed the frequency spectra of both type-0 and type-II PDC. To measure the spectrum of the multimode squeezed light under study, a self-made spectrometer was used, which includes a diffraction grating, a focusing lens, and a camera. The broadband spectrum falling on the diffraction grating was decomposed into space, after which it was focused on the camera matrix.

In addition, we performed numerical simulations to characterize the multimode squeezed light source using the Schmidt-mode theory [2]. We decomposed the two-photon amplitude in the set of independent collective (Schmidt) modes and inspected their shapes depending on the experimental parameters. We constructed the intensity spectra and squeezing in modes depending on the losses in the system.

Список литературы

[1] *L. La Volpe [et al.]*, Multimode single-pass spatio-temporal squeezing. Optics Express, **28**, 8 (2020).

[2] *P. Sharapova, [et al.]*, Schmidt modes in the angular spectrum of bright squeezed vacuum. Phys. Rev. Lett. **94**, 017402 (2015).

Krasnaya Polyana, Sochi, Russia March 1 – March 7, 2026
9th International School on Quantum Technologies

Non-Gaussianity Transfer and Generation Lambda-Type Light-Matter Interface

J.C. Benjamin Luna-Veronico[1,2*], Kirill Tikhonov[1,2,3,4], Polina Sharapova[5], Olga Tikhonova[6]

[1] *St. Petersburg State University, 7/9 Universitetskaya Nab., 199034 St. Petersburg, Russia*
[2] *Centre for Interdisciplinary Basic Research, HSE University, 190008, St. Petersburg, Russia*
[3] *Russian Quantum Center, Skolkovo, Moscow 143025, Russia*
[4] *P.N. Lebedev Physical Institute, Leninsky prospekt 53, 119991 Moscow, Russia*
[5] *University of Paderborn, Warburger Straße 100, D-33098 Paderborn, Germany*
[6] *Moscow State University, Leninskie Gory, 1, Moscow, 119991 Russia*
*E-mail: benjamin_lunaveronico@mail.ru

Abstract

The interaction of quantum light with multilevel atomic systems presents a rich landscape of non-classical phenomena, yet its theoretical description is often hindered by the exponential growth of the Hilbert space. In this work, we investigate a three-level Λ-system interacting with two quantized light fields. To overcome the infinite hierarchy problem inherent in the system of differential equations governing the light-matter interaction, we employ the cumulant expansion method. Beyond solving the equations of motion, we demonstrate that cumulants of order three and higher provide direct access to the non-Gaussian character of the quantum states. This approach significantly reduces computational overhead by bypassing the need to calculate the full density matrix and the subsequent integration of the Wigner function, allowing for the efficient characterization of quantum statistical properties directly from the solutions of the equations of motion.

Introduction

Three-level systems (3LS) in the Λ-configuration are fundamental to quantum optics, underpinning phenomena such as coherent population trapping (CPT) and electromagnetically induced transparency (EIT) [1]. While these effects are well-understood in the semiclassical regime, the nonlinear interaction with quantized light, such as squeezed or Fock states, introduces complex photon statistics and correlations that require a fully quantum-mechanical treatment [2].

A major challenge in modeling these systems is the "hierarchy problem" arising from the light-matter interaction. The equation of motion (EoM) for an Nth-order expectation value couples to $(N+1)$th-order (or higher) quantities, leading to an infinite chain of coupled differential equations [3]. Standard approaches often rely on the density matrix formalism in a truncated Fock basis[1]. However, this method becomes computationally intractable for high photon numbers or multimode fields due to the size of the density matrix.

In our work, we address this challenge by applying the method of cumulant expansions. We utilize them to fundamentally reformulate the problem. This method allows for a systematic truncation of the hierarchy by retaining correlations only up to a physically relevant order, thus rendering the system solvable without assuming a low photon number limit.

Non-Gaussianity and Cumulants

A key insight of this work is the direct link between high-order cumulants and the non-Gaussianity of the optical state. In the cumulant formalism, a state is Gaussian if and only if all cumulants of order $C \geq 3$ vanish[4]. Consequently, the presence of non-zero third or higher-order cumulants is a signature of non-Gaussian statistics. We exploit this property to evaluate the non-classicality of the generated light. Standard measures of non-Gaussianity, such as the negativity of the volume of the Wigner function, typically require the reconstruction of the full density matrix $\hat{\rho}$, followed by a Fourier transform to obtain the Wigner function $W(\alpha)$, and finally an integration over phase space [5]

Instead, we derive equations of motion governing the cumulant dynamics, which we then employ for our calculations. Since this method yields the time-evolution of these cumulants directly, we can evaluate the degree of non-Gaussianity immediately after solving the equations of motion.

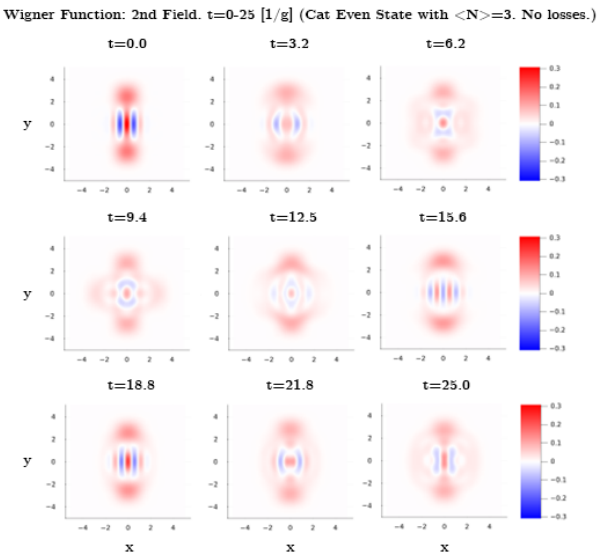

Figure 1: Wigner Function of one of the light fields. Generation of Non-Gaussian States (Compass State).

Results

The primary advantage of this method is the drastic reduction in computing time. Calculating the complete density matrix for fields with substantial photon numbers involves solving for $\mathcal{O}(N_{phot}^4)$ elements (for two modes), which is often prohibitive. In contrast, the number of relevant cumulants scales much more favorably.

By expressing the negativity of the Wigner function's volume in terms of cumulants, we avoid the intermediate steps of density matrix reconstruction and phase-space integration. Our results confirm that this cumulant-based metric accurately tracks the development of non-Gaussian features, such as those arising during the collapse and revival of Rabi oscillations or dark-state formation, at a fraction of the computational cost required by full density matrix simulations. This efficiency opens new avenues for exploring high-photon-number regimes and complex multimode interactions in quantum optical systems.

References

[1] *Rose H., Popolitova D.V., Tikhonova O.V., Meier T., Sharapova P.R.*, Dark-state and loss-induced phenomena in the quantum-optical regime of Λ-type three-level systems. Phys. Rev. A. Vol. 103. P. 013702 (2021).

[2] *Kira M., Koch S.W.*, Cluster-expansion representation in quantum optics. Phys. Rev. A. Vol. 78. P. 022102 (2008).

[3] *Rose H., Tikhonova O.V., Meier T., Sharapova P.R.*, Theoretical analysis of correlations between two quantum fields exciting a three-level system using the cluster-expansion approach. Proceedings Vol. 11999, Ultrafast Phenomena and Nanophotonics XXVI; P. 1199905 (2022).

[4] *Schack R., Schenzle A.*, Moment hierarchies and cumulants in quantum optics. Phys. Rev. A. Vol. 47. P. 3847 (1990).

[5] *Siyouri F., El Baz M., Hassouni Y.*, The negativity of Wigner function as a measure of quantum correlations. Quantum Inf. Process. Vol. 15. P. 4237–4252 (2016).

Krasnaya Polyana, Sochi, Russia March 1 – March 7, 2026
9th International School on Quantum Technologies

Morphing Supermodes of Multimode Squeezed Light in Dispersive SPOPO

Danil Malyshev[1,2*], **Kirill Tikhonov**[2], **Valentin Averchenko**[2]

[1] *Moscow Institute of Physics and Technology, Moscow, Russia*
[2] *Saint-Petersburg State University, St. Petersburg, Russia*
*E-mail: malyshev.wrk@yandex.ru

Abstract

The work is devoted to the generation of the multimode squeezed light in the synchronously pumped optical parametric oscillator (SPOPO) in the presence of group-velocity dispersion using the light supermode approach based on the Bloch–Messiah decomposition. Dispersion and cavity detuning are shown to significantly affect the structure of intermode correlations and the resulting squeezing spectra. To characterize the multimode properties of the generated radiation, we employ morphing supermodes theory serving as a convenient framework providing a compact description of multimode squeezed states in realistic dispersive optical systems.

Introduction

Squeezed light is an essential resource in the area of advanced quantum technologies. Consequently, the development of efficient methods for the generation, control, and detection of squeezed states remains a central problem. One of the most widely used platforms for producing multimode squeezed light is the synchronously pumped optical parametric oscillator (SPOPO), where pump photons are converted into correlated signal–idler pairs via nonlinear SPDC process inside the optical cavity.

In the real SPOPO setup, effects such as group-velocity dispersion introduce additional spectral correlations, so that the eigenmodes of the parametric process no longer diagonalize the system dynamics. As a consequence, squeezing is redistributed among frequency-dependent superpositions of modes that continuously vary across the spectrum. This motivates the introduction of morphing supermodes, which form a natural basis accounting for the full dispersive dynamics of the system. The morphing-mode description allows one to identify independently squeezed degrees of freedom and reveals fundamental limitations of standard homodyne detection in dispersive multimode regimes.

Theoretical description

The intracavity field of a SPOPO is described by Heisenberg–Langevin equations for the parametric modes, which can be described using slowly varying operators $a_n(T)$. The mentioned evolution depends on a variety of parameters likewise mode-depependent coefficients of the cavity losses γ_n, detunings Δ_n, parametric gain λ_n, and the mode coupling C_{nm} accounting for the dispersive correlations [1]. Due to this coupling, the parametric eigenmodes $a_n(T)$ no longer diagonalize the system dynamics. The latter indicates the need to introduce a new diagonal basis – morphing supermodes.

Introducing field quadratures and moving to the frequency domain leads to the input–output relation [2]

$$R_{\text{out}}(\Omega) = S(\Omega) R_{\text{in}}(\Omega), \qquad S(\Omega) = \sqrt{2\Gamma}(i\Omega + \Gamma - M)^{-1}\sqrt{2\Gamma} - I \tag{1}$$

where the transfer matrix $S(\Omega)$ fully characterizes the system dynamics. In the simplest two-mode case, the cavity may be treated as maintaining only two of Hermite-Gaussian modes – the 0th and the 2nd. The matrix M then has the block structure

$$M = \begin{pmatrix} \operatorname{Im}[G+F] & \operatorname{Re}[G-F] \\ -\operatorname{Re}[G-F] & -\operatorname{Im}[G+F] \end{pmatrix}, \tag{2}$$

with

$$G = \begin{pmatrix} C_{00} - \Delta & C_{02} \\ C_{20} & C_{22} - \Delta \end{pmatrix}, \qquad F = \begin{pmatrix} i\lambda_0/2 & 0 \\ 0 & i\lambda_2/2 \end{pmatrix}, \qquad \Gamma = \begin{pmatrix} \gamma_0/2 & 0 \\ 0 & \gamma_2/2 \end{pmatrix}. \tag{3}$$

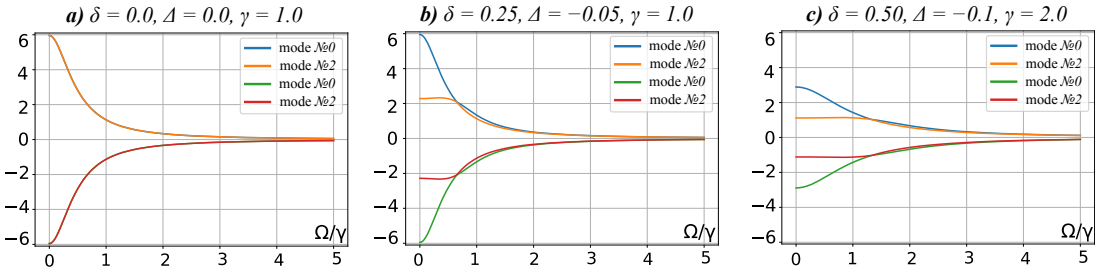

Figure 1: Morphing supermodes squeezing spectrum in case of equally amplified parametric modes $\lambda_n = 1$. System parameters: a) $\delta = 0.0$, $\Delta = 0.0$, $\gamma = 1.0$; b) $\delta = 0.25$, $\Delta = -0.05$, $\gamma = 1.0$; c) $\delta = 0.50$, $\Delta = -0.1$, $\gamma = 2.0$.

Here the off-diagonal elements $C_{02} = C_{20}$ originate from group-velocity dispersion and provide coherent coupling between the two parametric modes.

For all values of parameters, the transfer matrix $S(\Omega)$ is Ω-symplectic. That property guarantees the existence of the analytic Bloch–Messiah decomposition,

$$S(\Omega) = U(\Omega)\,\Sigma(\Omega)\,V^{\dagger}(\Omega), \tag{4}$$

where at all Ω values the above decomposition forms a regular SVD, and $\Sigma(\Omega)$ is diagonal matrix formed with th quadrature squeezing levels.

Morphing supermodes are defined by transforming the output field into the basis set by the unitary symplectic matrix $U(\Omega)$. In this basis, the squeezing transformation becomes diagonal, and each morphing supermode corresponds to an independent quantum harmonic oscillator, whose profile is given by

$$s_k(\Omega, \omega) = \sum_n U^*_{n,k}(\Omega)\mathrm{HG}_n(\omega), \tag{5}$$

where $\mathrm{HG}_n(\omega)$ is the n-th Hermite-Gaussian function. Thus, unlike standard parametric modes, morphing supermodes are frequency-dependent coherent superpositions of cavity modes whose composition continuously changes across the spectrum (or each round-trip of the cavity in the time domain), reflecting the influence of dispersion and detuning.

Results

The squeezing spectrum is therefore fully determined in the morphing-mode basis and can be controlled by varying experimentally accessible parameters such as cavity detuning Δ_n, parametric gain λ_n, and the dispersion strength, which is governed here by δ coefficient. Moreover, by modifying the system parameters one can vary the flat-band range, it is possible to obtain nearly flat-band squeezing spectrum in a broad range of Ω values, see figure 1. The obtained quantum light is highly desired in the protocols of non-Gaussian stated production, as well as in the quantum metrology problems [3].

Acknowledgments

This study was carried out under the financial support of the Russian Science Foundation (grant №24-22-00318).

References

[1] *Averchenko V. A., Malyshev D. M., and Tikhonov K. S.*, Effect of group-velocity dispersion on the generation of multimode pulsed squeezed light in a synchronously pumped optical parametric oscillator. New J. Phys. Vol. 26(12). P. 123017 (2024).

[2] *Gouzien E., Tanzilli S., D'Auria V., and Patera G.*, Morphing supermodes: A full characterization for enabling multimode quantum optics. Phys. Rev. Lett. Vol. 125(10) (2020).

[3] *Asavanat W. et al.*, Generation of highly pure Schrodinger's cat states and real-time quadrature measurements via optical filtering. Opt. Express. Vol 25(26). P. 32227 (2017).

Non-Gaussianity and Complex Superpositions in Cross-Kerr Systems with Squeezed Inputs

E.I. Mingazhitdinov[1*], **O.V. Tikhonova**[1,2]

[1] *Sarov Branch of Lomonosov Moscow State University, Sarov, Russia*
[2] *Faculty of Physics, Lomonosov Moscow State University, Moscow, Russia*
*E-mail: emildave@mail.ru

Abstract

Universal continuous-variable quantum computing requires deterministic non-Gaussian operations and specific resource states, such as Schrödinger cats and cubic phase states [1]. Standard generation methods are limited by the weak nonlinearity of optical media. In this work, we investigate a scheme [2] based on measurement-induced cross-Kerr nonlinearity, presenting a significant advancement over previous approaches.

Unlike earlier studies that utilized coherent signals, we investigate a regime where both input modes (signal and ancillary) are prepared in displaced squeezed vacuum states. We demonstrate that pre-squeezing the signal mode acts as a critical resource that synergizes with the filtering effect of the ancilla. This allows overcoming the limitations of previous schemes and generating states with more complex interference structures, as illustrated in Fig. 1.

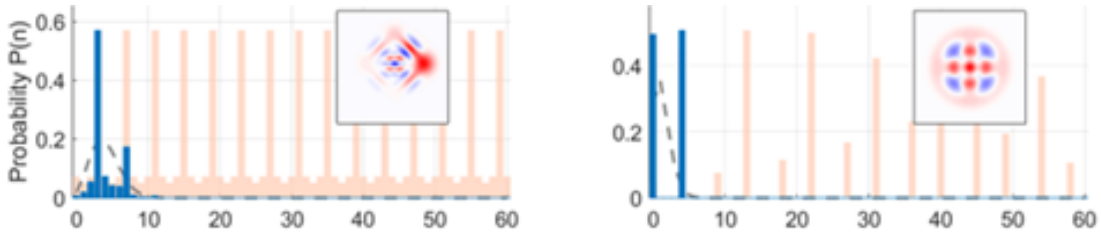

Figure 1: Fock state distributions and Wigner function insets of the generated states: (a) characteristic interference pattern and negativity due to ancilla squeezing; (b) optimized synthesis of the $(|0\rangle + |4\rangle)/\sqrt{2}$ superposition.

Global optimization of parameters for both modes has revealed new generation regimes. Specifically, as shown in Fig. 1(b), we demonstrate the capability to synthesize structured superpositions, such as the state $(|0\rangle + |4\rangle)/\sqrt{2}$, with fidelity $F > 0.99$. This result was unattainable using a classical coherent input. Furthermore, we confirm the achievement of deep nonlinear squeezing (cubic quadrature variance below -10 dB), which is critical for non-Gaussian quantum gates [3], opening new perspectives for quantum optical state engineering.

References

[1] *M. Mirrahimi et al.*, New J. Phys. **16**, 045014 (2014).

[2] *T. Tyc and N. Korolkova*, New J. Phys. **10**, 023041 (2008).

[3] *S. Lloyd and S. L. Braunstein*, Phys. Rev. Lett. **82**, 1784 (1999).

Frequency comb generation in a system with semiconductor laser coupled to two ring microresonators

Alina Golodukhina[1,2*], **Veronika Beliaeva**[1,2], **Artem Shitikov**[1], **Dmitriy Chermoshentsev**[1,3], **Igor Bilenko**[1,2]

[1] *Russian Quantum Center, Skolkovo, Moscow, Russia*
[2] *Faculty of Physics, Lomonosov Moscow State University, Moscow, Russia*
[3] *Moscow Institute of Physics and Technology, Dolgoprudny, Moscow Region, Russia*
*E-mail: golodukhina.an23@physics.msu.ru

Abstract

One laser source and one microresonator are usually used for Kerr frequency comb generation. In our study, a single laser simultaneously excites the modes of two ring resonators located on a single integrated platform, the backscattering from each of them returns to the laser implementing the SIL effect. This opens up new possibilities for generating dual frequency combs and multimode quantum compression in them.

Kerr-induced frequency combs allow for record-breaking precision in the measurement of optical frequencies and have applications in spectroscopy, metrology, integrated photonics, aerospace engineering [1]. Pumping a high quality factor microresonator ring (MRR) with Kerr nonlinearity by continuous laser radiation is One of the most effective ways to generate such microcombs. Due to the four-wave mixing process, pump photons are redistributed between the MRR modes, thereby forming an optical frequency comb [2]. The effect of locking the laser diode output frequency to the high-Q MRR mode frequency (the self-injection locking, SIL) allows for significant suppression of phase noise in the radiation and a substantial narrowing of the spectral linewidth [3]. As previously demonstrated, multimode quantum compression is possible in optical frequency combs generated in integrated ring microresonators [4].

A conventional setup for Kerr optical combs generation utilizes a single pump source and a single MRR. In this work we studied the system with two separated Si_3N_4 microresonators (with free spectral range (FSR) about 150 GHz and anomalous dispersion) on a single chip pumped with one DFB laser. The schematic depiction of the experiment is demonstrated in Fig. 1. The laser is butt-coupled to photonic integrated chip, where multimode interferometer (MMI) divides the input radiation into two coherent signals of equal intensity. The system of microheaters enables control and fine tuning the effective resonance frequency of each microring.

In the experiment the laser switched to SIL regime by fine tuning the MMRs resonance frequencies and the phase of modes propagating to each MRR individually. Within this study we observed several remarkable regimes, including: 1. Frequency locking of one microresonator and Kerr comb generation in the second; 2. Simultaneous Kerr comb generation in two microcavities (with different FSR); 3. Generation of a frequency comb inside a laser [5]. The optical spectra of a combination of Kerr microcomb and the multimode SIL is presented in Fig. 2. We measured output signal from each exit individually to analyze the dynamics in each MMR. In the top ring spectrum (Fig. 2a), the multimode regime is observed with parasitic lines. In the bottom ring the dominant effect is Kerr comb generation (Fig. 2b).

Thus, in our work, we studied new regimes of nonlinear interaction between a laser diode and a system of two microresonators. This significantly expands the scope of application of the self-injection locking effect and opens up opportunities for the further creation of compact double-comb sources and the study of quantum effects in them.

Figures

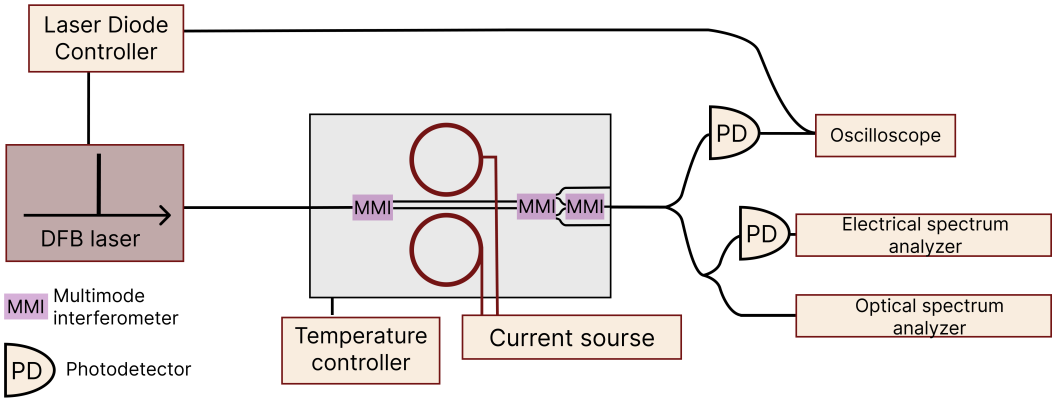

Figure 1: Scheme of the experimental setup

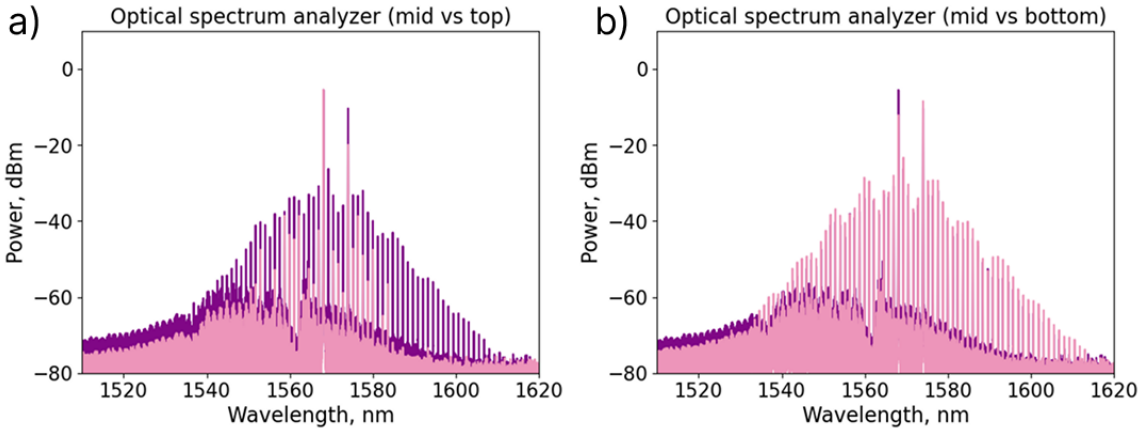

Figure 2: Combination of frequency microcomb and the multimode SIL. Comparison between middle output signal to (a) top and (b) bottom output signals

References

[1] *M. Kondratiev, V. E. Lobanov, A. V. Cherenkov, A. S. Voloshin, N. G. Pavlov, S. Koptyaev, and M. L. Gorodetsky*, "Self-injection locking of a laser diode to a high-Q WGM microresonator", Opt. Express 25, 28167–28178 (2017).

[2] *Chembo, Yanne K.*, "Kerr optical frequency combs: theory, applications and perspectives", Nanophotonics, vol. 5, no. 2, pp. 214-230 (2016).

[3] *Herr, T., Hartinger, K., Riemensberger, J. et al.*, "Universal formation dynamics and noise of Kerr-frequency combs in microresonators", Nature Photon 6, 480–487 (2012).

[4] *Yang, Z., Jahanbozorgi, M., Jeong, D., Sun, S., Pfister, O., Lee, H., & Yi, X.*, "A squeezed quantum microcomb on a chip", Nature Communications, 12(1), 4781 (2021).

[5] *Sokol, D. M., Dmitriev, N. Y., Chermoshentsev, D. A., Koptyaev, S. N., Masalov, A. V., Lobanov, V. E., & Shitikov, A. E.*, "Four-wave mixing in a laser diode gain medium induced by the feedback from a high-Q microring resonator", Photonics Research, 13(1), 59-68 (2024).

Benchmarking M-ary Quantum Random Number Generators in Advanced Optical Experiments

Anna Kretova[1*], **Daniil Reshetnikov**[1], **Anastasia Fominova**[1], **Kirill Tikhonov**[1]

[1] *Saint-Petersburg State University, Saint-Petersburg, Russia*
*E-mail: kretova.anya.a@gmail.com

Abstract

Random number sequences (RNSs) play a vital role in diverse scientific and engineering applications. They are critical to the integrity of classical and quantum cryptography, the accuracy of mathematical modeling and Monte Carlo simulations, and the core mechanics of fields as varied as secure communications and statistical sampling. The generation of truly random numbers depends on the intrinsic randomness of a physical process and is typically limited by electronic bandwidth and signal processing rates. Therefore, the most feasible solution for high-speed, real-time generation is to employ several parallel sources with lower individual entropy rates. In our work, we implement a multiplexing scheme to create a fast quantum random number generator, structurally tailored for high-bit-rate data transfer.

High-quality random number sequences (RNS) serve as a critical resource across science and engineering, being utilized for the sake of securing cryptographic systems, the accuracy of physical simulations, the validity of statistical methods and much more [1]. Among physical RNGs, quantum random number generators (QRNGs) based on the fundamental unpredictability of quantum processes are considered the top preference for achieving essential randomness quality.

However, the performance of practical QRNGs is often limited by the characteristics of their components. As QRNGs mostly operate in single-photon mode, a key constriction is the dead time of single-photon detectors, which significantly reduces the maximum generation rate. A promising method to temper this limitation is using multiple detectors in parallel, so called detector multiplexing. As discussed in prior research [2], such multiplexing schemes can effectively reduce the impact of individual detector dead time. Furthermore, multiplexed architectures allow to increase entropy yield beyond the binary domain. By processing signals from multiple detectors, one can generate random sequences over M-ary alphabets, potentially extracting more randomness per unit time.

In this work, we explore several multiplexed optical schemes designed for this purpose. Our primary focus is a novel hybrid source configuration, which we proposed and investigated in detail in our prior work [3]. This source combines a fast-rate semiclassical (coherent) source with a high-quality quantum source (heralded single-photon source). This combination allows for rapid random bit generation by leveraging the high photon flux of the semiclassical source while maintaining the certified randomness quality provided by the quantum component.

To further increase the preformance of the considered hybrid sourece, we implement a PBS-based multiplexing scheme (1) to significantly enhance the random number generation rate. We compare two operational regimes: a binary regime, whose quality depends critically on the alignment of the central PBS (red arrow), and an M-ary regime, which necessitates the precise alignment of a network of additional beam splitters (yellow arrows). A direct comparison of their maximum generation rates is performed. Sequence randomness is comprehensively assessed via the NIST statistical test suite and the NIST 800-90B entropy estimation suite. To quantify entropy extraction performance, we also compare results after post-processing with appropriate randomness extractors—including the V.F. Babkin method—for both binary and M-ary outputs.

The proposed multi-detector QRNGs are designed with a principle of simplicity, making them equally suitable for fundamental tests and practical integration. Furthermore, we demonstrate a novel application where these generators act as tools for the automated alignment and calibration of sensitive optical setups. In this method, the random sequences function as a stochastic probe, enabling precise adjustment of optical elements.

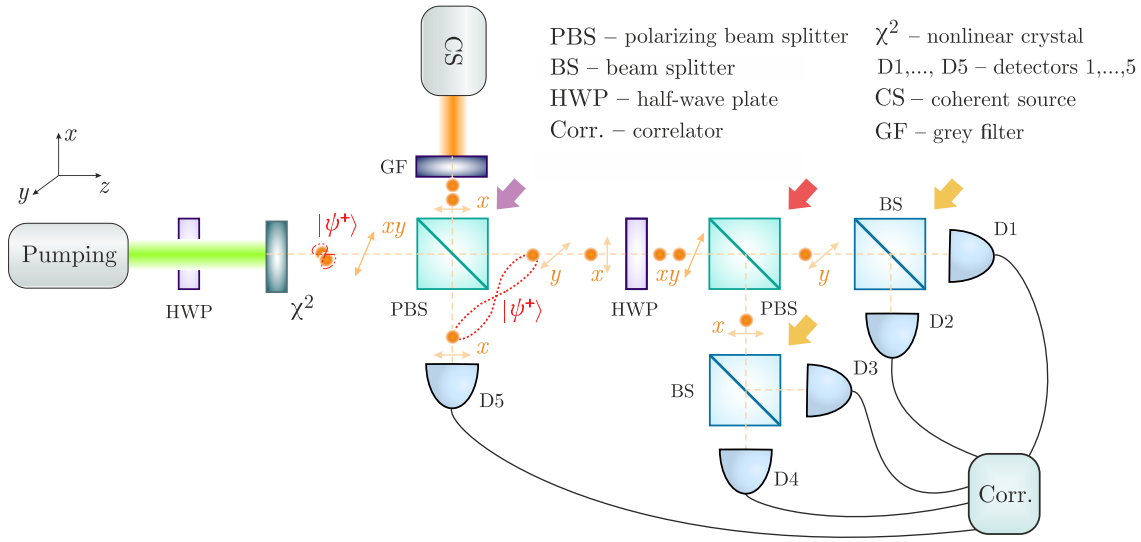

Figure 1: A schematic of the investigated QRNG setup. The first PBS (marked with a purple arrow) is used to mix the light from the two constituent sources. A second PBS (marked with a red arrow) splits the combined beam into two independent channels. Each of these channels is then further subdivided into two additional channels using auxiliary PBSs (marked with yellow arrows), creating a multi-detector array.

References

[1] *I. M. Arbekov and S. N. Molotkov*, Extraction of quantum randomness. Phys. Usp. **64**, 617 (2021).

[2] *B. Haylock at al.*, Multiplexed Quantum Random Number Generation. Quantum **3**, 141 (2019).

[3] *D. Reshetnikov, A. Kretova, A. Fominova, E. Vashukevich, T. Golubeva, K. Tikhonov*, Random Number Generators in Advanced Optical Experiments: A Comparative Analysis of Semiclassical, Quantum, and Hybrid Architectures (in preparation for publication)

Impact of Excitation Pathways on Single-Photon Emission: A PLE Study of Quasi-Resonant Excitation in C-Band InAs/InGaAs Quantum Dots on Metamorphic Buffers

Gleb Veyshtort[1*], **Alexey Veretennikov**[1], **Yuriy Serov**[1], **Aidar Galimov**[1], **Alexey Toropov**[1]

[1] *Ioffe Institute, Saint Petersburg, Russia*
*E-mail: gleb_veysh@mail.ru

Аннотация

We present a detailed spectroscopic study of quasi-resonant excitation pathways in C-band InAs/InGaAs quantum dots. We identify two distinct resonance types: non-selective (mediated by wetting layer states) and selective (direct intra-dot excitation). Time-resolved and correlation measurements link the non-selective mechanism to compromised single-photon purity.

Advances in quantum technologies drive the development of high-performance single-photon sources (SPSs). Semiconductor epitaxial self-assembled quantum dots (QDs) represent the most promising platform for on-demand single-photon generation [1]. SPS performance is typically characterized by brightness - the probability of photon emission per excitation pulse — and single-photon purity, which is determined by the probability of multi-photon emission.

Typically, QD-based SPSs are excited optically. When the excitation photon energy takes specific values between the exciton energy in the QD and the band gap of the matrix material, a resonant increase in the QD photoluminescence (PL) intensity may occur. This quasi-resonant excitation mode is widely used for SPSs as it enables high single-photon purity while allowing spectral separation of the PL from the excitation laser. Despite their practical importance, the underlying physical mechanisms of these resonances in specific structures are rarely studied in detail [2].

In this work, we investigate quasi-resonant excitation of InAs/InGaAs quantum dots emitting in the telecommunication C-band (1530–1565 nm). We study both an SPS based on a single QD embedded in a micropillar metamorphic cavity with distributed Bragg reflectors [3] and small QD ensembles in similar, but lower-quality-factor, microcavities. The single-QD device represents a high-performance source which, under resonant excitation, exhibits the highest reported brightness for the C-band. Here, we focus on a detailed spectroscopic study of its quasi-resonant excitation pathways to identify parasitic channels that could compromise single-photon purity.

To elucidate the excitation mechanisms, we performed photoluminescence excitation (PLE) spectroscopy on lower-quality-factor model structures exhibiting several closely spaced narrow lines in their PL spectra. Figure 1(a) shows the PL spectrum of one of the model structures containing four peaks, the PLE spectra of which are shown in different colors in figure 1(b). The obtained dependencies of the PL intensity on the excitation photon energy reveal two distinct types of resonances. A Type I (non-selective) resonance corresponds to the simultaneous excitation of several PL lines (areas 1 and 2 in the figure 1(b)). This phenomenon can be explained by features in the density of states of the wetting layer, which is formed during the self-assembled growth of QDs. We hypothesize that these features originate from the irregular surface of the underlying InGaAs metamorphic buffer layer, which is essential for redshifting the QD emission into the C-band. [4] Absorption in the wetting layer generates carriers that subsequently relax into multiple nearby QDs, causing luminescence. In contrast, type II (selective) resonances occurs only for a single PL line (area 3 in the figure 1(b)). This points to a direct excitation pathway, where a photon is absorbed via an excited state of the target QD itself, bypassing the wetting layer. Time-resolved PL measurements further corroborate the qualitative distinction between these two resonance types.

To assess the practical implications of these mechanisms, we investigated a single-QD SPS device under quasi-resonant excitation at different wavelengths. The PL decay kinetics at these resonances were found to follow either mono- or bi-exponential laws, with the pattern suggesting a possible correlation with the proposed resonance types (I and II). This supports the model of distinct carrier relaxation pathways for each mechanism: a multi-step capture process via the wetting layer (Type I) versus direct intra-dot relaxation (Type II). Furthermore, measurements of the second-order autocorrelation function

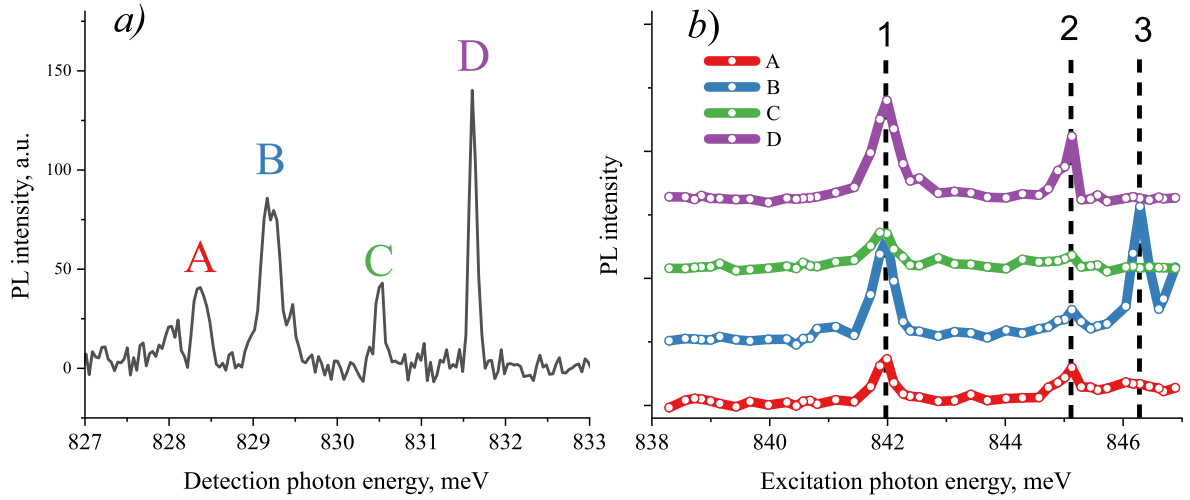

Рис. 1: a) A-D lines in the PL spectrum of the model structure, b) PLE spectra of A-D lines.

$g^{(2)}(0)$ suggest that excitation via non-selective resonances (Type I) could lead to a degradation of single-photon purity. Therefore, our results indicate that for optimal SPS performance, selective quasi-resonant excitation (Type II) appears to be preferable, while non-selective channels should be avoided.

The work was supported by Rosatom State Corporation in the framework of the Roadmap for Quantum computing (Contract №. 868/1734-D dated 22 September 2025)

Список литературы

[1] *Senellart P., Solomon G., White A.* High-performance semiconductor quantum-dot single-photon sources. Nature nanotechnology. **12.11**, 1026-1039 (2017).

[2] *Hauser N. et al.* Deterministic and highly indistinguishable single photons in the telecom C-band. arXiv preprint arXiv:2505.09695, (2025).

[3] *Veretennikov, A. I., et al.* Single-photon Emission in the Telecom C-Band in a Micropillar Cavity with an InAs/InGaAs Quantum Dot. JETP Letters **121.3**, 170-174 (2025).

[4] *Сорокин, С. В., et al.* Метаморфные гетероструктуры с квантовыми точками InAs/InGaAs для генерации одиночных фотонов в спектральном С-диапазоне. Письма в ЖЭТФ **121.1**, 37-43 (2025).

Free-Space Quantum Key Distribution over an Urban Atmospheric Link: System Design and Field Experiments

Vladislav Tretiakov[1*], **Andrey Klimov**[1], **Kirill Balygin**[1], **Veronika Vakhrusheva**[1,2]

[1] *Quantum Technology Centre of Moscow State University, Moscow, Russia*
[2] *SFB Laboratory, 127273*
*E-mail: tretiakov.vv18@physics.msu.ru

Abstract

We report on the development of a free-space quantum key distribution (QKD) system based on phase–time encoding, adapted from a commercially available fiber-based platform. Compared to our previous laboratory-oriented studies, the current work focuses on experiments over a 400 meters length real urban atmospheric optical link between the Main Building of Lomonosov Moscow State University and the Faculty of Physics. At this stage, the primary objective is to establish a stable free-space quantum channel and to investigate its performance under realistic atmospheric conditions.

Introduction

Quantum key distribution (QKD) enables provably secure communication based on fundamental principles of quantum mechanics. While fiber-based QKD systems have reached a high level of technological maturity [1], their applicability to long-distance links is fundamentally constrained by fiber attenuation. Free-space optical (FSO) channels represent an attractive alternative in scenarios where fiber deployment is impractical, including urban building-to-building links, mobile platforms, and satellite-based systems [2].

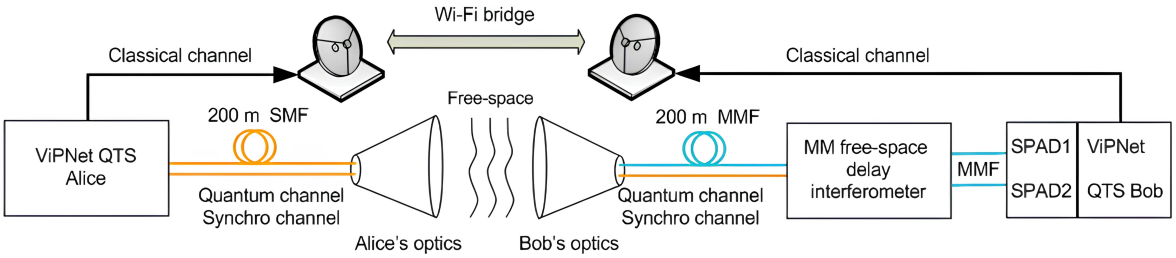

Figure 1: Simplified schematic of the AQKD system under development. The quantum and synchronization channels are integrated into a free-space optical link, while the service communication channel is implemented via a radio link.

However, atmospheric channels impose additional challenges related to turbulence-induced beam distortions and coupling losses, which severely limit the use of single-mode detection schemes. In our earlier work, we proposed and experimentally validated a practical approach for adapting a commercial fiber-based QKD system (ViPNet QTS [3]) to free-space operation by employing phase–time encoding and a free-space multi-mode delay interferometer. Figure 1 illustrates the general architecture of the developed atmospheric QKD system and the principle of phase-state analysis.

System architecture and Results

At the current stage, the QKD system has been deployed on a 400 meters length atmospheric optical link between two buildings of Moscow State University, with optical terminals installed at both ends of the link (see Figure 2). A stable free-space optical channel has been established, enabling long-term transmission tests and continuous monitoring of channel conditions. Ongoing experiments focus on the

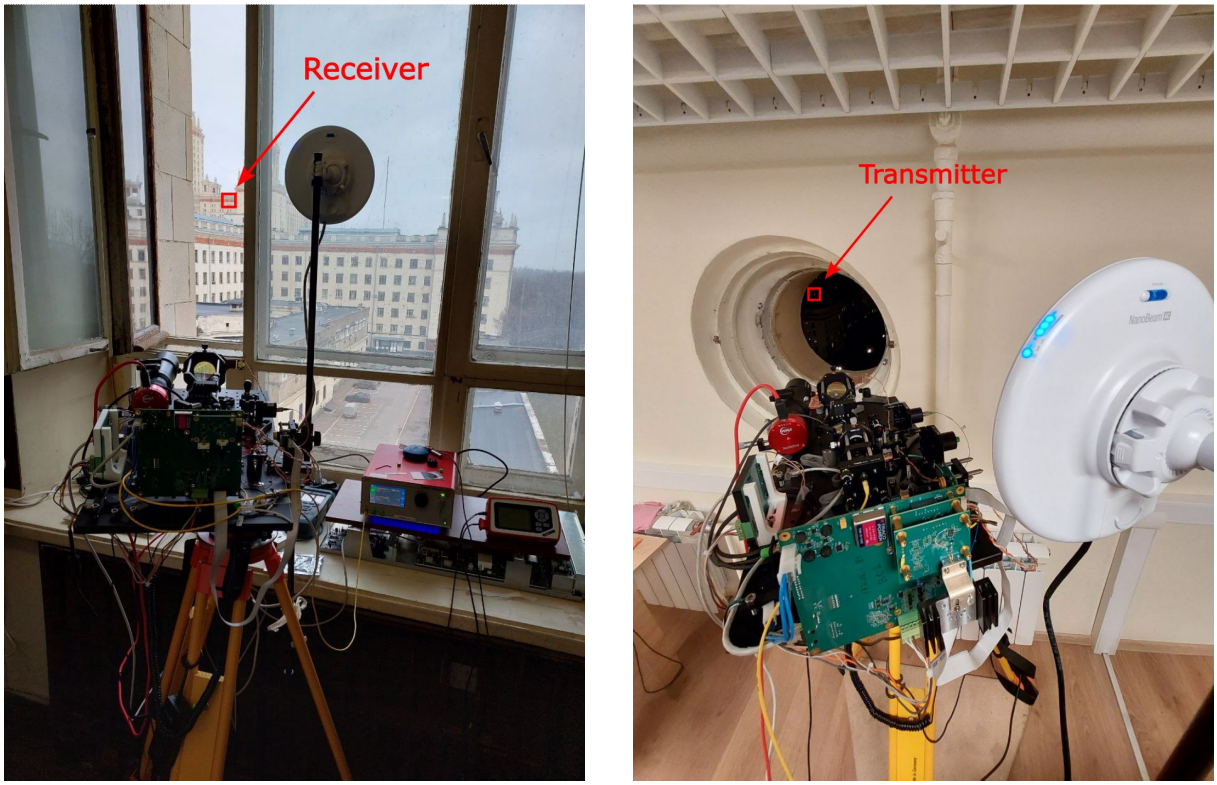

Figure 2: The deployed transmitter (left, Faculty of Physics) and receiver (right, Main Building of Lomonosov Moscow State University) terminals.

transmission of quantum states through the atmospheric channel, characterization of turbulence-induced fluctuations, and analysis of their impact on interference visibility and quantum bit error rate.

The multi-mode delay interferometer, previously optimized and tested under laboratory conditions [4, 5], is now operated in a field environment. Effects related to chromatic and modal dispersion, which were studied in detail in laboratory experiments, are taken into account at a qualitative level and are not expected to be the dominant performance-limiting factors for the current link length.

Based on the quantitative results obtained during laboratory QKD experiments, including a quantum bit error rate of about 4.5% and stable secret key rates on the order of hundreds of bits per second, we expect to demonstrate secret key generation over the atmospheric link by the time of the conference. The ongoing field trials are aimed at validating the robustness of the proposed system architecture under realistic urban atmospheric conditions and at identifying key parameters that limit performance in practical free-space QKD deployments.

The work was carried out within the framework of joint research and with the support of InfoTeCS JSC.

References

[1] Teng-Yun Chen, Jian Wang, Hao Liang, Wei-Yue Liu, Yang Liu, Xiao Jiang, Yuan Wang, Xu Wan, Wen-Qi Cai, Lei Ju, Luo-Kan Chen, Liu-Jun Wang, Yuan Gao, Kai Chen, Cheng-Zhi Peng, Zeng-Bing Chen, and Jian-Wei Pan. Metropolitan all-pass and inter-city quantum communication network. *Opt. Express*, 18(26):27217–27225, Dec 2010.

[2] Sheng-Kai Liao, Wen-Qi Cai, Wei-Yue Liu, Liang Zhang, Yang Li, Ji-Gang Ren, Juan Yin, Qi Shen, Yuan Cao, Zheng-Ping Li, Feng-Zhi Li, Xia-Wei Chen, Li-Hua Sun, Jian-Jun Jia, Jin-Cai Wu, Xiao-Jun Jiang, Jian-Feng Wang, Yong-Mei Huang, Qiang Wang, Yi-Lin Zhou, Lei Deng, Tao Xi, Lu Ma, Tai Hu, Qiang Zhang, Yu-Ao Chen, Nai-Le Liu, Xiang-Bin Wang, Zhen-Cai Zhu, Chao-Yang Lu,

Rong Shu, Cheng-Zhi Peng, Jian-Yu Wang, and Jian-Wei Pan. Satellite-to-ground quantum key distribution. *Nature*, 549(7670):43–47, August 2017.

[3] InfoTeCS. ViPNet QTS, 2025. Accessed: 2025-07-23.

[4] Jeongwan Jin, Sascha Agne, Jean-Philippe Bourgoin, Yanbao Zhang, Norbert Lütkenhaus, and Thomas Jennewein. Demonstration of analyzers for multimode photonic time-bin qubits. *Phys. Rev. A*, 97:043847, Apr 2018.

[5] V V Tretiakov, A N Klimov, K A Balygin, and S P Kulik. Laboratory demonstration of free space phase-time encoding quantum key distribution system with multi-mode delay interferometer. *Laser Physics Letters*, 22(9):095201, sep 2025.

Krasnaya Polyana, Sochi, Russia March 1 – March 7, 2026
9th International School on Quantum Technologies

Broadband optical injection attacks on the QKD transmitter

Klim Bondar[1,2*], **Ivan Sushchev**[1,2], **Daniil Bulavkin**[1], **Dmitriy Melkonian**[1], **Kirill Bugai**[1,3], **Anna Sidelnikova**[1], **Veronika Vakhrusheva**[1,2], **and Dmitriy Dvoretskiy**[1,3]

[1] *SFB Laboratory, LLC, 127273 Moscow, Russia*
[2] *Quantum Technology Centre and Faculty of Physics, Lomonosov Moscow State University, 119991 Moscow, Russia*
[3] *Bauman Moscow State Technical University, 105005 Moscow, Russia*
*E-mail: bondar.kd19@physics.msu.ru

Abstract

We experimentally investigate the effects of optical injection attacks on the transmitter side of QKD systems. Previous studies have primarily considered such attacks in the context of optical injection locking with slight frequency detuning between the master (Eve) and slave (Alice) lasers. Here, we demonstrate the impact of these attacks over a broad spectral range $\lambda = 1275 - 1650$ nm, showing a reduction in the relative key length under the decoy-state BB84 protocol.

Introduction

Quantum key distribution (QKD) enables two remote users (Alice and Bob) to share bit sequences that are, in principle, inherently secure against eavesdropping (by Eve) due to the fundamental laws of quantum mechanics. However, practical imperfections in optical components of real-world QKD systems introduce vulnerabilities. One such vulnerability is the laser seeding attack, in which Eve injects illegitimate optical radiation into Alice's laser diode cavity, increasing the energy (mean photon number) of her emitted pulses. Such an increase [1] compromises QKD security by altering the photon statistics of the transmitted states. Previous studies have analyzed the attack primarily in the context of optical injection locking, i.e., with low or negligible frequency detuning between Eve's master laser and Alice's slave laser. However, experimental evidence of the attack's effectiveness across a broad spectral range has not yet been reported.

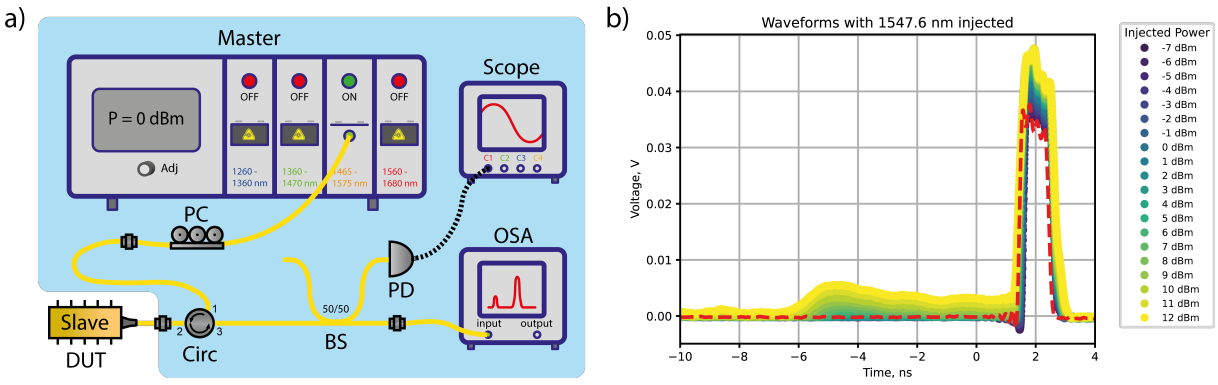

Figure 1: (a): Experimental setup for broadband optical injection into an Alice laser diode. Master is a module consisting of four tunable lasers, PC is a mechanical polarization controller, Circ is a fiber circulator, PD is a broadband PIN-diode, Scope is an oscilloscope, OSA is optical spectrum analyzer, and Slave is a slave laser diode. The solid yellow lines represent optical fibers, and the dotted black one represent electrical coaxial cable. (b): Typical waveforms observed during 1547.6 nm optical injection. Colored points represent waveforms under optical injection by fixed power, and the dotted red ones are unattacked Alice's waveform.

Results

Our experimental setup (Fig.1 (a)) implements the attack by injecting continuous-wave (CW) light from a wavelength-tunable laser module into a slave laser diode (DUT) via a fiber circulator. The diode's

output is detected by a broadband PIN photodiode, with the signal displayed on an oscilloscope and stored (Fig.1 (b)). Additionally, the optical spectrum of Alice's laser is recorded by OSA.

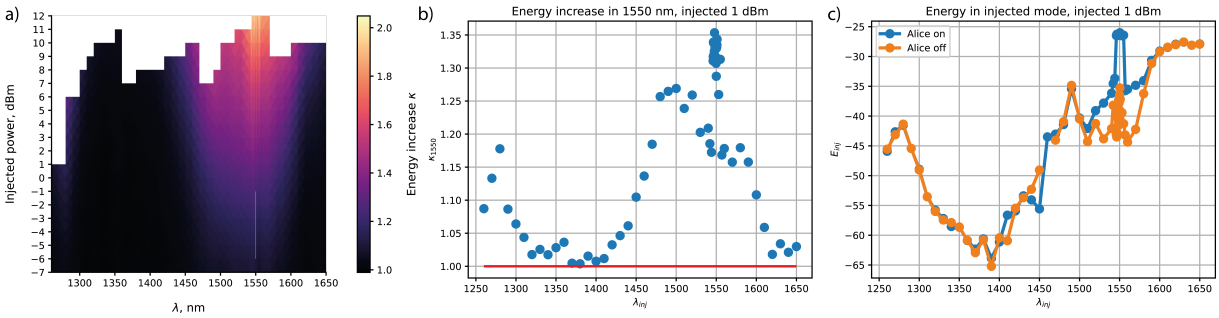

Figure 2: Dependence (a) of the energy increase κ in Alice's laser pulses on the injected power and wavelength, (b) of the energy increase κ_{1550} in legitimate Alice's mode on the injected wavelengths under fixed 1 dBm optical power, and (c) of the energy in injected mode on injected wavelength under fixed .

Measurements were performed both without an attack and with optical injection at wavelengths $\lambda = 1275-1650$ nm and powers $P = -7...12$ dBm. Pulse energies were normalized to the unattacked value to quantify the relative increase κ. The results, shown in Fig.2 (a), indicate the broadband energy increase in Alice's radiation. Furthermore, under shorter wavelengths injection, energy increase is observed only in legitimate spectral mode (see Fig.2 (b)), which indicates the optical pumping of the laser diode. At the same time, under near-legitimate wavelengths optical injection, the stimulated amplification of the tampered radiation is observed (Fig.2 (c)).

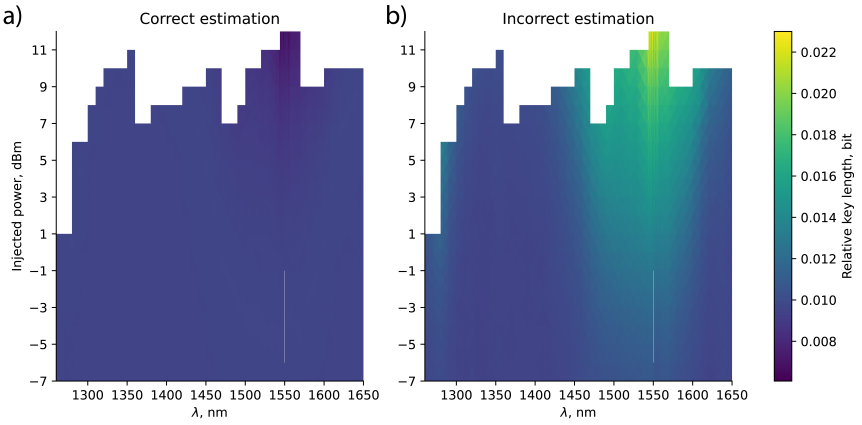

Figure 3: (a) Correct and (b) incorrect (realistic) estimate of the relative key length under Eve's optical injection attack, depending on the wavelength and injection power in decoy state BB84 protocol case.

The impact on secure key generation was evaluated under the BB84 decoy-state protocol, using the experimental parameters from [2]. Simulation results (Fig.3) show that the attack leads legitimate users to overestimate the fraction of single-photon component, and thus overestimate the unconditionally secure key length, generating part of the key from multi-photon component.

References

[1] *A. Huang, A. Navarette, S.-H. Sun, P. Chaiwongkhot, M. Curty, and V. Makarov*, Laser-seeding attack in quantum key distribution. Phys. Rev. Applied **12**, 064043 (2019).

[2] *L. C. Comandar, M. Lucamarini, B. Fröhlich, J. F. Dynes, A. W. Sharpe, S. W.-B. Tam, Z. L. Yuan, R. V. Penty, and A. J. Shields* , Quantum key distribution without detector vulnerabilities using optically seeded lasers. Nature Photonics **10**, 312-315 (2016).

Krasnaya Polyana, Sochi, Russia March 1 – March 7, 2026
9th International School on Quantum Technologies

Novel Isotropic Protocol for Scalable and Secure QKD Networks

Ivan Sushchev[1,2*]

[1] *SFB Laboratory, LLC, 127273 Moscow, Russia*
[2] *IQuantum Technology Centre, Faculty of Physics, Lomonosov Moscow State University, 119991 Moscow, Russia*
*E-mail: i.sushchev@icloud.com

Abstract

Scalable deployment of quantum key distribution is limited by cost, compactness, and security, especially in metropolitan networks. We consider a novel isotropic discrete-variable QKD protocol with continuous basis randomization that is naturally compatible with passive state preparation. The protocol provides intrinsic resistance to fake-state attacks, preserves practical key rates, and enables low-cost client devices for large-scale quantum networks.

Quantum key distribution (QKD) is widely regarded as a secure method for generating cryptographic keys protected by the laws of quantum mechanics. At the same time, large-scale deployment of QKD systems is limited by three closely related factors: scalability of quantum networks, high cost of hardware, and limited compactness of practical implementations. These limitations become especially important for metropolitan and access networks, where a large number of end users must be connected to a central node. In such scenarios, the so-called last-mile problem often determines whether QKD can be deployed in a practical and economically reasonable way.

A natural approach to scalable quantum networks is to concentrate complex and expensive hardware at a trusted central (backbone) node, while making client-side devices as simple and inexpensive as possible. This architecture is schematically shown in Fig. 1. It allows the number of users to be increased with moderate additional cost, but it also makes the overall security of the network strongly dependent on the measurement unit located at the central node.

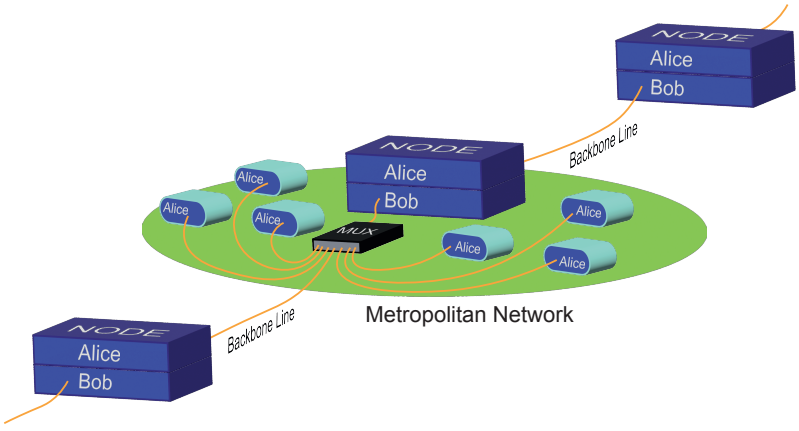

Figure 1: Metropolitan QKD network architecture. Expensive and complex hardware is concentrated at the central node (server), while client devices are strongly simplified to enable scalable deployment.

Several approaches to reducing the cost and size of QKD transmitters are actively being developed. Continuous-variable (CV) QKD systems rely on coherent detection and standard telecom components and have shown steady progress in performance and maturity [1]. However, such systems typically require stable local oscillators, high-speed analog electronics, and precise calibration, which complicates their use in highly simplified client devices. Also, CV QKD protocols lack complete proof of security. Another direction is passive state preparation, where the basis and bit values are randomized by the physical process itself rather than by active modulators. Fully passive transmitters have been experimentally demonstrated and offer exceptional simplicity, compactness, and low cost [2]. These properties

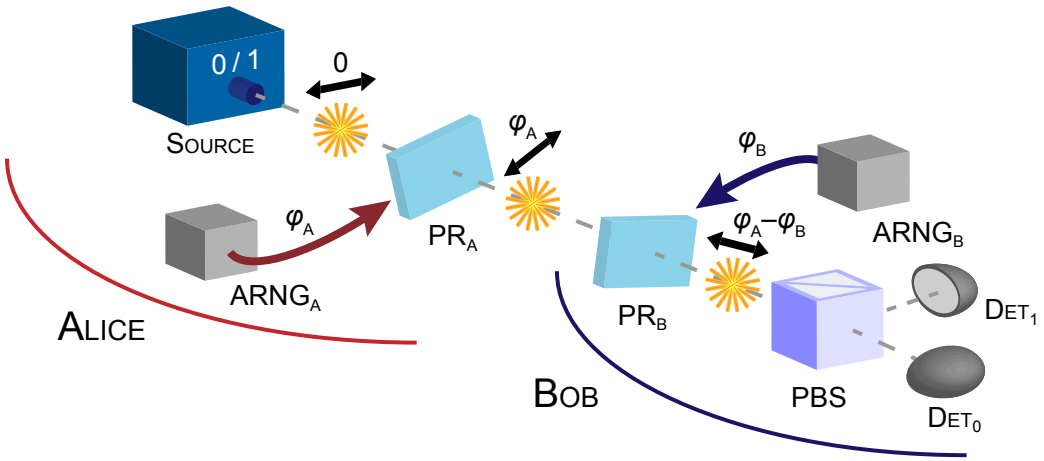

Figure 2: Schematics of the proposed protocol with polarization coding. Source, the source of horizontally (0) and vertically (1) polarized photons with equal probabilities; PR_A, Alice's polarization rotator; $ARNG_A$, Alice's analog random number generator; PR_B, Bob's polarization rotator; $ARNG_B$, Bob's analog random number generator; PBS, polarization beam splitter; Det_0 and Det_1, Bob's single-photon detectors.

make passive schemes especially attractive for large-scale metropolitan networks, provided that adequate security can be guaranteed.

At the same time, centralized receiver architectures make detector security a critical issue. Single-photon detectors are among the most vulnerable components of practical QKD systems. In particular, fake-state and detector-control attacks exploit non-ideal detector behavior and have been demonstrated experimentally [3, 4]. These results show that many detector-level countermeasures rely on assumptions that may not hold in realistic conditions. A conceptually strong solution is measurement-device-independent (MDI) QKD, which removes detector vulnerabilities by design [5]. However, MDI-QKD requires complex interference of independent sources and tight synchronization, which increases system cost and limits its suitability for cost-sensitive and highly scalable metropolitan networks.

In this context, a new point-to-point QKD protocol with built-in resistance to fake-state attacks was proposed in Ref. [6]. The protocol belongs to the class of discrete-variable QKD schemes and is based on continuous randomization of preparation and measurement bases. Alice prepares qubit states by applying random rotations with angles

$$\varphi_A \in [-\pi/2, \pi/2],$$

while Bob independently selects his measurement basis angles

$$\varphi_B \in [-\pi/2, \pi/2].$$

After the quantum transmission, Bob publicly announces his chosen angles. Alice then computes the mismatch angles

$$\Delta\varphi = \varphi_A - \varphi_B,$$

which determine the error probability for each detected bit. A principal schematic of the protocol for polarization encoding is shown in Fig. 2.

Unlike the BB84 protocol, the proposed scheme does not discard events with mismatched bases. Instead, all detection events are retained and processed probabilistically. Even in the ideal case without noise and eavesdropping, the raw key appears as white noise with an average error probability of 50%. By publicly disclosing a small subset of data and applying maximum-likelihood estimation, Alice and Bob can estimate the disturbance introduced by an eavesdropper. For collective attacks, the achievable

relative secret-key length can be written as [6]

$$\ell = 1 - h(\sin^2 \alpha) - \frac{1}{N}\sum_{j=1}^{N} h(e_j), \tag{1}$$

where α characterizes Eve's interaction with the quantum states, e_j is the error probability associated with the j-th basis mismatch angle, N is the key length, and $h(x)$ is the binary entropy function.

A key feature of the protocol is its intrinsic resistance to fake-state attacks. Because the measurement bases are continuously randomized, the probability that an attacker's basis closely matches Bob's basis is strongly reduced. Under realistic assumptions about detector response, the success probability of a detector-control attack scales with the cube of the angular precision. For typical experimental precision on the order of 1°, this probability is reduced to approximately 10^{-6}, leading to a strong reduction of the raw-key generation rate and making the attack ineffective in practice [6].

Importantly, the proposed protocol is particularly well suited for passive state preparation. In passive transmitters, the preparation basis is randomized by construction, without active modulation. The continuous and isotropic use of bases in the protocol turns this randomness into a useful cryptographic resource rather than a limitation. Detection events corresponding to different effective bases remain valuable for key generation, which significantly increases efficiency compared to standard protocols when used with passive sources.

In summary, the proposed isotropic QKD protocol offers a practical way to address security, scalability, and cost simultaneously. It provides built-in protection against fake-state attacks, is naturally compatible with passive state preparation, and is well suited for compact and low-cost client devices. These properties make the protocol a strong candidate for metropolitan and access QKD networks, where large-scale deployment and economic efficiency are critical.

I. S. Sushchev thanks S. N. Molotkov, D. A. Dvoretskiy, and S. P. Kulik for numerous discussions.

I. S. Sushchev also acknowledges the scholarship from the Foundation for the Advancement of Theoretical Physics and Mathematics, "BASIS."

References

[1] *Y. Zhang, Z. Li, Y. Wang, X. Wang, and H.-K. Lo*, Continuous-variable quantum key distribution system: Past, present, and future. Appl. Phys. Rev. **11**, 011306 (2024).

[2] *F. Y. Lu, X. Wang, Y. Liu, Z. Zhang, and H.-K. Lo*, Experimental demonstration of fully passive quantum key distribution. Phys. Rev. Lett. **131**, 110802 (2023).

[3] *A. Huang, S. Sun, Z. Zhang, and V. Makarov*, Testing random-detector-efficiency countermeasure in a commercial system reveals a breakable unrealistic assumption. IEEE J. Quantum Electron. **52**, 1 (2016).

[4] *Z. Wu, Y. Cao, Y. Liu, and X. Ma*, Hacking single-photon avalanche detectors in quantum key distribution via pulse illumination. Opt. Express **28**, 25574 (2020).

[5] *H.-K. Lo, M. Curty, and B. Qi*, Measurement-device-independent quantum key distribution. Phys. Rev. Lett. **108**, 130503 (2012).

[6] *I. S. Sushchev*, Point-to-point quantum key distribution resistant to fake-state attacks. APL Quantum **2**, 021301 (2025).

Methodology for estimating energy losses in satellite quantum communications systems taking into account atmospheric influences

Maksim Sapozhnikov[1*]

[1] *National Research Centre «Kurchatov Institute», Russia*
*E-mail: msapozh@jscc.ru

Аннотация

Current implementations of satellite quantum key distribution are significantly limited by atmospheric factors, primarily atmospheric turbulence caused by fluctuations in the air refractive index. These distortions determine the limits of the key QKD performance metrics: the generation rate of the filtered quantum key sequence and the quantum error rate per bit. Existing approaches to estimating energy losses in an optical channel either fail to account for the spatiotemporal inhomogeneity of a turbulent atmosphere or require excessive computational resources during modeling, which limits their applicability for the operational design and analysis of satellite quantum channels. A key result of this study is the developed methodology for calculating energy losses, taking into account the impact of atmospheric turbulence when calculating QKD performance. The application of the proposed methodology in numerical simulations of QKD experiments will improve the accuracy of estimating QKD performance metrics compared to existing approaches.

The development of wireless satellite quantum communications in the Russian Federation has been identified as a strategic priority and is institutionally enshrined within the state scientific and technological policy. A key tool for achieving this goal is the "Roadmap"for the development of the high-tech field of "Quantum Communications,"developed by Russian Railways in collaboration with leading scientific organizations, the expert community, and industry market participants. This Roadmap was approved by the Ministry of Digital Development, Communications, and Mass Media of the Russian Federation in 2020 and updated in 2022.

In the context of this strategy, the integration of quantum key distribution (QKD) technologies into a multi-tiered telecommunications infrastructure is of particular importance: from terrestrial fiber-optic and atmospheric lines to satellite channels that enable scaling of quantum networks to ensure the stable operation of distributed quantum networks in the face of geopolitical and technological uncertainty. Currently, research activity in the field of quantum communications in Russia is focused primarily on terrestrial and atmospheric links, despite the recognized need to include a space segment to ensure global coverage and commercial viability of systems [1]. Experimental studies have confirmed the compatibility of domestic atmospheric optical terminals with QKD equipment [2, 3]. However, scaling up quantum networks requires overcoming a fundamental limitation: the strong influence of the atmosphere on the parameters of the quantum channel for satellite-to-Earth and Earth-to-satellite paths [4]. Existing methods for estimating energy losses either simplify the physics of propagation, ignoring the spatiotemporal dynamics of turbulence, or require unacceptably high computational costs, making them of little use in the design and analysis of satellite systems.

This paper sequentially implements two stages of research. The first stage analyzes existing approaches to assessing the factors limiting the use of quantum key distribution in satellite quantum communication systems, with an emphasis on atmospheric phenomena as the main source of energy losses. The analysis established the applicability limits of the approaches considered. In particular, it identified conditions under which traditional calculation methods overestimate or underestimate the energy budget, which is unacceptable when designing quantum lines. Based on these findings, a methodology was developed for estimating energy losses in satellite quantum communication systems due to atmospheric processes. The methodology is based on atmospheric turbulence as the dominant factor and is constructed taking into account the physical mechanisms of loss formation during optical signal propagation along the satellite-to-Earth and Earth-to-satellite paths. Its application allows for increased accuracy in predicting performance indicators—in particular, key generation rate and quantum error rate—compared to traditional approaches.

In the second stage, the developed methodology was verified. This was accomplished through a quantitative and qualitative comparison of the results obtained using the proposed methodology with data from a full-scale satellite quantum key distribution experiment. The verification confirmed the viability

and validity of the proposed approach. The long-term significance of these results lies in increasing the reliability of calculations of the full energy budget of satellite quantum systems, which ensures the optimization of capital and operating costs at the feasibility study stage and contributes to increasing the profitability of the implementation of domestic global quantum network projects.

Список литературы

[1] *A.P. Ovsyannikov and B.M. Shabanov*, On an interuniversity quantum network project. Software and Systems. **36**, 695 (2022).

[2] *A.A. Boev, et al.*, Possibility of creating a modular system for quantum key distribution in the atmosphere. Pisma v Zhurnal Tekhnicheskoi Fiziki. **48**, 15 (2022).

[3] *D.V.Bolotov, et al.*, A Method for Estimating Losses in a Quantum Channel for Implementing Quantum Key Distribution Technology for Atmospheric Laser Communication Terminals. Wave Electronics and Its Application in Information and Telecommunication Systems. **5**, 57 (2022).

[4] *R.M. Muskan, R. Meena and S. Banerjee*, Analysing QBER and secure key rate under various losses for satellite based free space QKD. (2023).

Krasnaya Polyana, Sochi, Russia March 1 – March 7, 2026
9th International School on Quantum Technologies

Semidefinite Programming Methods for Multimode Continuous-Variable Quantum Channels: Application to the SCW Protocol

Daria Kargina[1*], **Roman Goncharov**[1]

[1] *Quantum Information Laboratory, ITMO University, Kadetskaya Line, 3, St. Petersburg, 199034, Russia*
*E-mail: dakargina17@gmail.com

Abstract

We study a prepare-and-measure discrete-modulation continuous-variable quantum key distribution protocol implemented in a subcarrier-wave architecture, in which Alice encodes information into a multimode coherent state and Bob performs heterodyne detection. Discrete modulation is realized by four-symbol phase-shift keying, and the signal amplitude is optimized by semidefinite conic programming. We also provide a finite-size security analysis against coherent attacks using the generalized entropy accumulation theorem and evaluate the resulting secret key rates over realistic Gaussian channels.

We consider a continuous-variable quantum key distribution (CV-QKD) scheme in a paradigm based on multimode states in a subcarrier-wave (SCW) protocol. The quantum channel between Alice and Bob is modeled as a standard Gaussian channel, through which a multimode state $|\Psi_x\rangle$ propagates. The channel is described by a transmittance η and excess noise ξ in shot-noise units.

Alice prepares a multimode state with $2S+1$ frequency modes, indexed by $k = -S, \ldots, 0, \ldots, S$. For each part she chooses an amplitude and a phase from the bias $\varphi_k \in \{0, \pi/2, \pi, 3\pi/2\}$, and forms a coherent state defined by complex amplitudes $\alpha_k(\beta)$:

$$\alpha_k = \alpha\, d_{0k}^{(S)}(\beta)\, \exp[-ik\,(\theta_1 + \varphi_k)]\,, \quad k \in \{-S, \ldots, -1, 1, \ldots, S\}, \tag{1}$$

where the real parameter $\alpha > 0$ is optimized by a conic (semidefinite) programming procedure in order to maximize the asymptotic secret key frame. The resulting multimode state held by Alice is $|\Psi_x\rangle = \bigotimes_k |\alpha_k^{(x)}\rangle$. The carrier mode $k = 0$ is excluded from the quantum description and is treated as a classical local oscillator controlled by the monitoring system.

The optimized finite-size key rate analysis is obtained by generalized entropy accumulation theorem (GEAT) (see Figure 1).

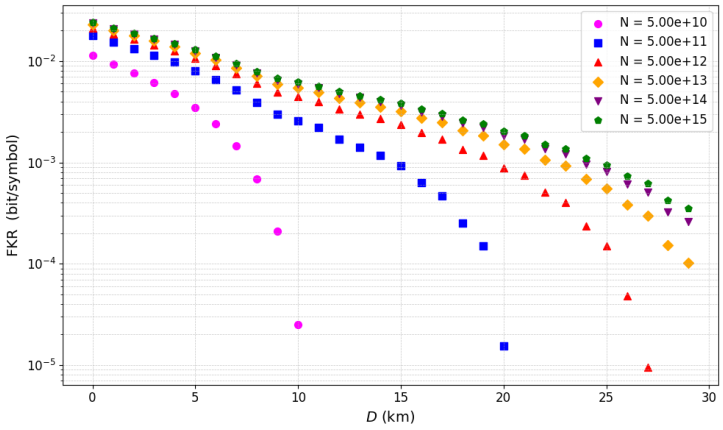

Figure 1: Secret key rate FKR depends on the distance D for different block lengths N. Parameters: $N_c = 12$, $\delta = 2$, $\Delta = 5$, $m = 0.85$, $J = 2$, $\epsilon = \epsilon_{PE} = \epsilon_{PA} = 10^{-10}$. Additional noise was included in the channel with a $\xi = 0.01$

This method is based on the work of Pascual-García *et al.* [1]. GEAT reduces the security proof against coherent attacks to the analysis of collective attacks through protocol decomposition. The key

applicability condition is the sequential protocol structure, where the adversary holds at most one quantum register at a time. Unlike the original EAT [2], GEAT for prepare-and-measure protocols does not require a virtual tomography step on Alice's subsystem, which removes additional statistical fluctuations and leads to improved finite-size key rates [3].

Finally, our results extend the finite-size security analysis of discrete-modulation CV-QKD to a realistic multimode subcarrier-wave implementation and show that semidefinite-programming optimization of the modulation amplitude yields the secret key rates over lossy and moderately noisy channels. Because the optimization and security proof depend only on the effective Gaussian parameters estimated from data, the same methodology can be straightforwardly adapted to other multimode or multi-carrier discrete-modulation CV-QKD protocols.

The work was carried out with the support of the Russian Science Foundation Grant No. The work was carried out with the support of the Russian Science Foundation Grant No. 24-11-00398.

References

[1] *Pascual-García C., Bäuml S., Araújo M., Liss R., Acín A.* Improved finite-size key rates for discrete-modulated continuous-variable quantum key distribution under coherent attacks. Phys. Review A. **2**, 022610 (2025).

[2] *Dupuis F., Fawzi O., Renner R.* Entropy accumulation. Comm. in Math. Phys. **3**, 867–913 (2020).

[3] *Metger T., Fawzi O., Sutter D., Renner R.* Generalised entropy accumulation. Comm. in Math. Phys. **11**, 261 (2024).